Technische Universität München

Lehrstuhl für Physikalische Chemie

Size-dependent Plasmonic Properties of Supported Silver Clusters and Cluster-Molecule Complexes

Tobias Lünskens

Vollständiger Abdruck der von der Fakultät für Chemie der Technischen Universität München zur Erlangung des akademischen Grades eines

Doktors der Naturwissenschaften

genehmigte Dissertation.

Vorsitzender:		Prof. Dr. S. Günther
Prüfer der Dissertation:	1.	Prof. Dr. U. K. Heiz
	2.	Prof. Dr. R. Nießner

Die Dissertation wurde am 12.07.2016 bei der Technischen Universität München eingereicht und durch die Fakultät Chemie am 06.09.2016 angenommen.

Eidesstattliche Erklärung

Hiermit bestätige ich, dass die der Fakultät für Chemie der Technischen Universität München zur Promotionsprüfung vorgelegte Arbeit mit dem Tiel Size-dependent Plasmonic Properties of Supported Silver Clusters and Cluster-Molecule Complexes am Lehrstuhl für physikalische Chemie unter Anleitung und Betreuung durch Herrn Prof. Dr. Ueli Heiz ohne sonstige Hilfe erstellt und bei der Abfassung nur die gem §6 Abs. 5 angegebenen Hilfsmittel benutzt worden sind. Die Dissertation ist in keinem anderen Prüfungsverfahren als Prfüngsleistung vorgelegt.

München, am _____ _____

Datum Unterschrift

Abstract

The plasmonic properties of size-selected, supported silver clusters are studied by surface second harmonic generation spectroscopy and by surface cavity ring-down spectroscopy under ultra high vacuum conditions. A resonance splitting for plasmonic modes oriented parallel and perpendicular to the surface is shown, which can be attributed to the anisotropic environment caused by the SiO_2 substrate. A blue shift of $\approx 0.2\,\mathrm{eV}$ in the plasmon resonance of ligand free clusters is observed for a decreasing cluster size from Ag_{55} to Ag_9, which is described by a theoretical model based on Mie theory. A capping layer of chemisorbed thiolate ligands shifts the plasmon resonance by $\approx 0.3\,\mathrm{eV}$ to lower energies, which can be attributed to an increased refractive index of the dielectric environment and a reduced free electron density inside the silver clusters. In addition to this general behavior clear differences are observed for Ag_{55} and Ag_{20} due to the varying surface to volume ratio.

Furthermore the thin film growth of π-conjugated molecules is studied by surface cavity ring-down spectroscopy. A shoulder in the absorption spectrum of a bis-pyrene is observed for coverages above one monolayer,

which can be attributed to intermolecular interactions.

Die plasmonischen Eigenschaften größenselektierter, geträgerter Silber-Nanopartikel werden mittels nicht linearer 'Second Harmonic Generation' Spektroskopie (SHG), sowie linearer 'Cavity Ring-Down' Spektroskopie (CRD) unter ultrahochvakuum Bedingungen untersucht. Die Plasmonresonanz verschiebt sich um $\approx 0.2\,\mathrm{eV}$ zu höheren Energien, wenn die Partikelgröße von Ag_{55} zu Ag_9 reduziert wird. Die gemessene Verschiebung ist in quantitativer Übereinstimmung mit einem auf der Mie Theorie basierenden Modell, welches mittels DFT berechnete, größenabhängige dielektrische Funktionen von Silber verwendet. Im Gegensatz zu Studien an Silber-Nanopartikeln, welche in kalten Edelgas-Matrizen eingebettet sind, wird selbst für die kleinsten untersuchten Nanopartikel eine einzige, plasmonartige Resonanz gemessen. Der größenabhängige Trend, welcher für größere Partikel bereits bekannt ist und mittels Mie Theorie erklärt werden kann, konnte somit bis hin zu molekülartigen Nanopartikeln bestätigt werden. Es wird gezeigt, dass die Polarisierbarkeit freier Leitungsbandelektronen innerhalb von Silber-Nanopartikeln durch die Adsorption von organischen Molekülen reduziert wird, was zu einem Verlust der gemessenen SHG-Intensität führt. Um den Einfluss von organischen Molekülen auf die plasmonischen Eigenschaften von Silber-Nanopartikeln zu bestimmen, wird

daher eine lineare optische Methode verwendet. Mittels CRD-Spektroskopie wird gezeigt, dass die Plasmonresonanz geträgerter Silber-Nanopartikel um $\approx 0.3\,\mathrm{eV}$ zu niedrigeren Energien schiebt, wenn Thiophenol auf die Proben aufgedampft wird. Diese Änderung kann der hohen Affinität von Thiolen gegenüber Silber und somit einer Chemisorption von Thiophenol auf den Silber-Nanopartikeln zugeordnet werden. Der gemessene Einfluss ist in qualitativer Übereinstimmung mit einer erhöhten dielektrischen Konstante des umgebenden Mediums, sowie einer Reduktion der freien Elektronendichte innerhalb der Silber-Nanopartikel. CRD-Spektroskopie wurde weiterhin dafür verwendet, die Adsorption und den Übergang zu einer geschlossenen Monolage π-konjugietrer Moleküle zu untersuchen. Oberhalb einer Oberflächenbedeckung von einer Monolage ist im Absorptionsspektrum eine Schulter zu erkennen, welche intermolekularen Wechselwirkungen zuzuschreiben ist.

Contents

List of Figures

List of Figures

1. Introduction

The plasmonic behavior of coinage metal nanoparticles, which is dominated by their localized surface plasmon resonance (LSPR), has been used to color glass for many centuries. The most popular example is the famous Lycurgus cup, which was crafted by the Romans in the 4th century and is exhibited in the British Museum in London. It appears green or red depending on whether light is reflected from or shining through the cup, respectively. Based on their strong absorption of light and the ability to enhance electro-magnetic fields, nowadays plasmonic coinage metal nanoparticles enable a wide range of applications like biological and chemical sensing [6, 63, 139, 206], plasmon assisted spectroscopy [102, 126, 157], energy harvesting [11, 37, 129] and plasmon assisted chemistry [125, 138, 149]. Regarding to these fields of research, silver is one of the most studied metals, because the LSPR of silver nanoparticles is located in the UV/VIS and it is exceptionally pronounced due to the absence of interband transitions in this spectral range, which would damp the LSPR. It has been shown, that the optical properties of silver nanoparticles depend, amongst others, strongly on their size [34, 105]. Therefore the size-dependent optical properties have

to be understood in order to optimize their plasmonic behavior. However, in the case of supported silver nanoparticles, which is the practically most relevant system for the applications mentioned above, experimental studies are limited to particle diameters above $\approx 1.5\,\mathrm{nm}$, due to the low surface coverages required to avoid agglomeration and the small excitation cross section of particles containing only a few tens of atoms [134, 158, 177]. This lack of information is particularly problematic in this size range, because substantial deviations from the plasmonic behavior of bigger particles are expected for molecular-like silver clusters [3, 61] and were observed for very small silver clusters embedded in cold rare gas matrices and in the gas phase [52, 116]. In order to overcome the experimental challenges, within this work the surface sensitivity of second harmonic generation spectroscopy is used in order to investigate molecular-like silver clusters supported onto a SiO_2 substrate.

Besides ligand-free metal clusters, monolayer-protected nanoparticles attracted a lot of interest in the past two decades, since thiolate-stabilized gold nanoparticles were synthesized for the first time in 1994 [25]. Not only gold but also thiolate-protected silver clusters have boosted, amongst others, the understanding of the size dependent optical properties [68]. However, chemisorbed thiolates change the optical properties of metal nanoparticles due to a reconstruction of the metal atoms, a change in the electron density inside the nanoparticle and an alteration of the dielectric environment [67, 151, 164]. Especially in the case of small particles with diameters below $\approx 2\,\mathrm{nm}$ strong deviations from a plasmonic behavior in form of distinct absorption features can be observed [32, 47, 210], which are not present in

the optical extinction spectra of ligand-free silver nanoparticles of similar size. However, since the ligand-layer is mandatory for the stabilization of such metal clusters, no experimental studies on the impact of the ligands on the optical properties under controlled conditions are available so far. Within this work the impact of the thiol-ligands on the optical properties of size-selected supported silver clusters is investigated under ultra-high vacuum conditions and the evolution of the extinction spectrum from the ligand-free clusters to a saturated system is monitored by means of surface caity ring-down spectroscopy.

2. Optical Properties of Metal Clusters

The optical properties of metal nanoparticles are dominated by the Localized Surface Plasmon Resonance (LSPR), a collective oscillation of the free conduction band electrons. This classical model is depicted in figure 2.1. In the case of small particles, an external electromagnetic field penetrates the whole particle and the homogeneous field inside the particle moves the free conduction electrons with respect to the positively charged lattice ions. The conduction electrons build up a negative charge at the particle surface that feels a restoring force due to the positive charge of the fixed lattice ions. If the

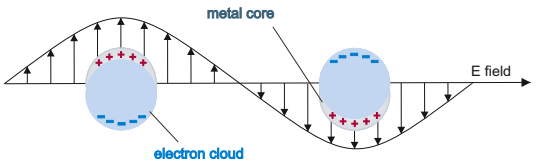

Figure 2.1.: Dipolar Localized Surface Plasmon Resonance excited by an External Electromagnetic Field.

external field is in resonance with this collective oscillation, a pronounced absorption is observed and a suspension of such particles appears colorful, if the absorption is in the visible region. Despite the strong absorption of small noble metal particles in the UV/VIS range of the electromagnetic spectrum, the ability for enhancement of the electromagnetic field around the nanoparticle is the most prominent feature of LSPRs. Both properties of the LSPR are used for energy harvesting [11, 129, 37], plasmon assisted chemistry [149, 125, 138], plasmon assisted spectroscopy [102, 157, 126], biological labeling and chemical sensing [206]. In order to provide the theoretical background for understanding this phenomena in this chapter the theory by Gustav Mie is introduced [143], which explaines the origin of the red color of small gold particles for the first time, and various factors that influence the extinction spectrum of small metal particles are discussed.
The interaction of electromagnetic fields with matter can be described with classical electrodynamics [46] and Mie was the first who solved Maxwell's equations for an electromagnetic field interacting with small spheres having the same dielectric constant as the bulk metal and that are surrounded by a homogeneous dielectric surrounding. For nanoparticles much smaller than the wavelength of light only a dipole oscillation contributes to the extinction spectrum and Mie theory is expressed in its dipole approximation as follows [143]

$$\sigma_{ext}(\omega) = 9\frac{\omega}{c_0}\epsilon_m^{3/2}V\frac{\epsilon_2(\omega)}{[\epsilon_1(\omega)+2\epsilon_m]^2+\epsilon_2(\omega)^2)} \tag{2.1}$$

where $\sigma_{ext}(\omega)$ is the frequency dependent extinction cross section, ω is the frequency of light, c_o is the speed of light, V is the particles volume, ϵ_m is

the dielectric constant of the surrounding medium and $\epsilon_1(\omega)$ and $\epsilon_2(\omega)$ are the frequency dependent real and imaginary part of the bulk metals dielectric function. The dielectric function of simple metals like alkali metals can be described well with the Drude-Sommerfeld model [105]. However the free 5s electrons of silver are described in good approximation with this model, too[1]. The basic principle of this theory is to describe the electrons in the metal as a free electron gas, consisting of independent electrons. The electrons can move freely between collisions, that can take place at lattice ions, other electrons, or phonons. Within this theory the dielectric function is expressed as

$$\epsilon(\omega) = \epsilon_\infty - \frac{\omega_p^2}{\omega(\omega + i\gamma_0)} \tag{2.2}$$

where ϵ_∞ is the high frequency dielectric constant, ω_p is the plasma frequency of free bulk electrons and γ_0 is bulk damping constant that describes the collisions of free electrons. If only the conduction electrons contribute to the dielectric function ϵ_∞ has got the value 1 and consequently

$$\epsilon(\omega) = 1 - \frac{\omega_p^2}{\omega(\omega + i\gamma_0)} \tag{2.3}$$

with its real and imaginary part

$$\epsilon_1(\omega) = 1 - \frac{\omega_p^2}{\omega^2 + \gamma_0^2} \tag{2.4}$$

$$\epsilon_2(\omega) = \frac{\omega_p^2 \gamma_0}{\omega\left(\omega^2 + \gamma_0^2\right)} \tag{2.5}$$

[1] Silver has got the electron configuration $[Kr]4d^{10}5s^1$.

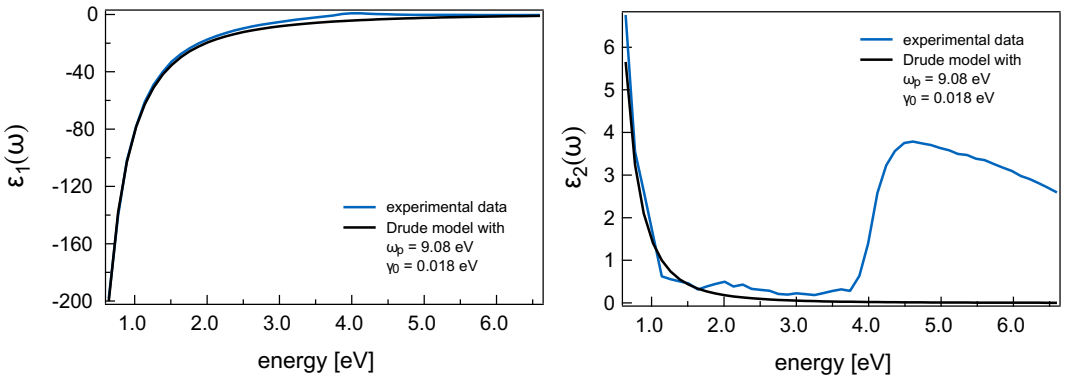

Figure 2.2.: Real part $\epsilon_1(\omega)$ and imaginary part $\epsilon_2(\omega)$ of the dielectric function of silver. The calculated Drude-type dielectric function represents the free 5s-electrons. The experimental data are taken from [94].

Figure 2.2 shows the real and imaginary part of the dielectric function for silver using equations 2.4 and 2.5 and the experimentally determined dielectric functions of bulk silver [94]. The experimentally measured dielectric function shown in blue exhibits strong deviations compared to the calculated Drude-type dielectric function shown in black above 3.8 eV. The reason for this are excitations from the deeper 4d-band electrons into the conduction band. In order to account for that the dielectric function has to be expressed in terms of interband contributions $\epsilon_{inter}(\omega)$ and intraband contributions $\epsilon_{intra}(\omega)$, whereas the free $5s^1$ electrons can be described with the Drude-Sommerfeld model.

$$\epsilon_{bulk}(\omega) = \epsilon_{intra/Drude}(\omega) + \epsilon_{inter}(\omega) \tag{2.6}$$

$$\epsilon_{inter}(\omega) = \epsilon_{bulk}(\omega) - \epsilon_{intra}(\omega) \tag{2.7}$$

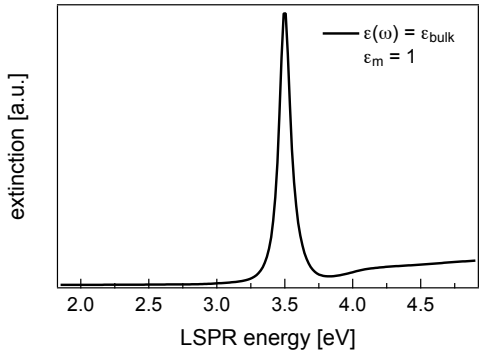

Figure 2.3.: Extinction spectrum of silver nanoparticles surrounded by vacuum, according to Mie theory .

The dielectric function is than expressed as

$$\epsilon(\omega) = \epsilon_{bulk}(\omega) - \epsilon_{intra}(\omega) + \epsilon_{intra/Drude}(\omega) \tag{2.8}$$

$$= \epsilon_{bulk}(\omega) + \frac{\omega_p^2}{\omega^2 + i\omega\gamma_0} - \frac{\omega_{p/Drude}^2}{\omega^2 + i\omega\gamma_0} \tag{2.9}$$

Using the bulk dielectric function Mie theory was very successful in describing the optical properties of small metal particles [105]. Figure 2.3 shows the calculated extinction spectrum of silver particles surrounded by vacuum using equation 2.1 and the experimental dielectric function from figure 2.2. The extinction spectrum shows a strong absorption at 3.5 eV corresponding to the LSPR of the free conduction band electrons in the silver particle. In addition the spectrum exhibits an onset above 3.5 eV which can be attributed to the excitation of interband transitions. The fact that the LSPR is located in an energy range well below the onset of the interband transitions is the reason for the intense LSPR of silver and justifies to treat silver in approxi-

mation as a simple Drude metal. If the LSPR is located in the same energy range as the intraband transitions the LSPR would be less pronounced due to a not negligible value of $\epsilon_2(\omega)$, as can be seen from the denominator in equation 2.1. This behavior can be observed in the case of gold and copper nanoparticles, which exhibit a much less pronounced LSPR compared to silver nanoparticles [194].

2.1. Size Effects

It is well known, that the optical properties of silver nanoparticles depend strongly on their size [34, 105] and this is also true for supported, molecular-like silver clusters, as will be shown in this work. Therefore in this section several theoretical concepts are described, which explain the size-dependent optical properties of coinage-metal nanoparticles.

Although Mie theory has been very successful in describing the optical extinction spectra of small metal particles down to a size of 20 nm, it has to be modified for very small particles that have to be treated within the dipole approximation ($d \ll \lambda$). Otherwise equation 2.1 would predict a size independent optical extinction spectrum, which is not observed in experimental studies [105]. Most extensions of classical Mie theory assume a size dependent dielectric function following Kreibig, who proposed that the scattering of free electrons at the particle surface becomes important, if the diameter of the particle is smaller than the free mean path of electrons l_0. The surface scattering causes an additional damping of the electron

oscillation and the bulk damping constant γ_0 has to be modified in order to account for this size effect

$$\gamma_0 = \frac{v_F}{l_0} \tag{2.10}$$

$$\gamma(r) = \gamma_0 + A\frac{v_F}{r} \tag{2.11}$$

Here v_F is the Fermi velocity of electrons in bulk silver and A is a phenomenological damping parameter. A is dependent on the scattering details and varies between 0 and 1. For small silver clusters in the gasphase a value of $A = 0.25$ was found [105]. Assuming that only the free $5s$ electrons, that can be described with the Drude model, suffer surface scattering, the Drude part of equation 2.9 is modified

$$\epsilon(\omega, r) = \epsilon_{bulk}(\omega) + \frac{\omega_p^2}{\omega^2 + i\omega\gamma_0} - \frac{\omega_p^2}{\omega^2 + i\omega\gamma(r)} \tag{2.12}$$

with its real and imaginary part

$$\epsilon_1(\omega, r) = \epsilon_{1,bulk}(\omega) + \frac{\omega_p^2}{\omega^2 + \gamma_0^2} - \frac{\omega_p^2}{\omega^2 + \gamma^2(r)} \tag{2.13}$$

$$\epsilon_2(\omega, r) = \epsilon_{2,bulk}(\omega) + \frac{\omega_p^2\gamma(r)}{\omega\left[\omega^2 + \gamma^2(r)\right]} - \frac{\omega_p^2\gamma_0}{\omega\left[\omega^2 + \gamma_0^2\right]} \tag{2.14}$$

Figure 2.4 shows the LSPR energy and width[2] for different particle diameters, calculated by feeding equations 2.13 and 2.14 into equation 2.1. For the dielectric constant of the surrounding medium ϵ_m a value of 1 was

[2] the width is shown as the full width at half maximum (FWHM)

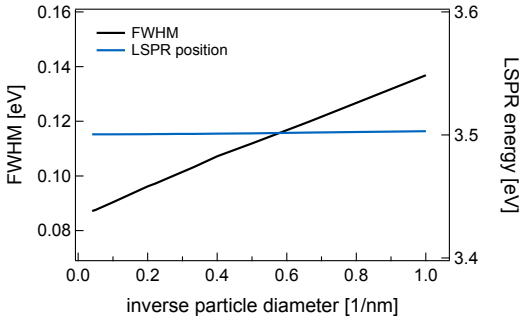

Figure 2.4.: Size dependent width and position of the Localized Surface Plasmon resonance according to the free mean path effect.

used, corresponding to particles surrounded by vacuum. Note that both, the LSPR energy and the FWHM for the bigger sizes match the values of the spectrum in figure 2.3, which corresponds to a 10 nm silver particles surrounded by vacuum. As can be seen, the main effect of the additional surface scattering with a decreasing particle diameter is a broadening of the LSPR, while the position remains almost unchanged. Thus the free mean path effect correctly describes the experimentally observed $1/R$ dependence of the LSPR width [12, 105, 120], but does not provide an explanation for the shift of the LSPR to higher energies with a decreasing particle diameter that is observed for silver nanoparticles [34, 73, 134, 158, 197]. Therefore further modifications were carried out, that either adopt the free electron spill out at metal dielectric interfaces for small particles [106, 127, 146, 172, 198], or account for quantum size effects (QSE) [167, 177]. Recently a model was presented, that account for both and analyzes the competition between free electron spill out and quantum size effects [147]. The assumption of a free electron spill out is in contrast to the classical Drude model with its

hard wall boundary conditions, which implies a uniform density of free electrons inside the metal particle without electron spill out into the free space. Due to the spill out the centroid of the charge oscillation associated with the LSPR is located outside the particle surface. In the case of simple s metals like alkali metals the electron density outside the particle feels a lower restoring force caused by the fixed, positively charged lattice ions. In consequence the LSPR shifts to lower energies with a growing influence of the surface and therefore with a decreasing particle size. In the case of silver the influence of the filled 4d band has to be considered. The screening of the d-electrons is very important in the bulk metal and the unscreened bulk plasma frequency ω_p is shifted from 9.08 eV to approximately 3.8 eV [105]. However the 4d band is very localized and excluded from the surface region where the electron spill out takes place. Thus the electron density outside the particle oscillates at the unscreened frequency, which results in an increased resonance frequency and therefore a shift to higher energies with a decreasing particle diameter. Following this approach, the shift of the LSPR depends on the quantity of the unscreened electron density outside the particle and the resonance frequency ω_{LSPR} can be expressed as

$$\omega_{LSPR}^2 = \omega_p^2 \left[\left(\frac{R_0}{R} \right)^2 + \frac{1 + 2 \cdot Re(d_r)/R}{\epsilon_\infty + 2\epsilon_m + 2\left(\epsilon_\infty - \epsilon_m^2\right) 2 \cdot Re(d_r)/R} \right] \tag{2.15}$$

where $Re(d_r)$ is a screening parameter, that is a measure of the centroid of the oscillating charge density and introduces the nonlocal correction of the classical Drude model. Positive values of $Re(d_r)$ describe a spill out of free electrons and thus a blueshift of the LSPR. Note that for $Re(d_r) = 0$ the term to the right in the parentheses of equation 2.15 has got the same

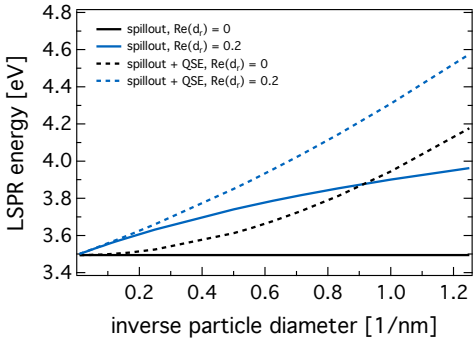

Figure 2.5.: Competition between the effect of surface screening and quantum size effects on the size dependent Localized Surface Plasmon Resonance of silver nanoparticles for two different screening parameters $Re(d_r)$.

resonance condition like equation 2.1 which assumes a dielectric function described by classical Drude theory. The term to the left in the parentheses accounts for quantum size effects due to splitting of energy levels, that can be observed for very small metal clusters consisting of only a few atoms per cluster [52, 117]. R_0 can be written in terms of the free electron density parameter r_s as $R_0 = 1.1a_0\sqrt{r_s}$ [147]. Using a dielectric constant of the surrounding medium $\epsilon_m = 1$ and a high frequency dielectric constant of silver $\epsilon_\infty = 5$ [146, 150], equation yields the size dependent LSPR energies shown in figure 2.5. The solid lines show the LSPR energies for the spill out of free electrons without quantum size effects[3], whereas the dashed lines show the combination of the spill out of free electrons and quantum size effects. The calculation was done for two different screening parameters $Re(d_r)$ in each case. The LSPR energies for $Re(d_r) = 0$ are shown in black

[3]Therefore the term to the left in the parentheses of equation 2.15 was neglected.

and the LSPR energies for $Re(d_r) = 0.2$ are shown in blue. As expected from Mie theory in combination with the classical Drude model, a neglect of quantum size effects together with a screening parameter $Re(d_r) = 0$ results in a size independent LSPR located at around 3.5 eV. Allowing for free electron spill out shifts the LSPR energy to higher energies with a decreasing particle diameter. Following the presented model, quantum size effects start to become important below a particle diameter of approximately 5 nm and cause an additional blueshift.

Both presented models, the free mean path effect and the free electron spill out are based on a modification of the bulk dielectric function in order to describe size effects. A different approach is to calculate the dielectric function depending on the size ab initio. A semiempirical model for the dielectric function of small silver clusters based on quantum mechanically calculations was combined successfully with Mie theory in order to describe the blueshift of the LSPR of size selected silver clusters [76, 134]. The analytical expression for the imaginary part of the size dependent dielectric function $\epsilon_2(\omega, r)$ within this model is given as follows[76]

$$\epsilon_2(\omega, r) = \frac{\omega_p^2 \left(1 - exp\left(-a_1 r\right)\right)^2 \left(\gamma_0 + \frac{a_3}{r\hbar}\right) \left[1 - exp\left(-\frac{r^3}{b_3^3}\right)\right] \omega}{\left[\frac{1}{\hbar^2}\left(\frac{1}{a_2 + b_2 r}\right)^2 - \omega^2\right]^2 + \left[\left(\gamma_0 + \frac{a_3}{r\hbar}\right) \left[1 - exp\left(-\frac{r^3}{b_3^3}\right)\right] \omega\right]^2} \quad (2.16)$$

Here a_1, a_2, a_3, b_1, b_2 and b_3 are fit parameters[4]. The size dependent real part of the dielectric function $\epsilon_1(\omega, r)$ can be calculated according to the

[4] $a_1 = 1.95\,\mathrm{nm}^{-1}$, $a_2 = 0.18\,\mathrm{eV}^{-1}$, $a_3 = 0.192\,\mathrm{eV}\cdot\mathrm{nm}$, $b_2 = 0.268\,\mathrm{eV}^{-1}\cdot\mathrm{nm}^{-1}$ and $b_3 = 0.2\,\mathrm{nm}$.

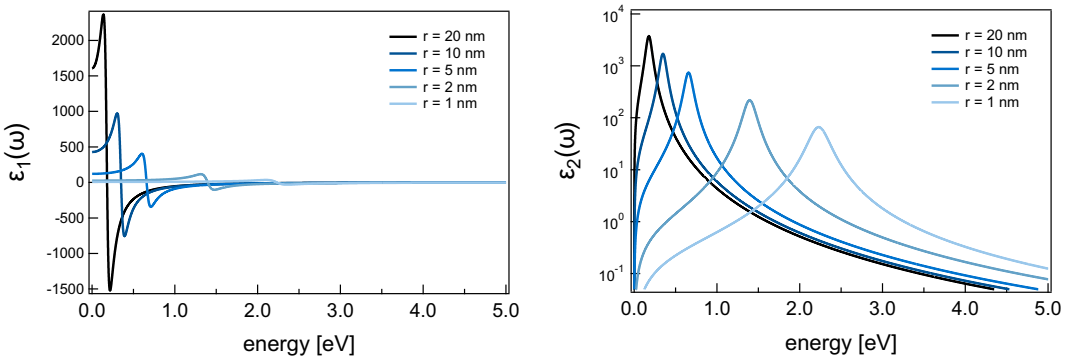

Figure 2.6.: Size dependent real part $\epsilon_1(\omega)$ and imaginary part $\epsilon_2(\omega)$ of the dielectric function of silver nanoparticles according to [76].

Kramer-Kronig relation

$$\epsilon_1(\omega, r) = 1 + \frac{2}{\pi} P \int_0^\infty \frac{\epsilon_2(\omega')\omega'}{\omega'^2 - \omega^2} d\omega' \tag{2.17}$$

Figure 2.6 show the as-calculated dielectric function for spherical silver particles with radii between 20 nm and 1 nm by use of equation 2.16 and 2.17. Note, that only intraband transitions are considered and that interband transitions from the 4d band to the conduction band are neglected. Furthermore it should be noted, that in the case of the imaginary part of the dielectric function a logarithmic scale was used. A size dependence of the dielectric function is clearly seen and it already becomes clear, that the LSPR shifts to higher energies with a decreasing particle size. Feeding the size dependent dielectric function into Mie theory results in the extinction spectra shown in figure 2.7. For the dielectric constant of the surrounding medium ϵ_m a value of 1.65 was used. All size dependent features that are observed experimentally in the extinction of small silver particles are present in figure 2.7. The LSPR shifts to higher energies, it broadens and its

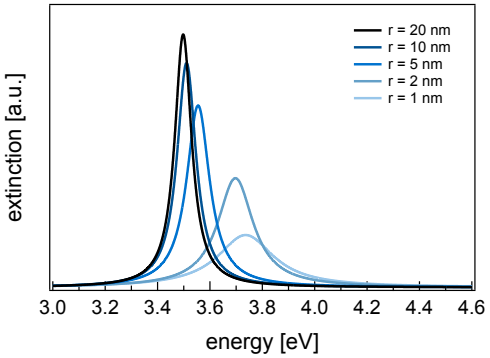

Figure 2.7.: Size dependent extinction spectra of silver nanoparticles due to combination of the size dependent dielectric function [76] and classical Mie theory for a dielectric constant of the surrounding medium $\epsilon_m = 1$.

intensity decreases for a decreasing particle size.

2.2. Shape Effects

Although classical Mie theory is only valid for spheres, other shapes like rods, cubes, triangles and prisms, just to name a few, have achieved much interest and it has been shown, that the extinction spectrum of metal nanoparticles depends strongly on their shape [31, 105, 118, 159, 162, 211]. In this chapter the optical properties of ellipsoidal in comparison to spherical particles will be examined in more detail, because an ellipsoidal shape is a more realistic approximation of a supported nanoparticle [39, 158], the system under investigation within this work. An ellipsoid has a volume $V_e = (4\pi/3)\,abc$. Here only an oblate spheroid will be considered, where

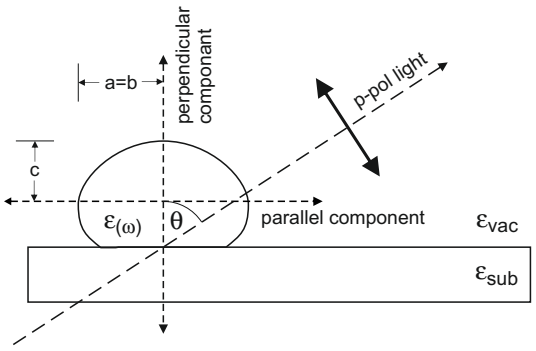

Figure 2.8.: Geomerty of optical extinction experiments.

$a = b > c$. In the case of supported particles the short symmetry axes c is oriented perpendicular to the surface, as shown in figure **??**. Following classical Mie theory the extinction $\sigma_{ext,i}$ along a particles axis i can be calculated as [20]

$$\sigma_{ext,i} = \frac{\omega}{c_0} \cdot \epsilon_m^{1/2} \cdot V_e \frac{\epsilon - \epsilon_m}{(\epsilon - \epsilon_m) L_i + \epsilon_m}. \tag{2.18}$$

L_i is the particle shape parameter and for an oblate spheroid it can be calculated as

$$L_a = L_b = \frac{R_{c/a}}{2\left(1 - R_{c/a}^2\right)^{3/2}} \left[\frac{\pi}{2} - \tan^{-1}\left(\frac{R_{c/a}^2}{\sqrt{R_{c/a}^2}}\right)\right] - \frac{R_{c/a}^2}{2\left(1 - R_{c/a}^2\right)} \tag{2.19}$$

$$L_c = 1 - 2L_a. \tag{2.20}$$

where the aspect ratio is given by $R_{c/a} = {}^{c}/_{a}$. Equations 2.19 and 2.20 show, that the threefold degenerated plasmon mode of a spherical metal nanoparticle splits into a twofold degenerated plasmon mode across the long particle axis $a = b$ and one plasmon mode across the short particle axis c. Note that in the case of a spherical particle, where the aspect ratio is

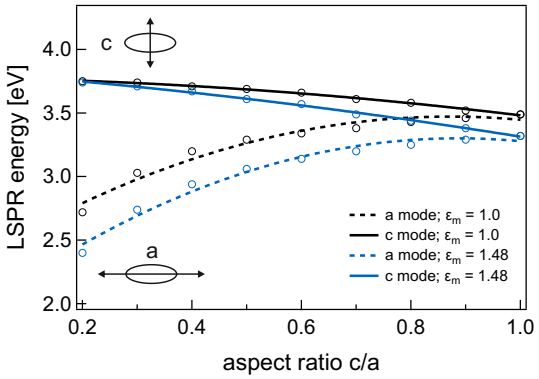

Figure 2.9.: Splitting of the Localized Surface Plasmon Resonance in elongated silver nanoparticles for two different dielectric constants ϵ_m of the surrounding medium.

1, $L_a = L_b = L_c = 1/3$ and equation 2.18 yields equation 2.1 from classical Mie theory. Figure 2.9 illustrates the influence of the aspect ratio on the position of the LSPR calculated with equations 2.19 and 2.20 and using the dielectric function ϵ of bulk silver [94]. Two different cases are shown. Firstly, a dielectric constant of the surrounding medium $\epsilon_m = 1$ was used, according to a particle surrounded by vacuum, shown in black. Secondly a dielectric constant of the surrounding medium $\epsilon_m = 1.48$ was used, according to the weighted dielectric constant of small silver clusters supported onto a quartz glass substrate [87], shown in blue. Compared to the single plasmon mode of a spherical particle $(aspectratio = 1)$, the plasmon along the short particle axis c is shifted to higher energies and the plasmon mode along the long particle axis a is shifted to lower energies, whereas the redshift of the long axis mode is much more pronounced. Note that in the case of supported particles the plasmon mode along the short particle axis corresponds to a

plasmon mode perpendicular to the surface and that s-SHG spectroscopy probes this mode exclusively, as described in section 3.2.2. Both, the long and the short axis mode corresponding to a higher dielectric constant of the surrounding medium (shown in blue) are shifted to lower energies compared to the plasmon modes of a particle in vacuum, which is explained in detail in section 2.3. For small silver clusters deposited onto quartz glass from the gas phase an aspect ratio of 0.86 was found [87]. As can be seen, such a deformation results in a plasmon splitting of approximately 0.1 eV . For a more pronounced plasmon splitting caused by a flattening of spherical particles smaller aspect ratios has to be assumed. A second important point that should be noted is the fact, that even the smallest aspect ratios, which are rather unrealistic for gasphase supported metal particles, in combination with the smallest possible dielectric constant of the surrounding yield a high energy mode smaller than 3.8 eV.

2.3. Dielectric Environment

The dielectric function of the surrounding medium ϵ_m has got a strong influence on the optical properties of metal particles, especially on the position of the LSPR. Compared to a single spherical metal particle surrounded by a homogeneous dielectric environment, the dielectric surrounding in this work is rather complex. An ensemble of silver clusters is supported onto a substrate, covered with organic molecules and surrounded by vacuum. In such a system mainly two properties of the dielectric environment can be

identified, which alter the extinction spectrum. Firstly both, a surface and a molecular layer in close proximity to metal clusters change the refractive index n_m of the surrounding. Secondly, the environment of supported particles is anisotropic due to the presence of the substrate and neighboring particles. The influence of these properties on the position and width of the LSPR of silver clusters is discussed separately in the following sections and are addressed again in the results chapter.

2.3.1. Refractive Index Changes

To demonstrate the influence of the refractive index of the surrounding medium n_m on the position of the LSPR, which is related to the dielectric constant ϵ_m by ϵ_m=n_m^2, in a first step a spherical metal particle surrounded by a homogeneous dielectric medium ϵ_m is considered. According to Mie theory, the extinction of such a system is directly altered, if the dielectric constant of the surrounding medium is changed. This behavior becomes clear, if one realizes, that the frequency of the oscillating electrons of a metal particle and the local electromagnetic field that extends beyond the physical boundaries of the particle into the dielectric environment are inseparable. The polarizabilty of the dielectric surrounding screens the surface charges, thereby lowering the frequency of the electron oscillation [44]. This effect on

the position of the LSPR can be quantified using the resonance condition[5]

$$\epsilon_1(\omega) + 2\epsilon_m = 0 \tag{2.21}$$

Assuming an ideal free-electron metal, the real part of the dielectric function $\epsilon_1(\omega)$ can be written within the Drude model as

$$\epsilon_1(\omega) = 1 - \frac{\omega_p^2}{\omega^2 + \gamma^2} \tag{2.22}$$

In the visible region, $\gamma \ll \omega_p$, and therefore (2.22) can be simplified to

$$\epsilon_1(\omega) = 1 - \left(\frac{\omega_p^2}{\omega^2}\right) \tag{2.23}$$

At resonance conditions

$$\omega = \frac{\omega_p}{\sqrt{2\epsilon_m + 1}} \tag{2.24}$$

As can be seen from equation 2.24, the position of the LSPR depends almost linear on the dielectric constant of the surrounding medium, which is illustrated in figure 2.10. This behavior was confirmed experimentally in different experiments, where the refractive index of the surrounding medium was the only changed variable. This was realized either by dispersing coinage metal particles in different solvents [5, 57, 156], surrounding silver nanoparticles with different solid matrices [84, 208], or by embedding surface confined silver nanoparicles in various solvent environments [53, 93, 135, 137, 140, 145]. It was found that different particle sizes, excitation modes and particle shapes show a different sensitivity to refractive

[5]Compare equation 2.1. The extinction shows a maximum, if the denominator is at its minimum.

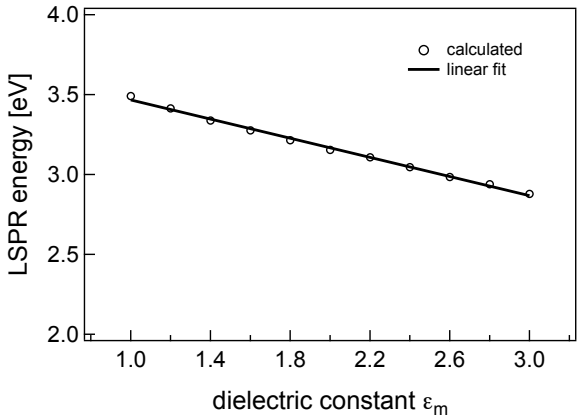

Figure 2.10.: Influence of the dielectric constant of the surrounding medium ϵ_m on the position of the Localized Surface Plasmon Resonance of silver nanoparticles.

index changes, which was confirmed by theoretical studies [99, 118]. Nevertheless, all systems follow the same trend. The LSPR shifts to lower energies with an increasing refractive index of the surrounding medium. Major work was carried out by Van Duyne and coworkers to optimize the local refractive index sensitivity of plasmonic silver structures in terms of chemical an biological sensing [63, 64, 65, 66, 93, 140, 142]. Recently it was possible to detect the adsorption event of a single molecule with a plasmonic nanostructure [7, 214], which emphasizes the importance of the local dielectric surrounding on the position of the LSPR. If metal particles are supported onto a substrate, or if they are covered with a thin layer of molecules, the dielectric environment is not homogeneous and the dielectric constant of the surrounding medium ϵ_m has to be replaced by an effective dielectric constant ϵ_{eff}, reflecting the complexity of the dielectric environment. In the case of supported particles ϵ_{eff} is somewhere between the value of the

substrate material and the value of the surrounding medium, for instance vacuum. One intuitive way to quantify ϵ_{eff} is to weight the dielectric constant of the substrate and the surrounding by the contact area A between the particle and the substrate[42, 105, 158, 192]

$$\epsilon_{eff} = A \cdot \epsilon_{substrate} + (1 - A) \cdot \epsilon_m \tag{2.25}$$

This assumption is rooted in the observation, that the LSPR shifts to lower energies, if particles are supported onto a substrate with a higher refractive index compared to the surrounding. In the case of particles surrounded by a thin dielectric layer, the dielectric constant and the thickness of the capping shell has to be considered. This is due to the fact, that the electromagnetic field of a LSPR extends beyond the physical boundaries of the metal particle. It is strongest at the surface of the particle and decays with distance [99, 165]. In various distance dependent studies it was shown, that the short and the long range dependence of the LSPR on a refractive index change can be explained reasonably well, assuming a single exponential decay of the electromagnetic field [6, 44, 63, 65, 66, 128, 142]. This was achieved by varying the thickness of the molecular layer surrounding the particles in solution, or by deposition of a dielectric layer on top of supported particles respectively. At short distances from the nanoparticle surface the LSPR shift follows a linear trend. At longer distances the refractive index dependent shift attenuates and levels off at a specific distance. Beyond this characteristic distance, the local electromagnetic field, and therefor the LSPR of metal nanoparticles, is not altered by the surrounding. Therefore the optical properties of ligand stabilized metal particles has to be described

as core-shell-particles consisting of a metal core and a thin dielectric layer, that are surrounded by a dielectric medium [5, 20, 57, 109, 156]. If the dielectric constant of the ligand shell is bigger than the dielectric constant of the surrounding medium, an increasing shell thickness results in an increased effective dielectric constant and the LSPR shifts to lower energies. If it is smaller than the dielectric constant of the surrounding medium an increasing shell thickness will shift the LSPR to higher energies. If the dielectric constant of the ligand shell equals the dielectric constant of the surrounding medium, the local dielectric environment is homogeneous and the LSPR is not affected, considering only refractive index changes.
The broken symmetry brought by the presence of the adjacent substrate lifts the degeneracy of the dipole plasmon modes oriented parallel and perpendicular to the substrate. It has been shown, that the dielectric constant of the substrate can be neglected for the plasmon mode parallel to the surface [103]. Therefore, different meaningful effective dielectric constants for the experiments done within this work show up and the resulting extinction spectra for spherical silver clusters using Mie theory are shown in figure 2.11. For $\epsilon_{substrate} = 2.3$ the dielectric constant of BK7 glass was used and for the dielecric constant of the surrounding medium the value for vacuum $\epsilon_{medium} = 1$ was used. In the case of thiol capped clusters the dielectric constant of bulk thiophenol $\epsilon_{shell} = 2.5$ was used for the molecular shell. For the plasmon mode perpendicular to the surface shown in blue, three different situations should be considered, whereby the dielectric constant of the substrate and the dielectric constant of the surrounding contribute equally to the effective dielectric constant, respectively. In the first case the

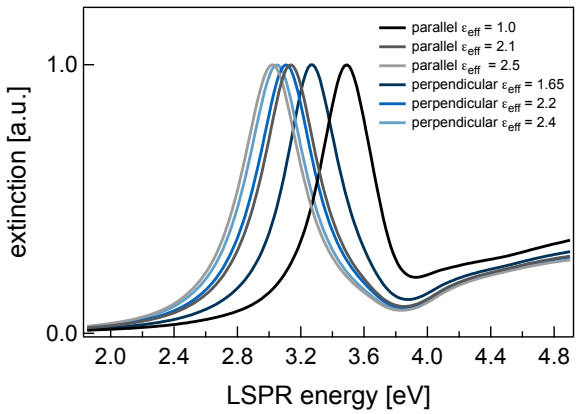

Figure 2.11.: Extinction spectra of supported silver nanoparticles for an excitation parallel and perpendicular to the surface, respectively. Different dielectric constants of the surrounding medium are considered, that represent the experimental situation within this work.

supported silver cluster is surrounded by vacuum, in the second case it is covered by a thick dielectric layer of thiophenol and in the third case it is covered by a dense packed monolayer of thiophenol so that the metal cluster still 'feels' the surrounding vacuum. In the latter case the ratio between the radius of the metal core and the radius of the complete core-shell particle is crucial for the effective dielectric constant [20]. A ratio of 0.55 was used, corresponding to the Wigner-Seitz radius of spherical Ag_{55} clusters and a shell thickness of 0.5 nm. Note that the extinction spectra of the core-shell particles, in figure 2.11 denoted with the corresponding effective dielectric constants $\epsilon_{eff} = 2.1$ and $\epsilon_{eff} = 2.2$ respictively, were calculated with an existing open source software [95]. The next situation that should be considered is the plasmon mode parallel to the surface. Again

the three borderline cases are highlighted, in which the particle is once surrounded by vacuum, once surrounded by a thick layer of thiophenol and once capped with a monolayer of thiophenol, still sensing the surrounding vacuum. Because the plasmon mode should be oriented strictly parallel to the surface, the influence of the substrate can be neglected [103]. These extinction spectra corresponding to the plasmon mode oriented parallel to the surface are shown in blue. As can be seen in figure 2.11, a system of supported silver clusters, covered with organic molecules exhibit several reasonable effective dielectric constants, which in turn are able to shift the LSPR over a wide range of the visible spectrum. Thereby plasmon modes oriented parallel and perpendicular to the surface has to be distinguished. For plasmon modes oriented parallel to the surface refractive index induced shifts of 0.5 eV are possible, whereas the LSPR located at 3.5 eV corresponds to a spherical silver cluster surrounded by vacuum and the LSPR located at approximately 3.0 eV corresponds to a spherical silver cluster surrounded by thiophenol. For plasmon modes oriented perpendicular to the surface refractive index induced shifts are less pronounced, because the adjacent dielectric substrate already increases the effective dielectric constant and shifts the LSPR towards lower energies. Again, the LSPR corresponding to a silver cluster surrounded by thiophenol is located at around 3.0 eV. This is due to the fact, that the refractive index of BK7 glass and thiophenol are similar, which cancels the unisotropy in terms of the effective dielectric constant of the surrounding. Besides the difference caused by unisotropy figure 2.11 illustrates, that for very small clusters with diameters around 1 nm, a dielectric shell with a thickness corresponding to a single monolayer

of molecules already alters the position of the LSPR appreciably.

2.3.2. Anisotropic Dielectric Environment

The symmetry of the surrounding of supported particles is broken due to the presence of the adjacent substrate and neighboring particles. The broken symmetry lifts the degeneracy of the dipole plasmon modes, even in the case of spherical particles, which alters the extinction spectrum in a way, that can not be explained with refractive index changes solely. First, considering interactions between neighboring particles, the optical properties of the ensemble are determined by the properties of the individual particles and the electrodynamic interactions between them [92, 136, 141, 168, 189]. The electrodynamic interaction is characterized by the coupling of near fields, which are caused by the light driven oscillation of electrons, on particles in close proximity. As shown in figure 2.12, the dipole-dipole interaction was found to be attractive for electromagnetic fields polarized parallel to the interparticle axis, which corresponds to a polarization parallel to the surface within the geometry of our experiment, and repulsive for electromagnetic fields polarized perpendicular to the interparticle axis, which corresponds to a polarization perpendicular to the surface within the geometry of our experiment. The attractive coupling causes a shift of the LSPR to lower energies and the repulsive coupling a shift to higher energies. The magnitude of the shifts depends on the strength of the interparticle coupling and therefore on the distance between the particles. An exponential like decay of the LSPR

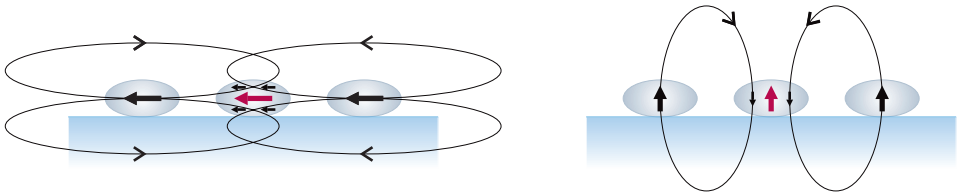

Figure 2.12.: Schematic illustration of interparticle coupling for an excitation parallel and perpendicular to the surface, respectively [133].

shift with interparticle distance was found, according to the decaying field intensity around the particles. Furthermore it was found, that the redshift of the LSPR caused by a parallel coupling is 2 times larger than the blueshift of the LSPR caused by a perpendicular coupling, and that the LSPR shift decay becomes negligible, if the gap between two particles exceeds 2.5 times the particle diameter. Note, that for a decreasing particle distance a transition from a coupled particle spectrum to a spectrum of an elongated particle, which is described in section 2.2, takes place [110, 168, 192]. For most of the spectra shown in this work, the coverage was kept well below 0.1 ML of clusters, which was found to be the threshold value for particle-particle interactions in the case of small silver clusters onto silica glass [77, 87]. However it should be noted, that in case of interparticle coupling the LSPR oriented parallel to the surface would be shifted to lower energies while the LSPR oriented perpendicular to the surface would be shifted to higher energies.

Apparently, the broken symmetry caused by the substrate surface is independent of the cluster coverage and has to be considered certainly. Even in the case of spherical particles the symmetry is broken and the elimination

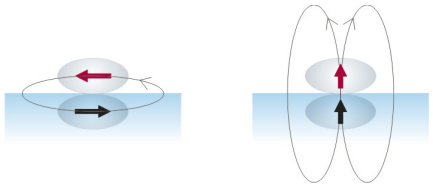

Figure 2.13.: Schematic illustration of the image charge of supported nanoparticles for an excitation parallel and perpendicular to the surface, respectively [133].

of the LSPR degeneracy results in a two-fold degenerated plasmon mode oriented parallel to the surface and one plasmon mode oriented perpendicular to the surface. The influence of a dielectric substrate onto these LSPR was considered for the first time within the dipolar approximation [209]. The polarization p on a metal particle under an external electromagnetic field was thought to create an image charge IC in the substrate, which in turn affects the LSPR of the metal particle. The polarization of the image charge p_{IC} is defined as

$$p_{IC} = \frac{\epsilon_{substrate} - 1}{\epsilon_{substrate} + 1} \cdot p \tag{2.26}$$

It increases the local field in the cluster as depicted in figure 2.13, shifting both plasmon modes to lower energies. As can be derived from equation 2.26 the influence of the the image charge in the substrate gets stronger with an increasing dielectric constant of the substrate material, which could be confirmed experimentally [85, 105]. In addition the effect of the image charge gets stronger with a decreasing distance between the center of the particle and the center of the image charge dipole. Therefore the redshift is more pronounced for smaller particle diameters and flat particles compared to spheres. However it has been shown, that the dipolar

approximation is not sufficient to describe the optical properties of supported particles. The substrate induced field causes an inhomogeneous electromagnetic field impinging the particle and higher order multipolar modes can be excited in addition to the dipolar mode, even for very small particles [16, 121, 123, 148, 159, 170, 173]. The main results of these studies on spherical and spheroidal particles above dielectric surfaces are two red-shifting dipolar plasmon modes in accordance to the image charge model and an additional quadrupolar plasmon mode at the high energy side of the extinction spectrum. It was found that the dipolar plasmon mode oriented perpendicular to the surface was shifted more to lower energies than the dipolar plasmon mode oriented parallel to the surface and that the energy of the quadrupolar plasmon mode is similar to the energy of the degenerated dipolar plasmon mode of the unsupported particle in free space. In the case of silver nanocubes onto dielectric surfaces actually blue shifted modes in comparison to the degenerated plasmon modes were observed [185, 213] and it could be shown, that the high energy mode corresponds to large electromagnetic fields away from the surface. This emphasizes the importance of the size, shape and substrate dependent electromagnetic field around metal nanoparticles on the position of the LSPR [69, 99, 165]. Regarding the optical properties of supported silver clusters highly interesting works have been carried out by Lazzari and coworkers based on the work of Bedeaux and Vlieger [15, 112, 114]. In a combined theoretical and practical study a blue shifted dipolar plasmon mode oriented perpendicular to the surface is reported for non interacting truncated silver spheres onto alumina. These results are discussed in detail further below. Similary, a blue shifted plasmon

mode oriented perpendicular to the surface is reported for non interacting truncated gallium spheres onto sapphire [4].

2.4. Chemical Interface Effects

Besides the optical properties of bare silver nanoparticles under UHV conditions, within this work the impact of organic molecules onto the optical properties of silver nanoparticles is investigated. Therefore, in this section several effects of the chemical surrounding, which influence the optical properties of silver nanoparticles are addressed.
In section 2.3 the surrounding of metal particles was treated as a non interacting matrix and only refractive index changes were considered, which is a simplification of real systems. It is known since long, that reactive matrices or adsorbates alter the extinction spectrum of small metal particles beyond the changed refractive index [19, 34, 90, 105]. A reason for the interactions are incompletely coordinated surface atoms, which can be the major part in very small particles with a high surface to volume ratio. Therefore chemical interface effects can alter the electronic structure and thus the optical properties of small metal particles dramatically. Here we will focus on the effect of adsorbates on the position and the width of the LSPR of small particles, which was first investigated systematically by Henglein, Mulvaney and Linnert [10, 81, 130, 150, 151, 188]. They obseved, that the reaction of metal particles in solution, especially silver particles, with different reagents like CN^-, SH^-, I^-, or metal ions cause a damping and a shift of the LSPR.

The shift of the LSPR can be attributed to a changed free electron density in the particles due to surface reactions, which can be understood from Drude theory. The dielectric function $\epsilon(\omega)$, and so the extinction spectrum of small metal particles depends, amongst others, on the density of free electrons n, which is a quantity in the expression of the plasma frequency ω_p

$$\omega_p = \sqrt{\frac{n \cdot e^2}{\epsilon_0 \cdot m_{eff}}} \tag{2.27}$$

where e is the elementary charge, ϵ_0 the dielectric constant of free space and m_{eff} the effective electron mass. In order to account for a variable density of free electrons in the particle, equations 2.12, 2.13 and 2.14 has to be modified. Assuming, that only the free electrons in the metal particle are effected by surface reactions, only the plasma frequency of the Drude part in equation 2.12 is modified

$$\epsilon\left(\omega, r\right) = \epsilon_{bulk}\left(\omega\right) + \frac{\omega_p^2}{\omega^2 + i\omega\gamma_{bulk}} - \frac{\omega_D^2}{\omega^2 + i\omega\gamma\left(r\right)} \tag{2.28}$$

with ω_D as the variable Drude-type plasma frequency. The real and imaginary part of the dielectric function are now given as

$$\epsilon_1\left(\omega, r\right) = \epsilon_{1,bulk}\left(\omega\right) + \frac{\omega_p^2}{\omega^2 + \gamma_{bulk}^2} - \frac{\omega_D^2}{\omega^2 + \gamma^2\left(r\right)} \tag{2.29}$$

$$\epsilon_2\left(\omega, r\right) = \epsilon_{2,bulk}\left(\omega\right) + \frac{\omega_D^2\gamma\left(r\right)}{\omega\left[\omega^2 + \gamma^2\left(r\right)\right]} - \frac{\omega_p^2\gamma_{bulk}}{\omega\left[\omega^2 + \gamma_{bulk}^2\right]} \tag{2.30}$$

In figure 2.14 the LSPR energy of silver particles surrounded by vacuum for different free electron densities is shown. The unchanged free electron density of silver $n = 5.8564 * 10^{28} m^{-3}$ [35] is used as reference and denoted

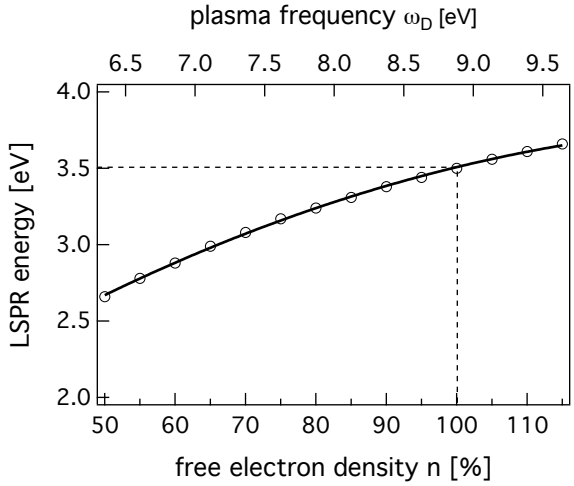

Figure 2.14.: Influence of the free electron density n on the position of the Localized Surface Plasmon Resonance of silver nanoparticles. The free electron density of bulk silver is denoted with 100%

by 100%. The corresponding plasma frequencies ω_D were calculated using equation 2.27 and are included in the top axis of the graph. The LSPR energy was calculated by feeding equations 2.29 and 2.30 into the classical Mie formula. Note, that the bulk plasma frequency corresponding to the unchanged free electron density results in a LSPR energy of 3.5 eVV, which was calculated in section 2 using bulk constants. A decreasing free electron density results in a shift of the plasmon resonance to lower energies, whereas an increased free electron density causes a LSPR shift to higher energies. This dependency of the LSPR energy was observed in experiments, where metal particles were charged electrochemically [33, 152, 160, 161, 200]. It was shown, that a negative charging of metal particles, which increases the free electron density, causes a blueshift of the plasmon resonance. Therefore

it can be concluded, that the presence of electron donors and acceptors shifts the LSPR to higher and lower energies, respectively. Noble metal particles are often synthesized with a capping layer of ligands, that prevent agglomeration, whereas amines and thiols are outstanding in the case of silver and gold nanoparticles [68]. Both, ligands binding with an amine and ligands binding with a thiol lower the free electron density inside the metal particle by locating charge in the bond to metal atoms, which results in a redshift of the LSPR resonance [14, 57, 81, 150, 156, 174, 203, 215]. The influence of thiols compared to amines was found to be more pronounced due to the strong, covalent interaction between thiols and silver or gold. The reduction of electron density and thus the redshift of the LSPR depend on the number of ligand molecules and the size of the particles. In size dependent studies a growing influence of the ligand layer on the extinction spectrum with a decreasing particle size was found. It has been shown that a layer of electron withdrawing ligands can compensate the size dependent blueshift discussed in section 2.1 and even reverse this trend into a redshift for particles smaller than approximately 10 nm in diameter [35, 164, 171, 190, 203]. It was possible to explain this behavior by replacing the macroscopic dielectric function, that represents a homogeneous density of free conduction band electrons across the whole particle diameter, by a dielectric constant accounting for the local environment. The metal core is described with the bulk dielectric function, whereas the 'skin' of the particle is described with a dielectric function, accounting for a reduced electron density. In the case of thiol ligands a reduction of the free electron density in the outermost particle layer by approximately 45% was determined.

Considering very small metal cluster with a high surface to volume ratio [6], an appreciable reduction of the overall free electron density can be expected, which would result in a significant redshift of the LSPR, according to figure 2.14.

As described in section 2.1, surface scattering leads to additional damping and thus broadening of the LSPR of small metal particles. Hence it is quite intuitive, that the chemical surrounding influences the width of the LSPR, which is commonly referred to as chemical interface damping [80, 86, 105, 120]. A matrix, or adsorbates around a small metal particle induce additional electronic states at the surface and the excited electrons of the plasmon oscillation may tunnel into and out of this surface states. During their residence time coherence is lost, thus chemical interface damping provides an extra decay channel for the LSPR. The extra damping is summarized in the phenomenological damping parameter A, which was introduced in equation 2.11. The damping parameter A varies between 0 and 1 and depends on the strength of the interaction between the surface and the matrix. In the case of silver particles surrounded by vacuum, A was found to be 0.25. If the particles are supported onto a substrate or surrounded by a matrix, the value of A increases, whereas different empirically determined values between 0.6 and 1 are reported [12, 86]. For small thiol capped noble metal particles the width of the LSPR could be described successfully with a value of $A = 1$ [59, 164], which illustrates that capping free particles with ligands is accompanied by a reasonable broadening of the LSPR.

[6] For example, an icosahedral cluster consisting of 55 atoms exhibits a surface to volume ratio of approximately 76%

3. Experimental

3.1. Setup and Sample Preparation

In order to investigate the size dependent optical properties of supported metal clusters and in order to determine the impact of organic ligands on the optical properties certain requirements to the experimental setup do exist, that are explained within this chapter. A detailed description may be found elsewhere [77, 96, 195]. To avoid contaminations of the cluster sample with adsorbates, the experiments were done under UHV conditions. A sketch of the differentially pumped UHV setup is shown in figure 3.1. The main parts of the setup are the cluster source to produce metal clusters (depicted in red), an ion optic to guide and mass select the produced size distribution of metal clusters (depicted in blue) and a laser and detection unit to measure prepared samples (depicted in green). The cluster source is a high frequency laser evaporation source similar to that described by Heiz et. al. [79]. The second harmonic of a pulsed Nd:YAG laser (Innolas Spitlight DPSS, 532 nm, 100 Hz, 70 $^{mJ}/_{pulse}$) is focussed onto a rotating metal target in order to ablate

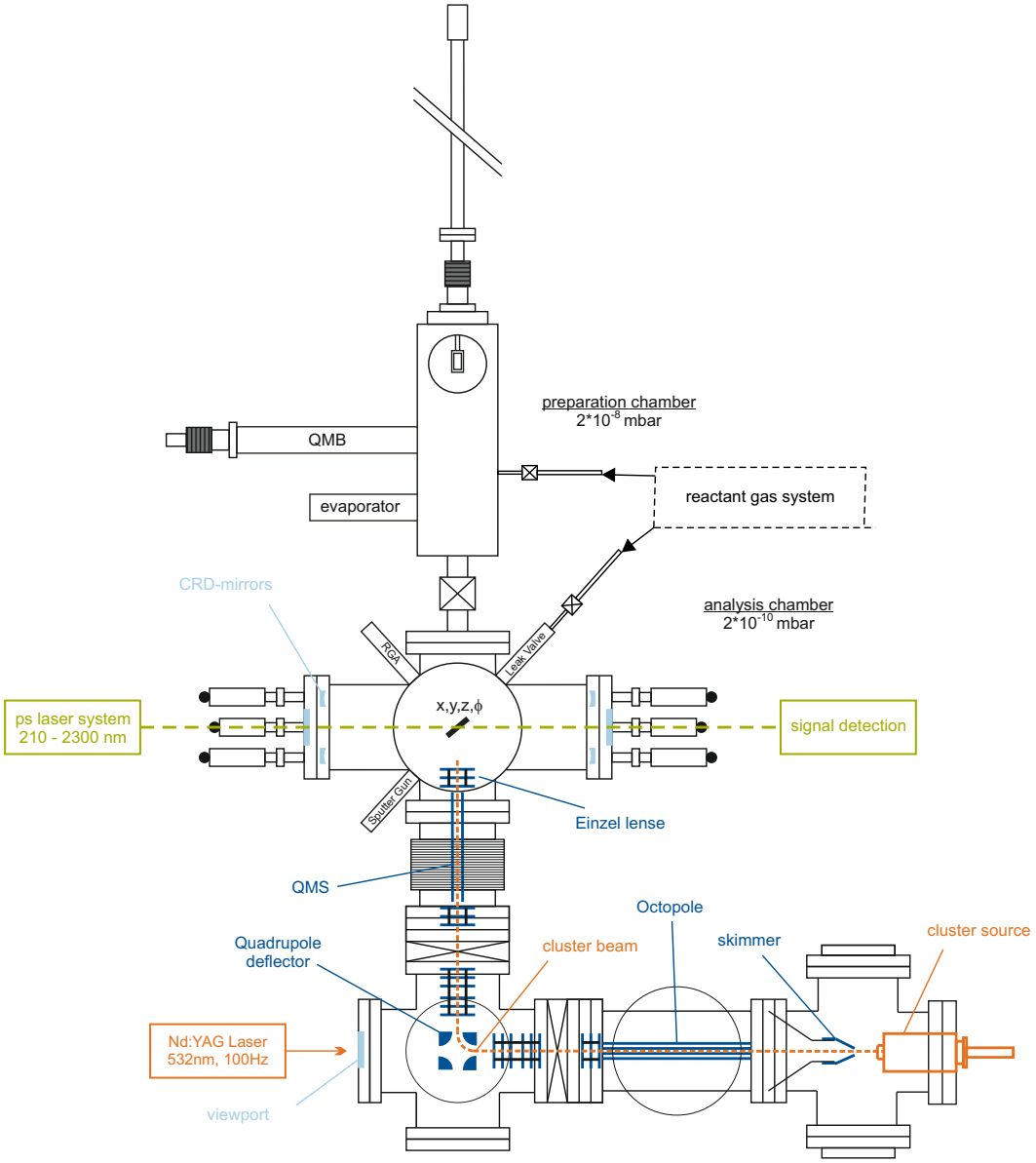

Figure 3.1.: Scheme of the experimental setup. The main parts are the cluster source to produce metal clusters (orange), an ion optic to guide and mass select the produced size distribution of metal clusters (blue) and a laser and detection unit to measure prepared samples (green) [133].

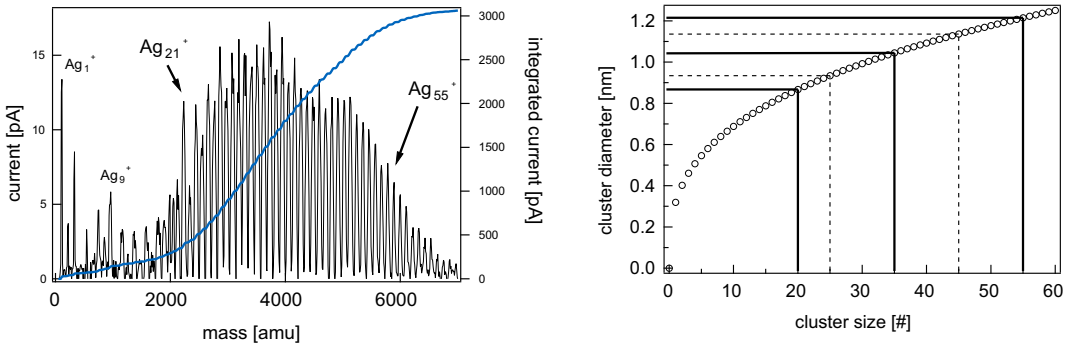

Figure 3.2.: Size distribution of positively charged silver clusters produced by the cluster source. On the right hand side the correlation between the cluster size and the diameter is shown for spherical clusters, based on the bulk density of silver atoms.

material. The produced metal vapor is cooled by collisions with *He* buffer gas (*He* 6.0, Air Liquide), which is dosed with a piezo valve. The piezo valve in turn is triggered by the evaporation laser, so that the metal vapor is expanded into an appropriate helium atmosphere. The formed mixture of neutral, positively and negatively charged clusters of different sizes is expanded into vacuum. The positively charged metal clusters are guided to a quadrupole mass filter (Extrel 5500 QMS, transmission 16000 amu.) with the help of an octopole and several stacks of Einzel lenses. A quadrupole deflector is used to to separate the charged clusters from the neutrals, which could not be mass separated by the QMS. A typical size distribution of positively charged silver clusters arriving at the QMS is shown on the left hand side of figure 3.2. The high abundance of some sizes can be explained with an increased stability due to a complete filling of electronic shells [45]. For example, Ag_9^+ and Ag_{21}^+ posses an exceptionally high abundance due

to the complete closure of the $1p$ and $2s$ shell, respectively[1]. Furthermore an even-odd fine-structure due to Jahn-Teller distortion can be observed. The overall integrated cluster current and the relative weight of individual sizes can be influenced by the pressure conditions inside the cluster source and the settings of the ion optics. On the right hand side of figure 3.2 the diameter of silver clusters is depicted against the cluster size. Assuming spherical clusters, the diameter D can be calculated as follows

$$D = 2a_0 r_s N^{1/3} \tag{3.1}$$

where $a_0 = 0.0529\,\text{nm}$ is the Bohr radius, $r_s = 3.02$ is the atomic Wigner Seitz radius and N is the number of atoms in the particle. It should be noted, that the Wigner Seitz radius is based on bulk properties and that the as-calculated diameters for small clusters are only an approximation. As marked with solid lines, Ag_{20} and Ag_{55}, two cluster sizes investigated in more detail within this work, have got diameters of approximately 0.9 nm and 1.2 nm respectively. Taking the size distribution shown on the left hand side as a basis, the mean size of unselected clusters, denoted as Ag_x within the framework of this work, is Ag_{35}[2]. Therefore silver clusters of unselected samples have got a mean diameter of approximately 1.0 nm. Because the size distribution does change slightly from measurement to measurement an error of the mean size of ± 10 atoms per cluster is assumed for unselected

[1]Note, that silver with an electron configuration of $[Kr]4d^{10}5s^1$ can be treated approximately as a simple $1s$ metal and that Ag_9^+ and Ag_{21}^+ therfore posses 8 and 20 free electrons respectively.

[2]For the unselected cluster samples Ag_x the QMS was operated in the RF-only mode and masses above 2200 amu were deposited.

samples, indicated with dashed lines on the right hand side of figure 3.2. Samples of supported silver clusters are prepared by deposition of positively charged silver clusters onto BK7 glass substrates (VWR International, borosilicate glass slabs, 0.15 mm thickness), which are sputtered before deposition (10 minutes, 1.5 keV, 1.5 mm spot size). BK7 glass slabs are used as substrates because they fulfill the requirements for the used spectroscopic techniques. Firstly they are highly transparent over the complete used wavelength range, which is a fundamental requirement, because all measurements are done in transmission mode. Furthermore the two surfaces of the glass slabs are plane parallel, which is important especially in the case of surface cavity ring-down spectroscopy (s-CRD), as described in section 3.2.1. A detailed characterization of the substrate material can be found elsewhere [193]. Due to the fact, that BK7 is an insulator, the positively charged clusters have to be neutralized during deposition. Neutralization is realized with the help of a low energy electron source, which is described in detail elsewhere [96, 193]. The deposition time has to be adapted to the cluster current, in order to prepare samples of size selected clusters with a sufficiently high coverage. However, for the preparation of size selected samples the coverage must not exceed $1 \cdot 10^{13} \mathrm{cm}^{-2}$, in order to avoid agglomeration [77]. Because only the total amount of deposited clusters can be calculated from the cluster current and the deposition time, the spatial distribution of the clusters onto the substrate has to be known, in order to determine the coverage. As can be seen from figure 3.3 a circular cluster spot with a diameter of approximately 10 mm and a gaussian distribution of clusters is produced onto the substrate with the used experimental setup. Therefore

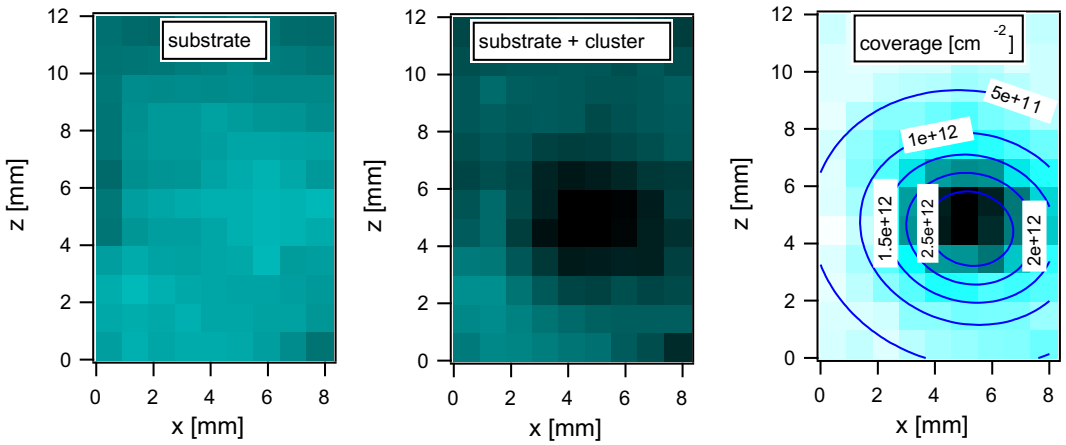

Figure 3.3.: Visualization of the cluster spot by means of CRD spectroscopy. A mapping of the optical losses measured at 450 nm is depicted for the clean BK7 substrate and the substrate decorated with unselected silver clusters. On the right hand side the difference between the decorated and the bare substrate is shown. This figure is taken from [133]

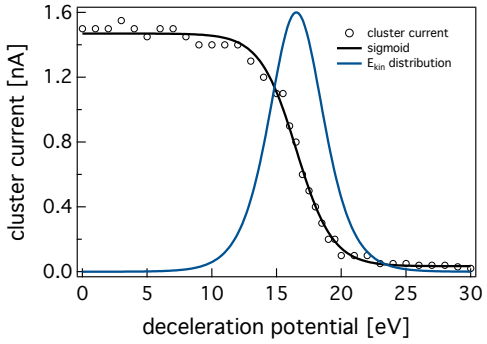

Figure 3.4.: Energy distribution of unselected silver clusters measured with a retarding field.

the coverage of the samples, that are measured at the center of the cluster spot, can be calculated from the cluster current and the deposition time. For the preparation of size selected samples it has to be ensured, that the clusters are not destroyed, when they impinge onto the surface. It has been shown that metal clusters with an energy of around 1 $^{eV}/_{atom}$ can be landed onto a substrate nondestructively [24, 202]. The energy distribution of unselected silver clusters Ag_x was measured by retarding field analysis and is shown in figure 3.4 The mean energy is around 16.5 eV with an energy distribution of approximately 3 eV. Because in this work unselected clusters have got a size above 20 $^{atoms}/_{cluster}$, it can be expected that the clusters are deposited under soft landing conditions. The as prepared samples can be measured inside the analysis chamber with a base pressure of $2 \cdot 10^{-10}$ mbar. To this end a picosecond laser system (EKSPLA, PG 401/SH) is available. It covers the wavelength range between 210 nm and 2300 nm, the pulse length is 33 ps and the pulse energy is around 1 $^{mJ}/_{pulse}$. For the signal detection the exper-

iment is equipped with a four channel oscilloscope (LeCroy, Waverunner 6051), a monochromator (MC, LOT-Oriel, Omni-λ300), two photomultipliers (PMT, Hamamatsu, H9305-03), a photodiode (Thorlabs, 201/579-7227) and two Pellin-Brocca prisms. As can be seen in figure 3.5, the detection unit is prepared for both used spectroscopic techniques and it is possible to switch between s-CRD and s-SHG spectroscopy by means of a folding mirror. In the case of s-CRD spectroscopy, the light leaking out of the optical cavity[3] is detected with a photomultiplier tube. In the case of s-SHG spectroscopy, the second harmonic light, which is the measured quantity in s-SHG experiments[4], is separated from the fundamental light by means of two prisms and a monochromator, before it is detected with another photomultiplier tube, too. A photodiode is used in order to detect the intensity of the laser, so that pulse to pulse fluctuations of the laser intensity can be taken into account [97].

To expose samples of supported silver clusters to organic molecules, a preparation chamber with a base pressure of $2 \cdot 10^{-8}$ mbar is connected to the analysis chamber. In order to evaporate organic molecules, the preparation chamber is equipped with a in-house design evaporator. The coverage can be monitored with the help of a quartz microbalance (INFICON, SL-A1E40). In order to dose molecules, that are gaseous or liquid under normal conditions, the preparation chamber is equipped furthermore with a gas dosing unit [77].

One part of the experimental setup that has changed during this thesis is the

[3] See section 3.2.1.

[4] See section 3.2.2.

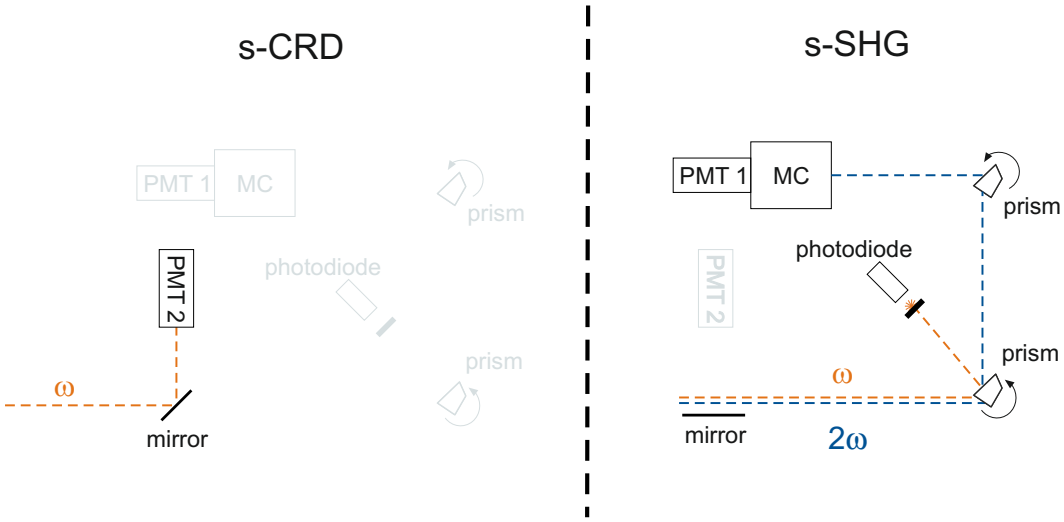

Figure 3.5.: Scheme of the detection unit.

sample holder, that is shown in figure 3.6[5]. The sample holder is designed in order to deposit metal clusters onto insulating substrates and in order to measure cluster samples with optical spectroscopy in transmission at variable temperatures. It is made of oxygen free copper and can be flange mounted directly to the LN_2 cryostat manipulator (1). It has got a quadratic base of approximately 60 mm and a hight of approximately 120 mm. The weight of the sample holder is approximately 800 g. The samples, which are mounted onto a stainless steel sample holder (4), can be inserted into the sample holder with the help of a manipulator. Underneath the sample an electron source (3) is attached, which enables the deposition of positively charged metal clusters onto insulating substrates [96]. Because the depo-

[5]The sample holder was designed and manufactured in collaboration with Kurt Ansperger: Konstruktion, Entwicklung und Bau von Prototypen.

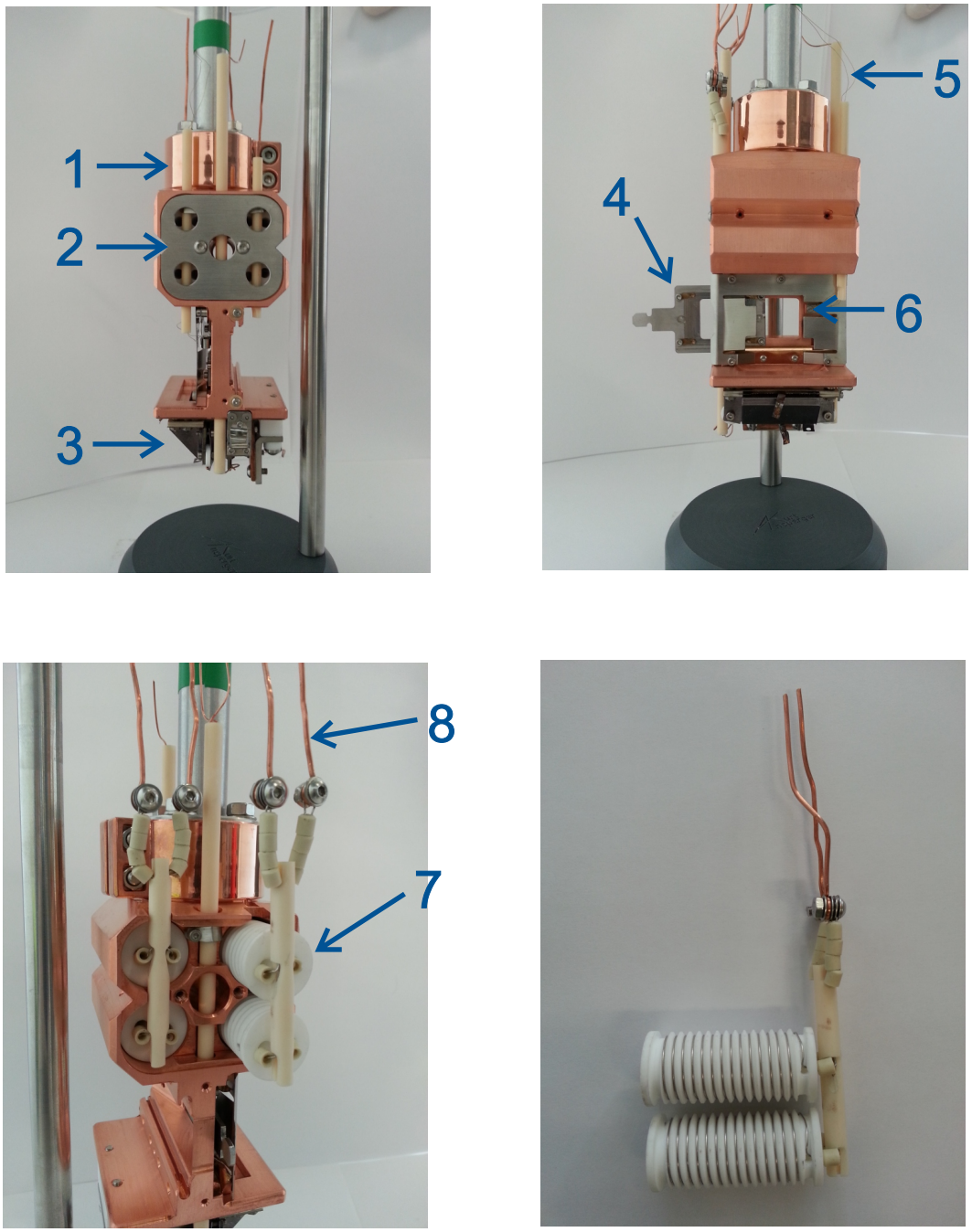

Figure 3.6.: Picture of the sample holder. 1) Flange connection to cryostat manipulator. 2) Holder for heating elements. 3) Electron source. 4) Substrate holder. 5)feedthrough for connection to electron source. 6) Position of thermocouple. 7)Heating element. 8) Connection for heating element.

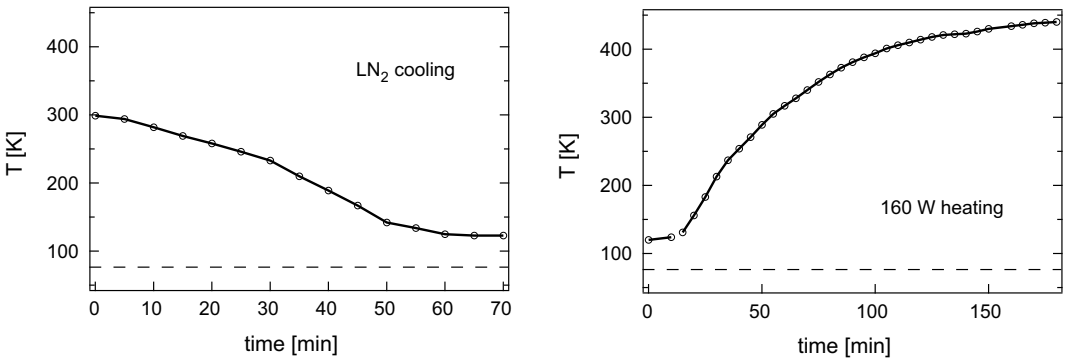

Figure 3.7.: Temperature behavior of sample holder. The temperature of LN_2 is marked with dashed lines.

sition of size selected clusters can take up to several hours it is important that the electron source is thermally isolated from the substrate. Otherwise the running electron source would heat the sample during deposition of metal clusters. Therefore the base of the sample holder (3), that is in thermal contact to the cryostat, shields the electron source and the electrons for neutralization are guided through a narrow slit to the sample surface. In order to heat the sample holder, it is equipped with four heating elements (6) that are placed above the substrate. The main body of each heating element is made of glass ceramic[6] and it is wrapped by a resistance wire[7]. Two heating elements each are connected in series and have an maximum output power of approximately 185 watts. The overall output power is therefore approximately 370 watts. In figure 3.7 the cooling and heating characteristic of the sample holder is shown exemplariliy. The temperature was measured

[6]Macor®
[7]NiCr $^{80}/_{20}$

at the edge of the substrate (position 6 in figure 3.6). The temperature of the sample holder falls from 300 K to 125 K within one our, when the cryostat is cooled with liquid nitrogen, as can be seen on the left hand side of figure 3.7. The graph on the right hand side of figure 3.7 illustrates, that the heating element is sufficiently dimensioned in order to heat the sample holder against the ongoing cooling above room temperature. For example, if the heating elements are driven with an output power of 160 W, which is less than half the maximum output power, the sample holder heats up to approximately 450 K within three hours. However the heat transfer from the sample holder to the center of the insulating glass substrate is very poor [96] and the determination of the exact sample temperature at the position of the cluster spot is difficult.

3.2. Spectroscopy

The small extinction cross section of silver nano clusters in combination with small surface coverages needed to avoid agglomeration require highly sensitive techniques for investigation. Therefore the used setup is equipped with two highly sensitive optical spectroscopic techniques. Firstly, linear Surface Cavity Ring-Down spectroscopy (s-CRD) and secondly nonlinear Surface Second-Harmonic-Generation spectroscopy (s-SHG) are available. The prefix 's' is used in order to distinguish from bulk measurements. Based on the s-SHG setup it is also possible to apply s-SHG Optical Rotatory Dispersion (s-SHG-ORD) in order to investigate chiral surface structures.

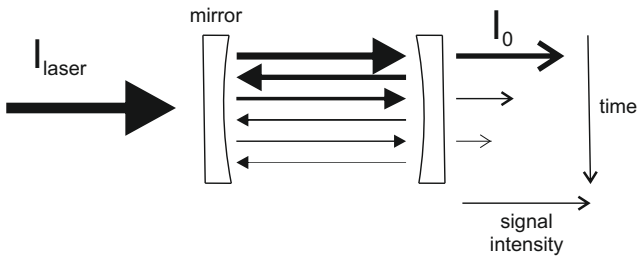

Figure 3.8.: Scheme of the Cavity Ring-Down principle.

Because no s-SHG-ORD spectra are presented in this work, this technique is not explained and the reader is referred to literature [77, 186, 196]. The description of s-CRD spectroscopy and s-SHG spectroscopy given in this chapter follows mainly the description that can be found in many reviews and textbooks [17, 23, 196, 205, 212].

3.2.1. Surface Cavity Ring-Down Spectroscopy

CRD is a spectroscopic technique in which the rate of absorption of a light pulse confined in an optical cavity is measured. The method can be traced back to measurements in order to determine the reflectivity of mirrors [8, 82] but was used quickly for absorption measurements [163]. The basic principle is illustrated in figure 3.8. The fraction of light that is coupled into an optical cavity bounces back and forth between the two mirrors. The intensity of the light inside the cavity decays due to imperfect reflectivity of the mirrors and the time dependence of the decay can be determined by measuring the portion of light leaking out of the cavity. Because of simplicity reasons in

the following description it is assumed that the light pulse coupled into the cavity is shorter than the cavity length L. The roundtrip time t_r of the pulse inside the cavity is given by

$$t_r = \frac{2L}{c} \tag{3.2}$$

where c is the speed of light. The intensity of light leaking out of the cavity depends on the reflectivity R of the mirrors

$$I_0 = I_{laser}(1 - R)^2 \tag{3.3}$$

where I_{laser} is the initial intensity of the laser. Under the assumption that both mirrors have got the same reflectivity, each roundtrip n reduces the intensity by the factor R^2 and therefore

$$I_n = I_0 R^{2n} = I_0 \cdot \mathrm{e}^{\ln R \cdot 2n} \tag{3.4}$$

Equation 3.4 can be expressed as a function of time t instead of a function of the number of roundtrips n.

$$I(t) = I_0 \cdot \mathrm{e}^{\frac{c \ln R \cdot t}{L}} \tag{3.5}$$

By replacing $\ln R$ by $(1 - R)$, which is a valid approximation for a high reflectivity, the exponential character of the decay is apparent

$$I(t) = I_0 \cdot \mathrm{e}^{\frac{c(1-R)t}{L}} \tag{3.6}$$

The time constant of the exponential decay is called ring-down time τ

$$\tau = \frac{L}{c(1 - R)} \tag{3.7}$$

which depends in the case of an empty cavity only on the length L of the cavity and the reflectivity R of the mirrors. In combination with equation 3.2 the loss of photons for a single pass Λ (loss per pass) can be calculated as

$$\Lambda = 1 - R \tag{3.8}$$

If an analyte is introduced into the cavity, scattering losses Λ_S and absorption losses Λ_A increase the loss per pass in addition to the imperfect reflectivity of the mirrors and therefore decrease the ring-down time τ. In that case the ring-down time and the loss per pass are given as

$$\tau = \frac{L}{c\left[(1-R) + \Lambda_S + \Lambda_A\right]} \tag{3.9}$$

and

$$\Lambda = (1-R) + \Lambda_S + \Lambda_A \tag{3.10}$$

Usually CRD is used as a gas phase technique. In order to measure supported metal clusters by means of s-CRD spectroscopy, the optical losses caused by the used substrate, that is introduced into the cavity, has to be kept as low as possible. In order to minimize the absorption losses it has to be highly transparent in the investigated wavelength range. In order to minimize the scattering losses the substrate has to be introduced to the cavity into Brewster's angle and the two surfaces of the substrate have to be perfectly plane parallel. Furthermore the substrate has to be thin in order to keep the displacement of the laser beam small. Glass slabs made for microscopy (Marienfeld) were found to satisfy all off these requirements

Table 3.1.: Reflectivity of CRD mirrors.

mirror pair [#]	range [nm]	reflectivity [%]
1	420-505	99.98
2	460-550	99.96
3	510-590	99.94
4	570-680	99.95
5	640-770	99.98

[193]. The high reflectivity of the mirrors required to obtain sufficient ring-down times restrict the choice to dielectric mirrors, which could exhibit a reflectivity of up to 99.99 % and more. However this mirrors have only a narrow range of high reflectivity and thus several different mirrors are needed in order to cover a wide wavelength range. A detailed description of the mechanism that is used in order to change and align mirror pairs under UHV conditions can be found elsewhere [96]. Table 3.1 summarizes the range and the experimentally determined reflectivity of the mirror pairs used within the framework of this thesis. In figure 3.9 a s-CRD spectrum of the used glass substrate is shown. The five mirror pairs cover the range between 420 nm and 770 nm, whereas neighboring mirror pairs exhibit an overlapping region. Note that the gap between 680 nm and 740 nm is due to the lack of laser light produced by the used laser system. The shown spectrum includes both, the losses caused by the substrate and the losses due to an imperfect reflectivity of the mirrors. Therefore the losses strongly increases at the optical edges of the individual mirror pairs due to a reduced

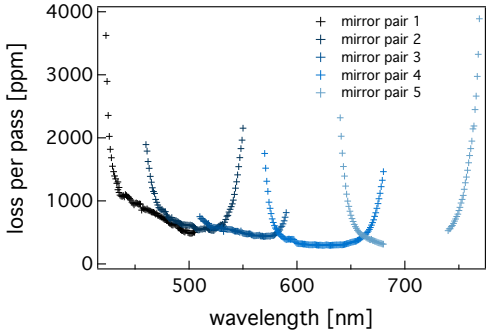

Figure 3.9.: s-CRD spectrum of the used BK7 glass substrates.

reflectivity. The growing loss at smaller wavelength λ is due to an increased scattering of light at the substrate surfaces following the wavelength dependent Rayleigh law. Because the scattering cross section is proportional to λ^{-4}, s-CRD measurements are restricted to the visible and near infrared wavelength range. It has been shown that s-CRD spectroscopy is suitable, in order to measure the extinction of small supported metal clusters [58, 98].

3.2.2. Surface Second Harmonic Generation Spectroscopy

Light can be described by a time and space varying electromagnetic field. The time dependent electric field component can be written as

$$E(t) = E_0 \cos(\omega t) \tag{3.11}$$

E_0 is a constant amplitude and ω is the angular frequency, given by $\omega = 2\pi c/\lambda$, with the wavelength λ and the speed of light in vacuum c. The interaction of the electric field with dielectric media causes induced dipole

moments inside the dielectric that oscillate with the same frequency as the applied field. As long as the intensity of the applied field is low, the polarization $P(t)$ of the medium, arising from the sum of the induced dipole moments, depends linearly on the electric field

$$P(t) = \epsilon_0 \chi E(t) \tag{3.12}$$

where ϵ_0 is the electric permittivity of vacuum and χ is the electric susceptibility. For very intense light, for example pulsed laser light, the relation between polarization and electric field is non linear[8] and the polarization is expanded in a Taylor series in terms of the total applied electric field

$$P(t) = \epsilon_0 \left(\chi^{(1)} E(t) + \chi^{(2)} E^2(t) + \chi^{(3)} E^3(t) + ... \right) \tag{3.13}$$

$\chi^{(2)}$ and $\chi^{(3)}$ are the second- and third-order susceptibilities, that characterize the nonlinear optical properties of the medium. Because the second-order susceptibility is responsible for SHG, higher order terms are not considered within this work. The second-order polarizability $P^{(2)}(t)$ is than given by

$$P^{(2)}(t) = \epsilon_0 \chi^{(2)} E^2(t) \tag{3.14}$$

If equation 3.11 is inserted into 3.14 it becomes clear that due to the nonlinear interaction an additional frequency independent term (optical rctification) and a term at the double frequency, which is responsible for the generation of the second harmonic, arise.

$$P^{(2)}(t) = \epsilon_0 \left(\frac{1}{2} \chi^{(2)} E_0^2 + \frac{1}{2} \chi^{(2)} E_0^2 \cos(2\omega t) \right) \tag{3.15}$$

[8] Compare figure 3.11.

The nonlinear optical response to an applied electric field in dielectric media can be described using an anharmonic potential as an approximation for the motion of bound electrons. The motion of electrons $x(t)$ can be described with

$$\frac{d^2x(t)}{dx^2} + 2\gamma\frac{dx(t)}{dx} + \omega_0^2 x + ax^2(t) = -\frac{e}{m}E(t) \tag{3.16}$$

where ω_0 and γ are the resonance frequency and damping constant of the anharmonic oscillator, and e and m are the charge and the mass of an electron. a is a parameter characterizing the strength of the nonlinearity. Although no general solution is known for equation 3.16 it can be solved for sufficiently weak applying fields by use of perturbation theory [22]. Then the nonlinear susceptibility in the case for second harmonic generation can be written as

$$\chi^{(2)} = \frac{Ne^3a}{\epsilon_0 m^2}\frac{1}{\left(\omega_0^2 - 4\omega^2 - 4i\omega\gamma\right)}\frac{1}{\left(\omega_0^2 - \omega^2 - 2i\omega\gamma\right)^2} \tag{3.17}$$

The signal intensity of the generated second harmonic light is proportional to the square of the second-order susceptibility and therefore

$$\left|\chi^{(2)}\right|^2 = \left(\frac{Ne^3a}{\epsilon_0 m^2}\right)^2 \frac{1}{\left(\left(\omega_0^2 - 4\omega^2\right)^2 + \left(4\omega\gamma\right)^2\right)}\frac{1}{\left(\left(\omega_0^2 - \omega^2\right)^2 + \left(2\omega\gamma\right)^2\right)^2} \tag{3.18}$$

$\left|\chi^{(2)}\right|^2$ possesses a maximum, whenever the denominator of equation 3.18 is minimum. As can be taken from the left hand side of figure 3.10 this is the case for $\omega = \omega_0$ and $\omega = \omega_0/2$. As a consequence a SHG spectrum of a system with a single resonance frequency exhibits two peaks. The first peak is observed, when the fundamental of the exciting light is in resonance with

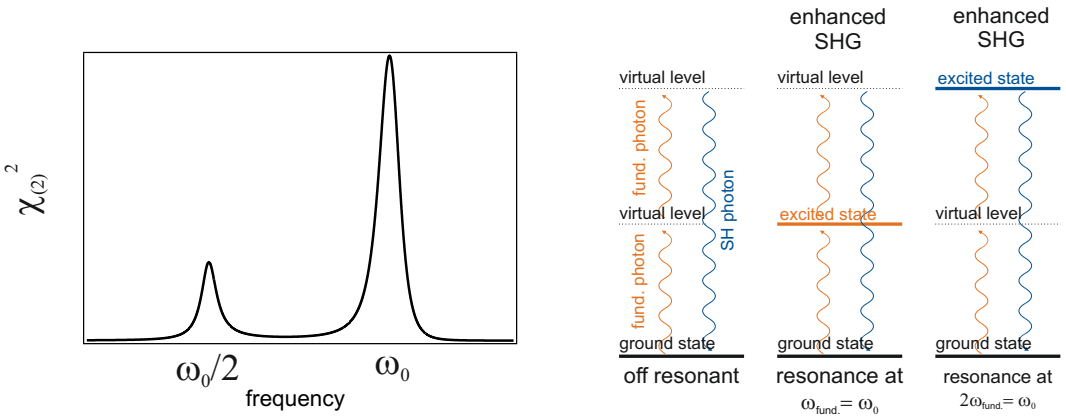

Figure 3.10.: Resonance enhanced second harmonic generation. The nonlinear susceptibility exhibits two maxima, which is visualized with a photonic picture.

the investigated system and the second peak is observed, when the second harmonic is in resonance with the system, as sketched within a photonic picture on the right hand side of figure 3.10. Because the generation of second harmonic light is enhanced when the transition energy is matched, SHG spectra are closely connected to extinction spectra. All s-SHG spectra shown in this work are measured with the second harmonic in resonance[9], because it has been shown that in order to measure samples of supported silver clusters non destructive, the energy input is too high, if the fundamental of the pulsed laser system is in resonance with transitions of silver clusters [195]. As mentioned above, s-SHG spectroscopy is a surface sensitive technique. The surface sensitivity can be attributed to distinct symmetry properties of the nonlinear susceptibility $\chi^{(2)}$. In centrosymmetric materials the nonlinear susceptibility is zero and thus no second harmonic light is

[9]With the exception of the spectrum shown in figure 4.10

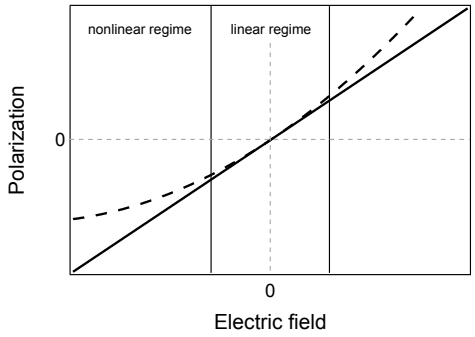

Figure 3.11.: Linear and nonlinear response the electric polarization with the strength of the applied electric field for a symmetric (dashed line) and a asymmetric (solid line) potential.

generated by centrosymmetric systems. This can be shown by Neumann's principle, which states that the sign and the magnitude of a physical property remain unchanged under symmetry operations. As can be taken from figure 3.11 the electric field and the polarization transform under inversion as $E \rightarrow -E$ and $P \rightarrow -P$, if a centrosymmetric potential is considered. Therefore, according to equation 3.14

$$-P^{(2)}(t) = \chi^{(2)}\left(-E(t)\right)\left(-E(t)\right) \tag{3.19}$$

$$= \chi^{(2)} E^2(t) \tag{3.20}$$

$$\Longleftrightarrow \; P^{(2)}(t) = -\chi^{(2)} E^2(t) \tag{3.21}$$

Because $\chi^{(2)} = -\chi^{(2)}$ is defined only for $\chi^{(2)} = 0$, no second harmonic light is generated in centrosymmetric systems. However, at the interface between two centrosymmetric media the centrosymmetry is broken and thus the generation of second harmonic light is allowed. S-SHG spectroscopy is a

widely used optical method in order to probe the surface chemistry of different interfaces [40, 181] and has been used in several studies, in order to probe the extinction of supported metal nanoparticles [9, 28, 89].

4. Results and Discussion

In this chapter the experimental outcomes of this work are presented and an interpretation as well as a classification regarding the existing literature is given. Because within the framework of this work two different spectroscopic techniques were used in order to investigate the optical properties of supported silver clusters in a first step Surface Second Harmonic Generation Spectroscopy (s-SHG) and Surface Cavity RingDown Spectroscopy (s-CRD) are compared and the differences in the extinction spectra are discussed. Then the optical properties of size selected supported silver clusters under UHV conditions using s-SHG spectroscopy are described. The investigated size range between Ag_{55} and Ag_9 link the range of bigger particles that can be described with bulk optical properties and the range of molecular like structures containing only a few atoms per cluster. The experimental results are discussed in an increasing order of complexity, based on the theoretical models described in chapter 2. In the next section cluster molecule interactions are presented with regards to the changed optical properties of silver clusters. Molecules with different types of functional groups are investigated using s-SHG and s-CRD spectroscopy. The last section describes the optical

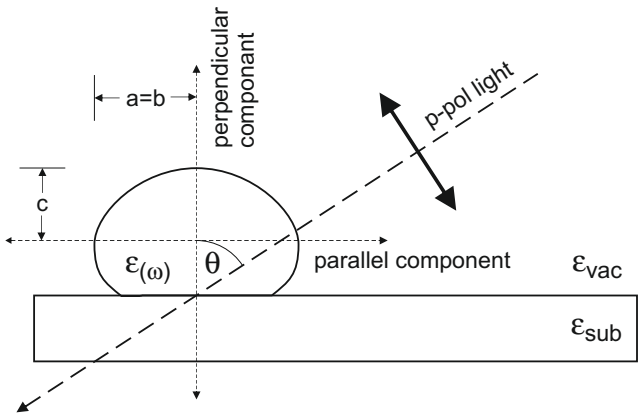

Figure 4.1.: Geomerty of optical extinction experiments.

properties of molecular structures of two different types of molecules with sub monolayer coverages using s-CRD spectroscopy.

4.1. Comparison between s-SHG and s-CRD Spectroscopy

The fundamental difference between s-SHG and s-CRD spectroscopy is the fact, that s-CRD is a linear and s-SHG a nonlinear optical technique, which has got far-reaching consequences for the data acquisition and interpretation. Figure 4.1 shows the geometry of optical extinction spectra used for all experiments within this work. The parallel polarized (p-polarized) incident laser beam impinges the substrate in Brewster angle $\theta = 57$ for the transition from vacuum to BK7 glass. Using this configuration, reflection

losses are minimized, which is a requirement for s-CRD spectroscopy, as discussed in chapter 3.2.1. Thus the incident light has got components polarized parallel and perpendicular to the surface of the substrate. It should be noted that p-polarized light is oriented parallel to the plane of incidence, not to be confused with parallel to the surface of the substrate. On the other hand s-polarization defines a plane of polarization perpendicular to the plane of incidence which is parallel to the substrate surface, respectively. As discussed in chapter 3.2.2 the generation of second harmonic light necessarily requires a non centrosymmetric electric environment. An electron oscillation driven by s-polarized light is oriented parallel to the substrate surface and takes place in a symmetric environment. Thus, this oscillation does not contribute to the generation of second harmonic light. On the other hand, an electron oscillation driven by p-polarized light has got a component perpendicular to the surface and takes place in an asymmetric environment. This electron oscillation does contribute to the generation of second harmonic light. Therefore in the used geometry of the optical extinction experiments the SHG signal can be attributed to a plasmon oscillation oriented perpendicular to the surface[1] . This relation is discussed for the used experimental setup in detail elsewhere [77, 194]. Nonetheless the results are depicted in figure 4.2 in order to clarify that the system of very small supported silver clusters investigated in this work can be interpreted within the electric dipole approximation [105, 153, 154, 155, 166]. If the sample is illuminated with p-polarized light under normal incidence

[1] An overview of selection rules for second harmonic generation in nanoparticles can be found in literature [54]

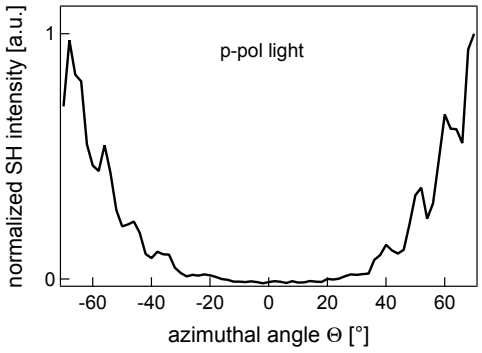

Figure 4.2.: SHG intensity of supported unselected silver clusters depending on the angle of incidence of the incoming laser light..

($\theta = 0$), the plane of polarization is oriented parallel to the surface. In this configuration only an electron oscillation parallel to the surface is excited, that does not allow for the generation of second harmonic light. With an increasing incident angle the polarization component oriented perpendicular to the surface grows and consequently the intensity of the generated second harmonic light increases. The lack of SHG signal under normal incidence emphasizes, that the s-SHG spectra shown in this work are dominated by the dipolar plasmon mode, therefore higher order multipolar modes are neglected. In the case of s-CRD spectroscopy the measured signal cannot be assigned to a certain orientation of the plasmon mode a priori due to the absence of symmetry rules in this linear technique. However it has been shown, that this signal corresponds to a plasmon oscillation oriented parallel to the surface [195]. Figure 4.3 shows typical spectra of supported silver clusters measured with s-CRD and s-SHG spectroscopy. Note, that the peak in the linear s-CRD spectrum is caused by absorption processes, whereas

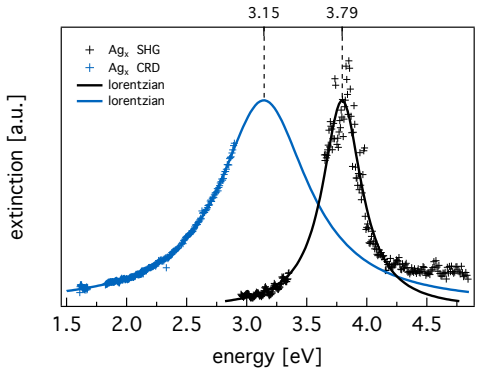

Figure 4.3.: LSPR dispersion of SiO_2 supported silver clusters with a mean diameter of 1 nm

the peak in the nonlinear s-SHG spectrum is caused by the generation of second harmonic light. Because these are inherently different processes, the intensity of the two spectra can not be compared. However, the position and the width of the two peaks can be compared among each others because both signals originate from the Localized Surface Plasmon Resonance of the supported silver clusters, as discussed in section 3.2. As can be seen, the two techniques cover different spectral regions. With s-CRD the spectral region from approximately $1.5 - 2.9$ eV is covered[2]. The limitation to this spectral region is due to scattering losses caused by the substrate, as elucidated in chapter 3.2.1. With s-SHG the spectral region from approximately $3.0 - 4.8$ eV is accessible[3]. It should be noted, that this photon energy does not correspond to the used fundamental photon energy, but the frequency doubled, second harmonic light. Thus a fundamental photon energy of ap-

[2] approximately $430 - 780$ nm
[3] approximately $250 - 420$ nm

proximately $1.5 - 2.4\,\text{eV}$ was used to measure this spectrum[4]. The limitation to this spectral region is due to the transparency of the used optics and the need for intensive laser light, as explained in chapter 3.2.2. Both spectra show a gap between 1.68 eV and 1.82 eV of fundamental light[5] which can be assigned to the lack of radiation provided by the used laser system. In addition to the measured data the lorentzian fits of this data are shown in figure 4.3. In the case of the s-SHG spectrum the signal intensity above 4.2 eV is not considered for the fit of the LSPR of the free 5s electrons, as it can be assigned to interband transitions from the 4d band to the conduction band[6]. Unfortunately, in the s-CRD spectrum the peak maximum of the LSPR is not resolved. Nonetheless the measured onset can clearly be assigned to the LSPR of supported silver clusters, as shown in chapter 4.3, and the lorentzian fit gives the position and width of the LSPR, if the error is chosen sufficiently large. Interestingly, with s-CRD and s-SHG different signals are detected. The LSPR measured with s-CRD is located at around 3.2 eV with a FWHM of approximately 0.9 eV, whereas the LSPR measured with s-SHG is located at around 3.8 eV with a FWHM of approximately 0.4 eV. Because multipolar resonances can be ruled out and the coverage of approximately $6 * 10^{12} cm^{-1}$ is too low for interparticle effects, only the presence of the substrate can be responsible for the observed differences. As discussed in chapter 2.2 the presence of the substrate causes a deviation from a perfect spherical shape of supported clusters and provides an unisotropic dielectric

[4] approximately $500 - 840\,\text{nm}$

[5] Consequently, in the second harmonic spectrum this gap shows up from $3.36 - 3.64\,\text{eV}$

[6] Compare section 2.

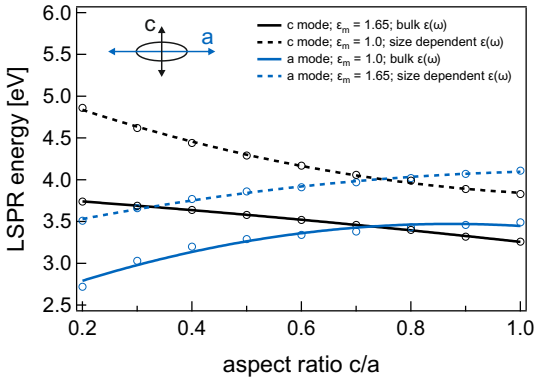

Figure 4.4.: LSPR dispersion of silver clusters in an unisotropic dielectric environment for different axis ratios. The bulk dielectric function [94] (solid lines) and a size dependent dielectric function [76] (dashed lines) were considered

environment. Both effects lead to an elimination of the threefold degenerated LSPR of spherical particles surrounded by a homogeneous dielectric environment resulting in a mode splitting. The effects of an unisotropic refractive index and the deviation from spherical shape are shown in figure 4.4. The LSPR energies were calculated by feeding the dielectric function of bulk silver [94] (solid lines) into equation 2.18. For the a-mode, oriented parallel to the surface, a dielectric constant of the surrounding medium $\epsilon_m = 1$ was used, assuming that the presence of the substrate does not influence this plasmon oscillation in terms of the refractive index. For the c-mode, oriented perpendicular to the surface, a dielectric constant of the surrounding medium $\epsilon_m = 1.65$ was used, assuming that the refractive index of vacuum and the substrate contribute equally to the effective dielectric constant. The unisotropic refractive index results in a parallel plasmon oscillation, that is located at higher energies than the perpendicular plasmon

oscillation, which is in harsh contrast to the experimental results. To reverse the position of the two plasmon modes, deviations from a spherical shape has to be allowed. In order to get the measured difference of approximately 0.6 eV, an axis ratio of 0.35 has to be applied, which is far away from the experimentally derived axis ratio of 0.89 in the case of small, quartz glass supported silver clusters [87]. However, the as derived LSPR energies of approximately 3.1 eV (a-mode) and 3.7 eV (c-mode) match the experimental results quite well. As shown in figure 3.2, the mean diameter of unselected silver clusters in this work is approximately 1 nm with a size distribution of 10%. Using the dielectric function of bulk silver to calculate the LSPR energies is therefore questionable. Thus the dielectric function for spherical silver clusters with a diameter of 1 nm was calculated using equation 2.16 and 2.17 to estimate the LSPR energy for different axis ratios. The results are presented in figure 4.4 with dashed lines. As can be seen, both plasmon modes shift to higher energies. To realize an energy difference of 0.6 eV, a slightly higher axis ratio of 0.44 is necessary, which is however still quite unrealistic. Additionally the calculated LSPR energies for an axis ratio of 0.44 are far away from the experimental results. Using the same effective dielectric constant of the surrounding medium for both plasmon modes can not explain the huge energy splitting of 0.6 eV, too, if realistic axis ratios are assumed, as can be seen from figure 2.9. It can be concluded that neither an unisotropic refractive index, nor a deviation from a spherical shape can be responsible for the experimental observed mode splitting and especially the different widths of the measured plasmon modes are not explained by the considered models. Therefore the influence of the unisotropic dielectric

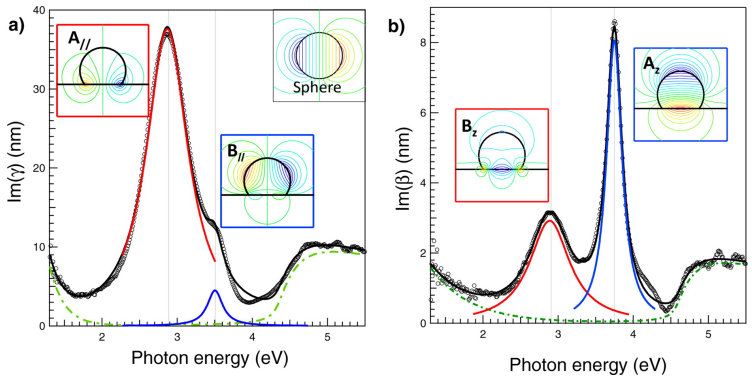

Figure 4.5.: LSPR of alumina supported silver nanoparticles for excitations parallel (left hand side) and perpendicular (right hand side) to the surface. Taken with permission from [112].

environment has to be considered in terms of the image charge that is build up in the dielectric substrate, when a supported particle is excited with an electromagnetic field. As explained in chapter 2.3.2 this has to be done under consideration of the electromagnetic field around the supported particle and interfacial damping, which in turn depends on the particle shape and the nature of the support material. Lazzari and coworkers studied the decomposition of the LSPR of oxide supported silver nanoparticles in various studies [111, 112, 113, 114, 115] and showed, that the assumption of supported truncated spheres enables for interpretation of the observed features. Figure 4.5 shows the results for silver nanoparticles supported onto alumina [112]. The spectra has been measured by optical spectroscopy during vapor deposition growth and it was possible to differentiate between p- and s-polarization. Figure 4.5 a) corresponds to a polarization parallel to the surface and figure 4.5 b) corresponds to a polarization perpendicular to the

Table 4.1.: Comparison of the experimental found plasmon dispersion with literature values.

	own data		Lazzari et al. [112]	
	a-mode	c-mode	a-mode	c-mode
position [eV]	3.2 ± 0.2	3.8 ± 0.05	3.3	3.8
FWHM [eV]	0.9 ± 0.1	0.4 ± 0.1	0.8	0.4

surface. With A and B in the insets, dipolar and quadrupolar components are denoted. Note, that for the smallest particle sizes with diameters of approximately 3 nm, the quarupolar components B were nor observed. Figure 4.5 depicts the results for larger particles with a diameter of approximately 10 nm and a relatively large coverage of almost $1 * 10^{12} cm^{-1}$. As can be seen, the extinction spectrum exhibits two dipolar plasmon modes, a broad, low energy mode oriented parallel to the surface and a sharp high energy mode oriented perpendicular to the surface. In the case of the smallest investigated particle size, where interparticle coupling can be neglected, the parallel plasmon mode is located at 3.3 eV with a FWHM of 0.8 eV, and the perpendicular plasmon mode is located at 3.8 eV with a FWHM of 0.4 eV. These values are in good agreement with the experimental results shown in figure 4.3 and are summarized in table 4.1. As can be seen, slight differences are found in the case of the a-mode, which is oriented parallel to the surface. As described above, within this work this mode is detected with s-CRD spectroscopy. The fact that the LSPR is not resolved completely using s-CRD and the resulting large error might be an explanation for the deviations.

Furthermore the different substrate materials (SiO_2 vs. Al_2O_3), different particle sizes (1 nm vs. 3 nm) and possibly different shapes (gasphase deposited vs. vapor deposition growth) might explain the differences. Nevertheless the perpendicular oriented c-mode, which can be measured accurately with s-SHG spectroscopy is in excellent agreement with the work by Lazzari et al.. It can be concluded, that the supported silver clusters within this work can be thought as deformed spheres, which exhibit a low energy plasmon mode oriented parallel to the surface and a high energy plasmon mode oriented perpendicular to the surface. The low energy mode is detected with s-CRD spectroscopy whereas the high energy mode is detected with s-SHG spectroscopy.

4.2. Size Dependence

The optical properties of small silver nanoparticles are dominated by their Localized Surface Plasmon Resonance. The position and the width of the LSPR depend, despite other factors, strongly on the particle size, as described in section 2.1. In order to investigate the size dependence, the size has to be variied independently from other factors such like the surface chemistry. Several size dependent studies of ligand free silver clusters are reported for supported particles [158, 166, 167, 175, 177], for particles in the gasphase [197] and for particles embedded in rare gas matrices [34, 51, 52, 71, 72, 116], ranging from diameters of 20 nm down to the molecular like dimer Ag_2. With one exception [175] the studies on supported

particles are restricted to particle diameters bigger than approximately 1.5 nm, due to the need of low coverages, in order to prevent agglomeration, in combination with the low cross section of very small particles. The low excitation cross section of very small particles could only be circumvented by accumulation of isolated particles in a rare gas matrix. Therefore a lack of information exists in the small size regime in the case of supported clusters, which represent the practically most relevant system. For example, silver nanoparticles are a suitable candidate for solar energy harvesting devices, due to their strong absorption in the UV/visible range and their ability to enhance an incoming electromagnetic field [11, 38, 129]. In order to optimize the efficiency of such devices, the extinction has to be tuned, which requires a sound understanding of the optical properties of supported particles. Beside this practical question there is a fundamental interest in this size range, because it links the scalable properties of bigger particles, that usually follow a phenomenological $1/R$ law with the molecular like optical properties of very small particles. It has been found, that for silver clusters bigger than approximately Ag_{20} the extinction spectrum is dominated by a single strong absorption, corresponding to the plasmon resonance of the free conduction electrons. The extinction spectrum of even smaller particles exhibit multiple absorption peaks due to the distinct energy splitting of the conduction band in this size range. However this behavior has only be found for silver clusters embedded in cold, weakly interacting rare gas matrices due to the afore mentioned reasons. It is unknown, how the LSPR of supported silver clusters evolves, if entering the small size limit. Therefore within this work the optical properties of size selected supported silver clusters ranging from

Ag_{55} to Ag_9, corresponding to diameters between approximately 1.1 nm and 0.7 nm if spherical particles are assumed, were investigated by means of s-SHG spectroscopy. The power of s-SHG spectroscopy for the investigation of small supported metal clusters with a low surface coverage has been proved [134, 195] and a detailed description of the measured spectra and the data treatment can be found elsewhere [77, 194]. Here the focus is on the interpretation of the experimental results, but it should be noted that s-SHG spectra of supported silver clusters exhibit a single peak as depicted in figure 4.3 even for the smallest sizes and that the spectra are corrected for influences caused by the support and other parts of the optical setup. In figure 4.6 the experimentally determined LSPR energies, taken from a lorentzian fit of the measured spectra, are depicted against the inverse particle diameter, a presentation that allows the size evolution to be plotted from bulk (1/D=0) to molecular like clusters [62]. For the presentation the clusters are assumed to have a spherical shape and the particle diameter is expressed as

$$D = 2a_0 r_s N^{1/3} \tag{4.1}$$

where $a_0 = 0.0529\,\text{nm}$ is the Bohr radius, $r_s = 3.02$ is the atomic Wigner Seitz radius and N is the number of atoms in the particle. As already mentioned in section 3.1, this calculation is based on bulk values and the calculated particle diameter is only an approximation. Nevertheless this presentation is chosen in order to ensure a good comparability with literature, as shown below. The LSPR of supported silver clusters shifts to higher energies by approximately 0.2 eV if the cluster size is decreased from Ag_{55} to Ag_9. This

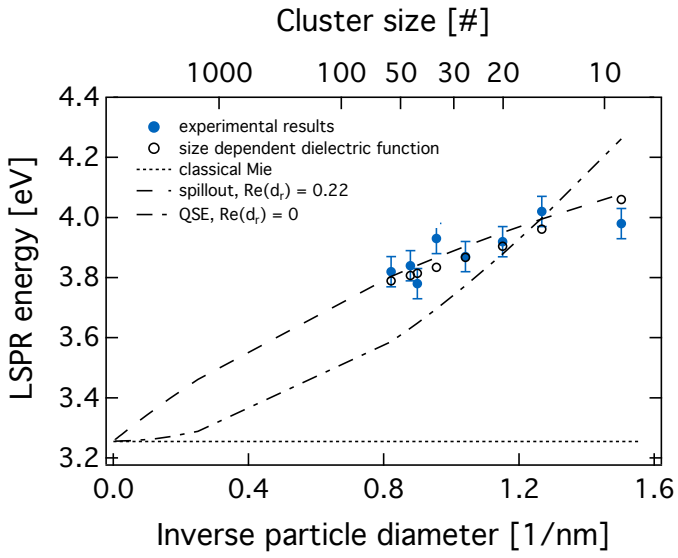

Figure 4.6.: Experimentally derived plasmon energies of SiO_2 supported size selected silver clusters in comparison to different theoretical models.

Table 4.2.: Comparison of the experimental found plasmon dispersion with literature values.

size [#]	diameter [nm]	position [eV]	FWHM [eV]
9	0.6656	3.98	1.2
15	0.7892	4.02	0.8
20	0.8686	3.92	0.8
27	0.9600	3.87	0.9
35	1.0467	3.94	0.6
42	1.1123	3.78	0.5
45	1.1382	3.84	0.7
55	1.1269	3.82	0.7

shift with a decreasing particle size is not supported by classical Mie theory, which uses the dielectric function of the bulk material to describe the extinction of small particles and predicts a size independent plasmon resonance at approximately 3.26 eV, depicted as the dotted line. This LSPR energy corresponds to an effective dielectric constant of the surrounding medium $\epsilon_m = 1.65$, where the assumption of equally contributing dielectric constants of the substrate $\epsilon_{BK7} = 2.3$ and the surrounding vacuum $\epsilon_{vac} = 1.0$ was made. This assumption is justified due to the fact, that s-SHG spectroscopy only probes the plasmon oscillation oriented perpendicular to the surface, and that the near field around supported particles corresponding to this oscillation was found to be concentrated at the particle/substrate-interface and at the particle/vacuum-interface [112]. Within classical Mie theory a size dependent shift of the LSPR could be explained, if a size dependent aspect ratio of the supported particles is assumed. A decreasing aspect ratio $R_{c/a}$ results in a shift to higher energies of the plasmon resonance oriented perpendicular to the surface, as shown in figure 2.9. However an almost constant or even increasing aspect ratio of supported silver clusters for a decreasing particle size was found [158, 204], which would cause a shift to lower energies or no shift at all, respectively. As discussed in section 2.1 the physical boundaries of a metal particle can not be described as a hard barrier for the free electrons inside the particle. Electron density may spill out beyond the physical boundaries of the particle, whereas the portion of free electron density outside the particle increases with a growing surface to volume ratio. In the case of silver with it's filled 4d electron band, an increasing free electron density outside the particle results in a shift of the

LSPR to higher energies. Therefore a theoretical model that accounts for the spill out is used to fit the experimentally observed shift of the LSPR [147]. Equation 2.15 was used to calculate the LSPR energy[7], whereas for the dielectric constant of the surrounding medium again a value of 1.65 was used. For the bulk plasma frequency ω_p a value of 9.08 and for the high frequeny dielectric constant ϵ_∞ a value of 4.475 was used. The resulting LSPR energies are depicted as a dashed line in figure 4.6. The best agreement with our experimental results is found for a screening parameter $Re(d_r) = 0.22$. Note that for the high frequency dielectric constant ϵ_∞ a slightly different value than 5.0 [146, 150] was used in order to match the bulk limit of the LSPR energy of 3.26 eV predicted by classical Mie theory. In the case of using $\epsilon_\infty = 5$ the best agreement with our experimental results is found for a screening parameter $Re(d_r) = 0.33$. This emphasizes, that a quantification of the spill out effect is difficult. Nevertheless the experimentally derived blueshift of the LSPR is in good agreement with the model of free electron spill out. The deviations might be caused by different contact areas between the clusters and the substrate for different sizes. The ratio of the particle surface in contact with vacuum and the particle surface in contact with the substrate probably changes in the investigated size range significantly for different cluster sizes due to distinct cluster structures. Therefore the electron spill out into free space exists in varying degree, which is not considered in the theoretical model, assuming spherical particles surrounded isotropically by an dielectric. In a next step quantum mechanical effects are

[7] In order to consider the electron spill out solely, the left term in the parentheses, which accounts for quantum size effects, was neglected.

considered, which become important for very small metal clusters, where the energy levels in the conduction band are discretized and only certain electronic transitions are allowed. For ultra small free clusters sophisticated TDDFT calculations are available, which however become computational demanding, if the particle size increases or supported particles are considered. Here an analytical model is used that is based on the quantum confinement of free electrons inside the physical boundaries of the particle and which was successful in describing various experimental results [147]. The dashed-dotted line in figure 4.6 depicts the outcome of equation 2.15 when a screening parameter $Re(d_r) = 0$ is used, thus reflecting a situation without spill out of free electrons. This model predicts a blueshift of the LSPR due to quantum size effects (QSE) far greater than the experimentally observed one. Between Ag_{55} and Ag_9 the LSPR is expected to shift by approximately 0.7 eV, while only a shift of approximately 0.2 eV is measured. For some reasons the analytical QSE model, which was used in a similar way in reference [177] to explain the experimental results, is not valid in the investigated size range. Eventually full quantum mechanical calculations are needed in order to describe quantum size effects in metal clusters consisting of only a few atoms correctly. In a last step the size dependence of the dielectric function, discussed in section 2.1 in detail, is considered explicitly instead of modifying the bulk dielectric in a size dependent way. Equations 2.16 and 2.17 are the analytical formulations for the size dependent real and imaginary part of the dielectric function of silver, which is derived from quantum mechanically calculated dielectric functions of distinct cluster sizes [76]. Using this equations the dielectric

function of the cluster sizes investigated within this work are calculated assuming spherical clusters. The LSPR energies that are calculated by feeding this dielectric functions into classical Mie theory are shown as hollow circles in figure 4.6. Again a dielectric constant of the surrounding medium $\epsilon_m = 1.65$ was used. The LSPR energies predicted by this semi empirical approach are in agreement with the experimental results on a quantitative level. The small differences in the energy might be due to deviations of the cluster shape from sphere like clusters as assumed in the theoretical model. Additionally the cluster support, which is not considered in the analytical formulation might influence the dielectric function, resulting in the observed differences. Besides the LSPR position and the intensity, the width is the third characteristic measure of the lorentzian shaped plasmon resonance. With a decreasing particle size the width should increase caused by additional surface scattering, as described in section 2.1. However, as can be seen from table 4.3 only a tendency towards an increasing width, but no clear trend is observed for a decreasing particle size. However it should be noted, that the experimental error for the FWHM was determined as $\pm 0.2\,\mathrm{eV}$, so the expected $1/R$ trend might get lost in the big error. Again a different contact area between the clusters and the substrate for different cluster sizes might be a reason for the deviation from the expected trend, because electronic states of the substrate adjacent to the cluster surface provide an extra decay channel for the plasmon resonance, as described in section 2.4. A higher proportionate area of the cluster surface in contact with the substrate material for a distinct size in comparison to other sizes would thus result in an extra broadening of the plasmon resonance and

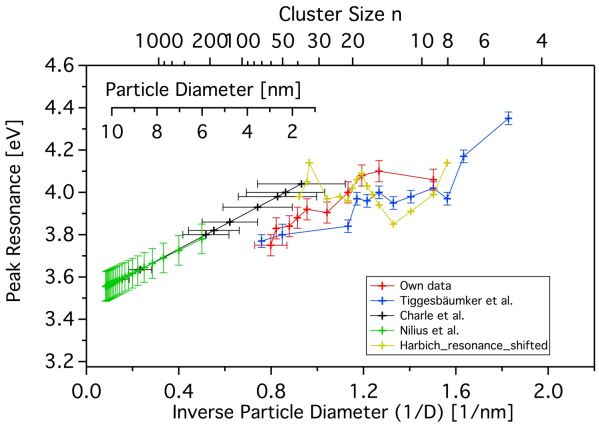

Figure 4.7.: Experimentally derived plasmon energies of SiO_2 supported size selected silver clusters (red curve) in comparison with literature. This figure is taken from [77]

perhaps blur the expected $1/R$ trend. Another possibility for the absence of clear trend might be, that the classical assumption of a collective electron oscillation, that gets scattered at the particle surface is not valid for cluster sizes, consisting of only a few atoms per cluster. Eventually the extinction spectra of very small supported silver clusters exhibits multiple distinct peaks as the extinction spectra of small silver clusters in weakly interacting rare gas matrices. In this case the single peak in the s-SHG spectra measured in this work could be the weighted mean of the distinct peaks, broadened by the interaction with the substrate. However, the single observed peak has got a symmetrical lorentzian shape for all investigated cluster sizes and follows the expected trend in terms of the resonance position.

Figure 4.7 compares the LSPR energy determined within this work with selected works on silver nanoparticles reported in literature [34, 52, 158, 177, 197]. Note, that the shown results of the different studies are scaled in a

way, that accounts for the different supports and matrices and is described in detail elsewhere [62, 77]. The blueshift of the LSPR of silver nanoparticles for a decreasing size measured within this work is in good agreement with literature values. The trend known for supported particles of bigger sizes (shown in green and black) continues for particles smaller than 2 nm and the shift of the LSPR is in the same order as known for silver clusters in the gasphase (shown in blue) or silver clusters embedded in rare gas matrices (shown in yellow). Interestingly the dispersion of the LSPR into distinct peaks known from very small silver clusters in rare gas matrices is not observed in the case of SiO_2 supported silver clusters and the single resonance behaves like a classical plasmon resonance down to a size of Ag_9.

4.3. Cluster Molecule Interactions

Based on a sound knowledge of the optical properties of size selected supported silver clusters, the question arises how the optical properties are altered, if the system is exposed to molecules. The scientific interest in ligand capped metal clusters, especially gold and silver, has increased enormously during the past two decades due to the ease of size selective synthesis and exact knowledge of the structure [25, 68, 91]. In this field of research one focus is on chiral metal clusters since optical activity located in metal based transitions was shown the first time for monolayer protected gold clusters [55, 191]. It has been shown, that chiral ligands can rearrange the metal core in a chiral fashion and that the chirooptical properties depend on many

factors like the particle material and size, the used ligand, the number of ligands and so forth. However, since the ligand layer is mandatory for the stabilization of the metal clusters, the impact of the ligand layer on the optical properties of the metal cluster can hardly be extracted from such studies. Furthermore optical activity has not been measured up to now in the case of supported metal particles, representing the most interesting system in terms of asymmetric heterogeneous catalysis, a potential application of chiral metal particles [60]. Nonlinear s-SHG spectroscopy has been shown to be powerful in order to investigate chiral surfaces [26, 27, 186, 196]. The corresponding techniques are analogs of linear Optical Rotatory Dispersion and Circular Dichroism and are called s-SHG-ORD (Surface Second Harmonic Generation Optical Rotatory Dispersion) and s-SHG-CD (Surface Second Harmonic Generation Circular Dichroism) respectively. It was shown, that the CD effect in the nonlinear analog is orders of magnitudes bigger than within the linear technique, which enables the investigation of chiral surface species with sub monolayer coverage and very small effects [176]. Our spectroscopic setup was successfully used for the study of supported chiral molecules [78] and the next step would be the investigation of supported chiral metal clusters.

4.3.1. s-SHG Studies

Several molecules, whose chemical structures are shown in figure 4.8, were used to study cluster molecule interactions in the case of supported sil-

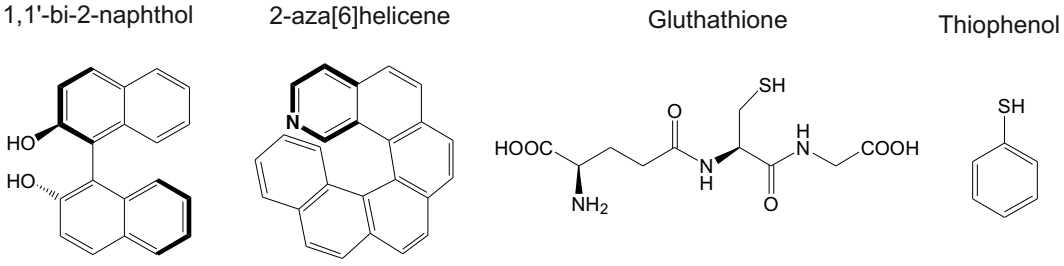

Figure 4.8.: Structural chemical formulas of molecules used to study cluster molecule interactions by means of SHG spectroscopy. 1,1'-bi-2-naphthol, 2-aza[6]helicene and glutathione are chiral and Thiophenol is achiral.

ver clusters by means of s-SHG spectroscopy. 1,1'-bi-2-naphthol (Binol), 2-aza[6]helicene and glutathione were chosen as chiral molecules in order to investigate chirooptical properties of supported silver clusters under controlled UHV conditions. Binol and helicenes posses axial chirality whereas glutathione posses a stereogenic center. Glutathione was used because it has been shown, that gold and silver clusters capped with enantiomerically pure glutathione exhibit optical activity in metal based transitions [30, 50, 108]. Binol was used because of it's well understood nonlinear optical properties when supported onto SiO_2 glass slabs [78]. Additionally the correlated dithiol (BINAP) has been used successfully to synthesize chiral metal particles [56]. The helicene was used in order to test a chiral molecule with as little functional groups as possible and Thiophenol was used as simple test molecule. In order to determine the influence of the molecules on the optical properties of supported silver clusters, samples of unselected clusters were prepared under UHV conditions as described in section 3.1 and the extinction spectrum was measured by means of s-SHG

spectroscopy prior to molecule exposure. The molecules were evaporated on top of the clusters in the preparation chamber, with a base pressure of approximately $2 \cdot 10^{-8}$ mbar. The overall duration of the sample inside the preparation chamber was kept well below two minutes. It has been shown, that a period of two minutes inside the preparation chamber at a pressure of $3 \cdot 10^{-8}$ mbar only alter the s-SHG spectrum slightly, so that changes can be attributed to interactions with evaporated molecules[8]. Binol, glutathione and the helicene are solids at ambient conditions, so they were evaporated onto the silver clusters with use of an evaporator for organic molecules. The applied temperature for the evaporation process was kept low, so that no thermal decomposition takes place during evaporation and the molecules are intact onto the surface [77]. The coverage was monitored with help of a quartz microbalance. Thiophenol is liquid at ambient conditions, so it was leaked into the preparation chamber and the cluster sample was exposed to a background pressure of $3 \cdot 10^{-6}$ mbar for 30 seconds. On the left hand side of figure 4.9 s-SHG extinction spectra of unselected silver clusters Ag_x with a coverage of approximately $1 \cdot 10^{13} cm^{-2}$ are shown[9] , if exposed to Binol. On the right hand side the lorentzian fits of the LSPR located at around 3.7 eV are depicted with normalized intensities for a better comparison. It should be noted, that the signal intensity above approximately 4.0 eV, which can be attributed to interband transitions, is not considered for the fit. Binol was evaporated in several steps and the s-SHG spectra were measured

[8] see App2

[9] Samples of unselected silver clusters Ag_x have got a size distribution between approximately Ag_{21} and Ag_{60}, as schown in section 3.1.

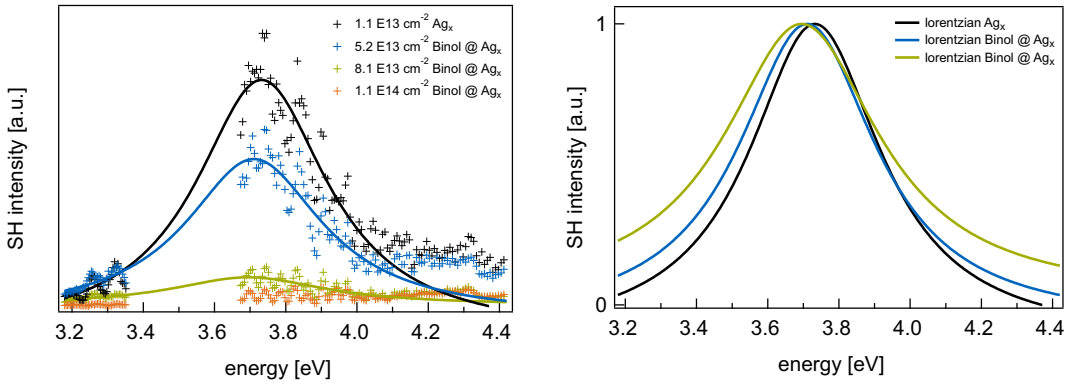

Figure 4.9.: s-SHG spectra and corresponding lorentzian fits of supported silver clusters interacting with Binol. The Binol coverage of $1 \cdot 10^{14} cm^{-2}$ corresponds to a full monolayer.

subsequently after each evaporation step. With an increasing coverage of evaporated Binol the LSPR signal intensity decreases until no signal is left at a coverage of approximately $1 \cdot 10^{14} cm^{-2}$. Assuming a size of 1 nm^2 for Binol molecules, this coverage corresponds to a full monolayer of molecules [107]. The corresponding s-SHG spectrum depicted in orange exhibits an oscillation pattern below an energy of approximately 4.0 eV, which can be attributed to interferences between second harmonic light generated at the front and back of the used SiO_2 support and indicates an accurate measurement [97, 194]. A single monolayer of Binol molecules adsorbed onto SiO_2 does not generate SH signal intensity due to a transition dipole moment oriented parallel to the surface, as shown in an earlier study [78]. Up to a coverage of a full monolayer a slight shift to lower energies and a broadening of the LSPR can be observed with an increasing coverage. The shift could be explained with an increased effective dielectric constant

Table 4.3.: Fit parameters of spectra shown in figure 4.9.

	$\theta[cm^{-2}]$	norm. int. [a.u.]	position [eV]	FWHM [eV]
Ag_x		1	3.73	0.45
Binol 1 @ Ag_x	$5.2 \cdot 10^{13}$	0.66	3.71	0.47
Binol 2 @ Ag_x	$8.1 \cdot 10^{13}$	0.15	3.70	0.53

of the surrounding medium and the broadening with a reduced lifetime of the plasmon resonance due to chemical interface damping. However both, the shift and the broadening are within the error of the fit, so the loss of the SHG signal corresponding to the LSPR of silver clusters with an increasing coverage of molecules is the only reliable observation. Interestingly the complete loss of the signal coincides with a full monolayer of molecules, suggesting that silver clusters interacting with molecules do not contribute to the generation of second harmonic light. A similar behavior is observed in the case of the other tested molecules, too, as shown in the appendix A.2. The interaction of supported silver clusters with organic molecules, regardless of the type of molecules with different functional groups, therefore results in the loss of the SHG signal corresponding to the LSPR. At this point it is important to note, that the intensity of the generated second harmonic light depends on the polarizability of the free conduction electrons in the metal particle. It is known that the polarizability is reduced, if electron density is located in chemical bonds between metal clusters and a capping layer of molecules [74, 104]. Therefore the silver clusters might still be present on the substrate in an intact form, but the generation of second

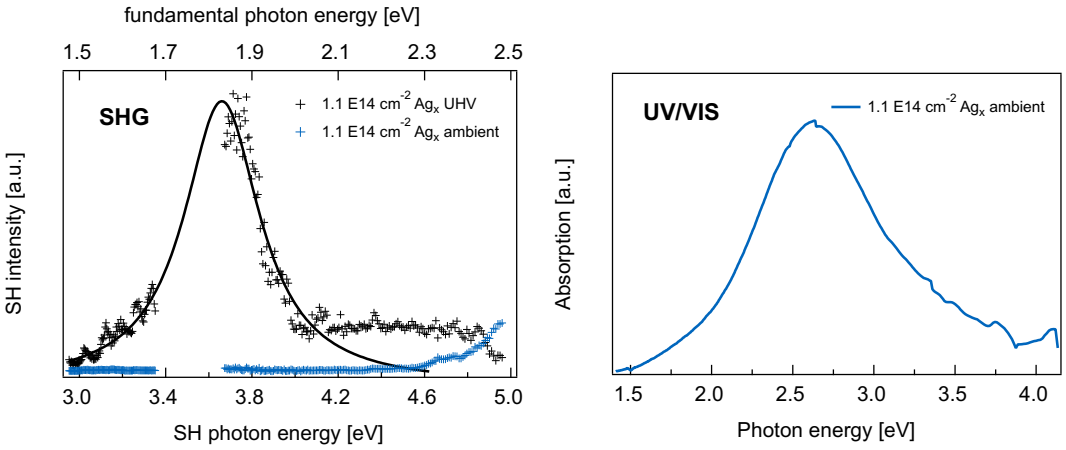

Figure 4.10.: Nonlinear s-SHG and linear UV/VIS extinction spectra of supported silver clusters. On the left hand side the s-SHG spectra before (black) and after (blue) exposure of the sample to molecules is shown.

harmonic light might be suppressed. In section 3.2.2 it is explained, that the generation of second harmonic light is enhanced if either the fundamental or the second harmonic is in resonance with the LSPR and it has been shown that in the used experimental arrangement the latter is the case [195]. Because the enhancement of the second harmonic is stronger, if the fundamental is in resonance with the LSPR energy, this modified experimental arrangement would offer the opportunity to verify the above assumption of a decreased polarizability of the free electrons. However the second harmonic light would have an energy of around 7.4 eV (approximately 170 nm), if the fundamental is in resonance with the LSPR located at around 3.7 eV, a spectral range that is not covered by the used setup. Figure 4.10 shows the experimental results obtained with a spectroscopic setup that was extended to the UV as much as possible. On the left hand side the

s-SHG spectrum of supported silver clusters under UHV conditions with a coverage of approximately $1 \cdot 10^{14} cm^{-2}$ is depicted in black. The coverage was increased in comparison to the experiments shown in figure 4.9 in order to get a strong signal intensity and in order to measure the sample with a standard UV/VIS spectrometer, having a lower sensitivity than surface sensitive s-SHG spectroscopy. The UV/VIS absorption spectrum, measured after exposure of the sample to molecules, is depicted on the right hand side of figure 4.10. Because the UV/VIS spectrometer is not implemented to the UHV setup, the sample had to be transferred to ambient conditions for the measurement. Subsequently the sample was transferred back to UHV in order to measure another s-SHG spectrum, depicted in blue on the left hand side of figure 4.10. Note that in the graph on the left hand side both, the fundamental and second harmonic photon energies are depicted. Fundamental light with an energy from $1.5 - 2.5\,\text{eV}$ was used to generate second harmonic light, which is the measured quantity, with an energy from $3.0 - 5\,\text{eV}$. Several important features can be extracted from figure 4.10. First of all, the UV/VIS spectrum clearly exhibits a strong absorption peak, which can be attributed to the plasmon resonance of the silver clusters. Therefore a decomposition of supported silver clusters caused by cluster molecule interactions can be excluded as the reason for the loss of the SHG signal shown in figure 4.9. Secondly, the LSPR shifted from 3.66 eV to 2.66 eV. The difference of 1.0 eV might be a combination of the LSPR dispersion between resonances oriented parallel and perpendicular to the surface, as explained in section 4.1, and the influence of the molecules onto the position and width

of the LSPR[10]. For oxide supported silver clusters with high coverages an energy difference of 0.8 eV between the plasmon resonance oriented parallel and perpendicular to the surface was measured [112], suggesting that the resonance detected with the UV/VIS spectrometer is that one oriented parallel to the surface. The fact, that the LSPR is broader when measured with the UV/VIS spectrometer supports this assumption [112]. The additional energy difference might be due to oxidation of the silver clusters, which shifts the LSPR to lower energies, as discussed in section 2.4. Measuring another s-SHG spectrum after transferring the sample back to UHV, the initial LSPR at 3.66 eV is gone as can be seen from the blue curve on the left hand side of figure 4.10, in accordance with the results shown in figure 4.9. Interestingly an SHG intensity onset on the high energy side of the spectrum can be observed which could be attributed to the case where the fundamental is in resonance with the LSPR. Unfortunately the peak is not fully resolved, however the onset of the peak starts at a fundamental photon energy of approximately 2.3 eV, which is again 0.8 eV 'bluer' than the onset of the plasmon resonance measured with the UV/VIS spectrometer. This energy difference again can be explained with one plasmon mode oriented parallel to the surface and one plasmon mode oriented perpendicular to the surface. Note, that the selection rules for the SHG process are the same, irrelevant if the fundamental or the second harmonic is in resonance with the transition. Therefore s-SHG spectroscopy exclusively probes the plasmon resonance oriented perpendicular to the surface, independent on the

[10]Because the UV/VIS absorption spectrum was measured under ambient conditions other effects like the oxidation of the silver clusters should influence the spectrum, too.

experimental arrangement. Of course the comparison of not fully resolved peaks measured with different spectroscopic techniques is inaccurate and can only give a hint. However, these measurements suggest that the polarizability of free conduction electrons inside silver clusters is reduced due to cluster-molecule interactions, which suppresses the generation of second harmonic light considerably. It can be concluded, that nonlinear s-SHG spectroscopy can not provide further insights into the interactions between supported silver clusters and organic molecules under the used experimental conditions and that a linear spectroscopic technique has to be used in order to get more information about the influence of organic molecules on the optical properties of supported silver clusters.

4.3.2. s-CRD Studies

In contrast to nonlinear s-SHG spectroscopy, s-CRD spectroscopy is a linear optical method and therefore it should be less sensitive to a reduced hyperpolarizability due to cluster molecule interactions. Unlike studies with a conventional UV/VIS spectrometer, as shown in the previous section, it has got the strong advantage to enable UHV studies with sub monolayer sensitivity [193]. Therefore it is possible to measure the influence of organic molecules on the optical properties of size selected supported silver clusters, which require small surface coverages in order to prevent agglomeration. Because the interactions between metal clusters and molecules takes place at the cluster surface, Ag_{55} and Ag_{20} were chosen as cluster sizes with different

surface to volume ratios in order to measure the influence of thiophenol on the optical properties of silver clusters. In the case of thiolate stabilized coinage metal clusters in solution a clear correlation between the cluster size n and the number of thiolates m was found, whereas the number of thiolates is given as $m = n^{0.605} \cdot 10^{0.42}$ [43, 68]. Following this expression a Ag_{55} cluster should be surrounded by approximately 30 ligands and a Ag_{20} cluster should be surrounded by approximately 16 ligands, corresponding to 55% and 80% with regards to the number of atoms respectively. Although the cluster structure and the number of ligands is unknown in the case of supported clusters[11], a different surface to volume ratio can still be expected for these two cluster sizes, which should be reflected in the extinction spectra. Thiophenol was used as ligand because it was shown, that thiophenol and it's derivates form stable complexes with silver clusters in solution via a thiolate bonding [1, 13, 21, 70, 75]. Additionally thiophenol is non resonant in the investigated spectral range, which simplifies the interpretation of the spectra. In order to study the impact of thiophenol on the optical properties of supported silver clusters, cluster samples were prepared under UHV conditions as described in section 3.1 and a s-CRD spectrum was measured subsequently. Afterwards thiophenol was leaked into the preparation chamber with a background pressure of $2 \cdot 10^{-6}$ mbar and the cluster sample was exposed to that atmosphere for a certain time[12],

[11] Ag_{55} is a geometrically closed shell cluster and has got an icosahedral shape in the gase phase [83, 178], whereas Ag_{20} is geometrically and electronically a closed shell cluster with an tetrahedral gas phase structure [45, 100]

[12] A mass spectrum of the thiophenol atmosphere can be found in appendix A.2

followed by the measurement of another s-CRD spectrum. It was shown that the base pressure of the preparation chamber of $2 \cdot 10^{-8}$ mbar does not change the extinction spectrum of supported silver clusters, if the sample is placed in the preparation chamber without dosage of organic molecules[13]. Therefore changes in the extinction spectrum can unambiguously be assigned to cluster molecule interactions. The evaporation was retried until no changes in the s-CRD spectrum could be observed. As described in section 3.2.1 a complete s-CRD spectrum is subdivided into several separate parts, each covered with an individual set of mirrors. The measurement of an individual part requires an adjustment of the corresponding mirror pair accompanied with an experimental error. To circumvent this experimental error the evolution of the s-CRD spectrum during the evaporation of thiophenol was monitored with a single mirror pair, so that the readjustment of the optical setup between the evaporation steps was not neccessary. Finally again a full spectrum was measured from the saturated system. The impact of thiophenol upon unselected silver clusters with a mean diameter of 1 nm $\pm$ 10 % is shown in figure 4.11. On the left hand side the extinction spectrum of the bare clusters is depicted in black and the final spectrum after exposure to Thiophenol is depicted in blue. Additionally lorentzian fits of the measured data are shown as solid lines. On the right hand side of figure 4.11 the evolution of the extinction during evaporation of Thiophenol is shown, monitored with a single mirror pair, whereas the exposure to thiophenol is denoted in Langmuir[14]. Note that normalized intensities are

[13] See appendix A.2

[14] $1L = 1.33 \cdot 10^{-6} mbar \cdot s$

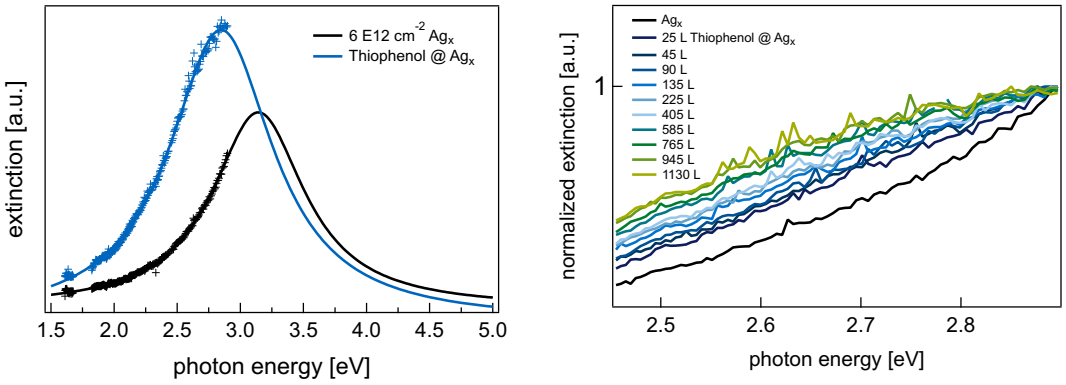

Figure 4.11.: Influence of thiophenol on the extinction spectrum of unselected silver clusters. On the left hand side the extinction spectra of bare and saturated silver clusters is shown, whereas on the right hand side the evolution of the extinction under thiophenol exposure is shown.

depicted. The same measuring procedure as for the unselected samples was done for size selected samples of Ag_{55} and Ag_{20} and the spectra are shown in figure 4.12. The corresponding evolution of the extinction during evaporation of thiophenol can be found in appendix A.2. As can be seen, and as already mentioned in section 4.1, the s-CRD spectra of bare silver clusters are not resolved completely and the fit parameters should be taken with care. However, in accordance to the expected size effect, the LSPR of bare samples is located at approximately 3.2 eV and 3.1 eV for Ag_{20} and Ag_{55} respectively, whereas the resonance of Ag_{20} is slightly broader. Both, the position and the width are in good agreement with literature, as shown in section 4.1. Furthermore the difference in the position of around 0.1 eV and the difference in the FWHM of around 0.2 eV is in quite good agreement with the experimental results presented in section 4.2, which were obtained

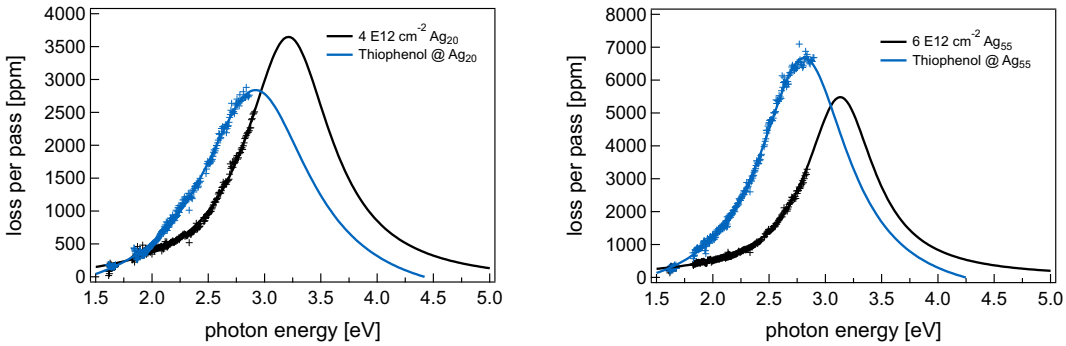

Figure 4.12.: Influence of thiophenol on the extinction spectrum of size selected Ag_{20} and Ag_{55} clusters.

with s-SHG spectroscopy. These agreements indicate a sufficient accuracy of the fit in order to compare the impact of thiophenol on different cluster sizes, although the peak is not resolved completely. After evaporation of thiophenol the peak maximum or at least the inflection point is resolved, resulting in an accurate fit. The reproducibility of the measurement was shown in the case of Ag_{55} with several individual samples[15]. For the peak position a standard deviation of $\pm 0.02\,\text{eV}$ was determined and for the FWHM a standard deviation of $\pm 0.3\,\text{eV}$ was determined. In all experiments the LSPR of supported silver clusters shifts to lower energies and broadens, if exposed to thiophenol. As can be taken from table 4.4, after exposure to thiophenol the LSPR of Ag_{20} and Ag_{55} are located at around 2.92 eV and 2.82 eV respectively, so the resonances of both cluster sizes shifted by approximately 0.3 eV to lower energies. As described in section 2.4 this shift might be caused by a higher dielectric constant of the surrounding medium ϵ_m or a reduced

[15] see appendix A.2

Table 4.4.: Comparison of the thiophenol induced LSPR shift and broadening for different cluster sizes.

	Ag_x		Ag_{20}		Ag_{55}	
	bare	Thiophenol	bare	Thiophenol	bare	Thiophenol
position [eV]	3.1	2.85	3.2	2.92	3.1	2.82
FWHM [eV]	0.9	1.0	0.9	1.2	0.7	0.9

electron density inside the metal clusters. It has been shown that thiophenol, and other thiols in general, chemisorb onto a silver surface if they impinge from the gas phase [2, 18, 101, 132, 179]. The reaction takes places via the formation of a covalent bonding between the sulfur and silver, whereas the SH bond of the thiol dissociates. Although this mechanism was found for extended silver surfaces it is assumed that thiophenol chemisorbs onto small supported silver clusters, too, as known from silver nanoparticles in solution [36, 48]. Because chemisorbed thiolate ligands reduce the electron density and increase the dielectric constant of the surrounding at the same time, the observed shift is propably a combination of these two effects. Additionally to thiophenol chemisorbed to silver clusters, thiophenol molecules adsorbed onto the SiO_2 substrate or thiophenol physisorbed in multilayers on top of the clusters might influence the LSPR via an increased dielectric constant of the surrounding, too. In order to gain a better understanding of the investigated system figure 4.13 shows the evolution of the LSPR position against thiophenol exposure, whereas the LSPR positions are taken from the fits of the peak sections shown on the right hand side of figure 4.11. These

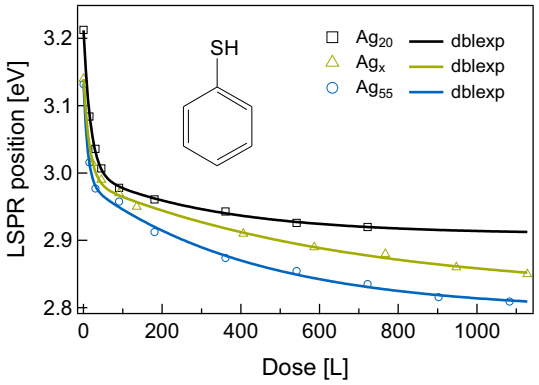

Figure 4.13.: Evolution of the LSPR position under thiophenol exposure for different cluster sizes.

fits were done on the basis of the completely measured s-CRD spectra before and after the evaporation of thiophenol in order to get values as precise as possible. Again, the reproducibility was shown in the case of Ag_{55} and can be found in appendix A.2. For both cluster sizes, as well as for unselected samples, the LSPR position shows a double exponential characteristic under exposure to thiophenol.

$$y_0 + A_1 \exp\left(\frac{-(x - x_0)}{\tau_1}\right) + A_2 \exp\left(\frac{-(x - x_0)}{\tau_2}\right) \tag{4.2}$$

A rapid shift at the beginning, characterized by the fit parameters A_1 and τ_1 is followed by a slow shift, characterized by A_2 and τ_2, indicating two different processes that take place at different time scales. Because thiophenol directly chemisorbs onto a silver surface from the gas phase without the appearance of physisorbed precursor states [2, 18], a combination of physisorption and consecutive, kinetically hindered chemisorption can be excluded as the reason for the observed double exponential characteristic. In

Table 4.5.: Fit parameters of the double exponential LSPR shift of supported silver clusters under thiophenol exposure.

	$y_0[eV]$	A_1	$\tau_1[L]$	A_2	$\tau_2[L]$
Ag_{20}	2.91	0.21	18	0.09	335
Ag_{55}	2.80	0.15	11	0.19	428
Ag_x	2.82	0.15	16	0.17	657

that case physisorbed thiophenol would increase the dielectric constant of the surrounding medium and the formation of the thiolate bonding would decrease the free electron density inside the silver clusters, further shifting the LSPR to lower energies. To exclude this mechanism experimentally, a sample of unselected silver samples was prepared, measured and exposed to thiophenol as described. However the evaporation was halted after the first evaporation step and the sample was stored in UHV for 30 minutes, which corresponds to the typical duration between two evaporation steps. Subsequently another spectrum was measured before the evaporation of thiophenol was continued. As can be seen in figure 4.14, the s-CRD spectrum does not change, if the sample is stored in UHV. When the evaporation of thiophenol is continued, the LSPR of supported silver clusters continues to shift to lower energies, indicating that the system is not saturated after the first evaporation steps, and that at least the rapid shift of the LSPR at the beginning of the evaporation can be assigned to chemisorption of thiophenol to supported silver clusters. In order to verify this assumption, a sample of unselected silver clusters was exposed to benzene under the same

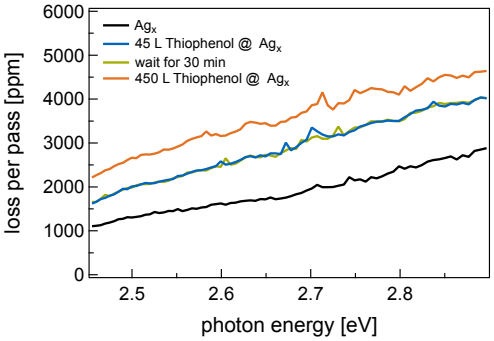

Figure 4.14.: Time behavior of the extinction of supported silver clusters covered partially with thiophenol. The duration of 30 minutes corresponds to the typical duration between two evaporation steps.

conditions as for the experiments with thiophenol[16]. In contrast to exposure to thiophenol, the shift of the LSPR shows a single exponential decay, which can be attributed to Langmuir adsorption of benzene onto supported silver clusters and shows a time constant of the shift that is an order of magnitude larger than the time constant of the fast process in the case of thiophenol evaporation[17].

$$y_0 + A \exp\left(\frac{-(x - x_0)}{\tau}\right) \tag{4.3}$$

Therefore the rapid shift at the beginning of thiophenol evaporation can unambiguously be assigned to chemisorption of thiophenol to silver clusters. The slow LSPR shift in the case of thiophenol evaporation might be caused either by chemisorption of thiophenol, too, or it might be due to additionally physisorbed thiophenol. In both cases several arguments for

[16] A mass spectrum of the benzene atmosphere can be found in appendix A.2

[17] The determined fit parameters are $A = 0.25$ and $\tau = 251$.

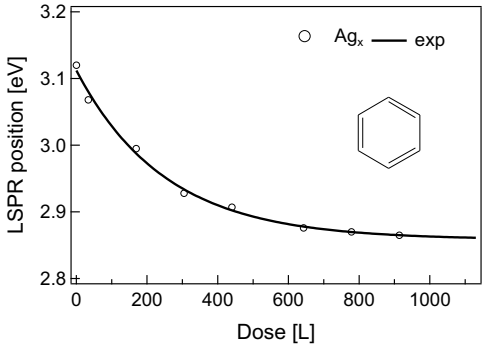

Figure 4.15.: Evolution of the LSPR position of unselected silver clusters under benzene exposure.

and against it do exist. In order to examine, if the formation of multilayers is responsible for the slow shift of the LSPR, cooled samples and samples held at room temperature of unselected silver clusters were exposed to thiophenol[18]. Assuming that thiophenol behaves similar to benzene, multilayers that might be present in the case of cooled samples should desorb at room temperature [187], resulting in a lower dielectric constant of the surrounding medium, which in turn should shift the LSPR. As can be seen from figure 4.16, experiments done at different temperatures result in almost identical extinction spectra, suggesting that no multilayers of thiophenol are formed under the present experimental conditions. This assumption is supported by the experimental observation, that the extinction spectrum of supported silver clusters saturated with thiophenol almost does not change, if stored in UHV for 24 h[19]. However it can not be excluded, that thiophenol

[18]As described in chapter 3.1, the temperature of the cooled sample is difficult to determine, therefore no exact temperature is given.

[19]See appendix A.2

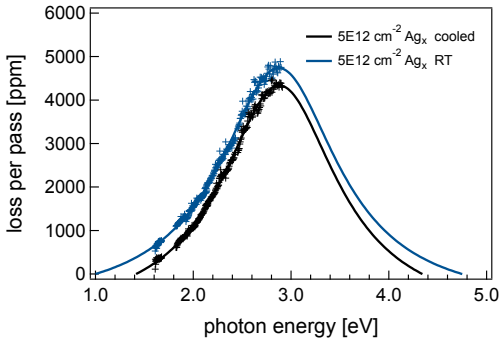

Figure 4.16.: Effect of sample temperature on the influence of thiophenol onto the extinction of supported silver clusters. Note that measurements of two individual samples with approximately the same coverage is shown.

physisorbed onto the SiO_2 substrate in the vicinity of supported clusters is responsible for the slow shift due an increased dielectric function of the surrounding. In particular it has been shown that the local electric field around supported silver clusters, if excited with light polarized parallel to the surface as it is the case in s-CRD experiments[20], is located close to the surface [112, 185]. The absence of a double exponential characteristic of the LSPR position if silver clusters are exposed to benzene however rather indicate, that the slow LSPR shift is caused by chemisorption, too. As can be taken from table 4.5 in the case of Ag_{55} the slow shift accounts for more than the half of the total LSPR shift. As described in section 2.3.1 and as can be seen from figure 2.11, a monolayer of thiophenol around Ag_{55} accounts for approximately 70% of the change in the dielectric function of the surrounding, if going from the value $\epsilon_m = 1$ for vacuum to $\epsilon_m = 2.1$

[20]Compare section 4.1

for a monlayer of thiophenol (bulk thiophenol has got a dielectric constant of $\epsilon_m = 2.5$). Because of the linear relation between the dielectric constant of the surrounding and the LSPR position, the fast LSPR shift caused by chemisorbed thiophenol should therefore cause the bigger share of the overall shift, in particular as chemisorbed thiophenol additionally includes the shift due to a reduced free electron density. In the case of Ag_{20} the slow shift accounts for a smaller share compared to the fast LSPR shift, in accordance with the assumption of physisorbed thiophenol. The fact that the amount of the slow shift is smaller in the case Ag_{20} compared to Ag_{55} could be explained with the fact, that the perturbation of the local electromagnetic field around metal clusters due to adsorbed ligands is more pronounced in the case of smaller particles [35]. Thus the sensing ability for dielectric constant changes in the surrounding of the clusters should be weaker in the case of Ag_{20}. Assuming that the slow LSPR shift is also caused by chemisorbed thiophenol, the two observed time regimes could be explained by different sticking probabilities of thiophenol onto different geometrical sites [36, 169] or by a sterically hindered closure of the ligand layer after the adsorption of the first molecules [180, 207]. However, in order to unambiguously assign the slow shift of the LSPR to physisorption or to chemisorption further temperature dependent experiments would be necessary, because in contrast to physisorption, chemisorption of thiophenol onto silver shows the expected, strong temperature dependence [199]. The comparison of experiments done with thiophenol and benzene indicates, that the bigger portion of the LSPR shift caused by the interactions with thiophenol is due to an increased dielectric constant of the surrounding

instead of a reduced electron density. In the case of unselected silver clusters thiophenol causes a shift of approximately 0.3 eV, whereas benzene causes a shift of approximately 0.2 eV. The interaction between benzene and silver was found to be very weak and can be described by physisorption character [29, 131], so it can be assumed, that the shift of 0.2 eV is due to an increased dielectric function of the surrounding. As can be taken from figure 2.10, a shift of 0.2 eV would be observed, if the dielectric constant of the surrounding is increased by a value of 0.8, which is in good agreement with a monolayer of benzene[21]. Because benzene has got a slightly smaller dielectric constant than thiophenol, at least 0.2 eV of the observed LSPR shift in the case of thiophenol should be caused by an increased dielectric function of the surrounding medium, implying only a small reduction of the free electron density inside the metal cluster. This might be the reason why after reaction with thiophenol the smaller Ag_{20} cluster is still located at higher energies than Ag_{55}, although the blueshift of the LSPR for a decreasing cluster size was found to reverse in the case of thiolate protected silver clusters due to the growing influence of the thiolate ligands [164, 190].

4.4. Thin Film Growth of π-conjugated Molecules

Besides the investigation of the optical properties of supported silver clusters, within this work the thin film growth of 1,4-Di-n-octyloxy-2,5-bis(pyren-1-

[21] Benzene has got a dielectric constant of $\epsilon_{benzene} = 2.1$, so in the case of a monolayer or a lose film a slightly smaller value should be considered

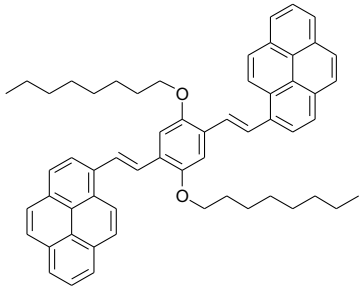

bis-pyrene

1,4-Di-n-octyloxy-2,5-bis(pyren-1-ylethenyl)benzene

Figure 4.17.: Structural chemical formula of the investigated bis-pyrene compound.

ylethenyl)benzene (bis-pyrene) was studied by means of s-CRD spectroscopy. In bis-pyrene two pyrene rings are bridged by a bis(vinylene)henylene unit, as can be seen in figure 4.17. It is known that such molecules have versatile electronic and optical properties, making them promising materials for organic photovoltaic (OPV) and organic light emitting diodes (OLED) [49, 119, 144]. In order to improve such devices it is mandatory to understand the thin film growth of π-conjugated molecules [119]. In figure 4.18 the absorption spectra of a thick bis-pyrene film evaporated onto a BK7 glass substrate and bis-pyrene in a THF solution (tetrahydrofuran) are shown. Both spectra exhibit a strong absorption at around 440 nm, which can be attributed to to the long-axis polarized ^1L_a transition [122, 124]. In the case of bis-pyrene in THF solution the peak is located at slightly higher wavelength, which can be attributed to a positive solvatochromism effect due to solvent molecules. The absorption spectrum of bis-pyrene in the molecular film exhibits additionally a shoulder located at around 505 nm. The fact that this shoulder is not present in the spectrum of bis-pyrene in solution suggests, that it is caused by interactions of the transition dipole moments

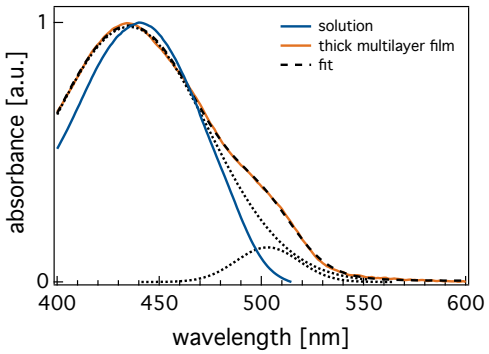

Figure 4.18.: Absorption Spectra of bis-pyrene in Solution and bis-pyrene deposited onto a BK7 Glass Substrate.

of neighboring molecules. In order to confirm this assumption figure 4.19 shows the coverage dependent evolution of the absorption spectrum of bis-pyrene evaporated onto BK7 glass substrates under UHV conditions. On the left hand side normalized spectra between coverages of $1.6 \cdot 10^{13} cm^{-2}$ and $1.2 \cdot 10^{14} cm^{-2}$ are presented in the wavelength range, where the shoulder is observed in the thick film spectrum. Note that the shown wavelength range is covered by a single CRD mirror pair, which minimizes the experimental error[22]. On the right hand side the complete s-CRD spectra of bis-pyrene coverages of $1.6 \cdot 10^{13} cm^{-2}$ and $1.2 \cdot 10^{14} cm^{-2}$ are depicted. It can clearly be seen, that the normalized intensity of the shoulder located at around 505 nm increases with the coverage and saturates above approximately $6.6 \cdot 10^{13} cm^{-2}$. Therefore the shoulder located at around 505 nm can clearly be assigned to interactions between bis-pyrene molecules in the thin film. The saturation of the intensity of the shoulder can be explained

[22]Compare section 4.3.2

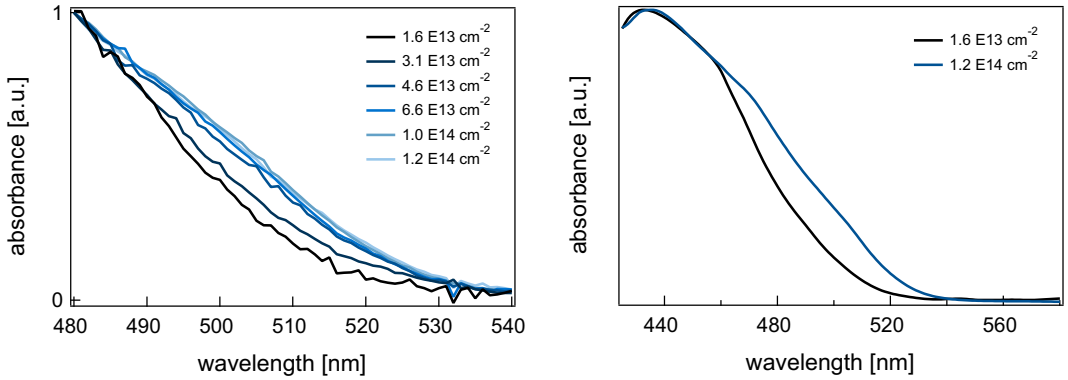

Figure 4.19.: Coverage dependent intensity evolution of the shoulder located at around 505 nm. On the right hand side full s-CRD absorption spectra of bis-pyrene supported onto a BK7 glass substrate with a coverage below and above a monolayer are depicted. Note that the molecular density of a full monolayer is approximately $3 \cdot 10^{13} cm^{-2}$

with a transition to a bulk like structure, in which additionally deposited molecules contribute equally to the increased intensity of the main peak and the shoulder respectively. However it is not clear whether the shoulder is due to interactions between molecules lying side by side or due to interaction between molecules stacked one above the other. By means of STM spectroscopy the molecular density of a full monolayer of bis-pyrene lying flat onto Au(111) was determined as approximately $3 \cdot 10^{13} cm^{-2}$ [119]. The facts, that at this coverage the shoulder has got a relative weak intensity and that the intensity of the shoulder saturates at twice that coverage suggests, that the shoulder is more likely caused by molecules stacked one above the other. As soon as the second monolayer of molecules is closed, additional molecules contribute equally to the intensity of both peaks and the intensity

of the shoulder saturates. In that case the observed intensity of the shoulder at a coverage of $3 \cdot 10^{13} cm^{-2}$ may be caused by molecules deposited on top of other molecules before the first monolayer is fully closed, or due to an inaccurate determination of the coverage with help of the quartz microbalance. However it can not be excluded, that the shoulder is due to interactions between molecules lying side by side. In that case it could be concluded, that bis-pyrene growth in islands onto BK7 glass and that the first monolayer is closed at a coverage of approximately $6.6 \cdot 10^{13} cm^{-2}$, because a fully closed monolayer would indicate the transition to the bulk like structure.

.

5. Summary and Outlook

In summary, this work presents studies on the plasmonic behavior of size-selected supported silver clusters by means of surface second harmonic generation spectroscopy and surface cavity ring-down spectroscopy under ultra high vacuum conditions. The energy of the plasmon resonance of supported silver clusters smaller than 1.5 nm is measured successfully for the first time. The plasmon resonance is shown to blue shift by ≈ 0.2 eV for a decreasing particle size from Ag_{55} to Ag_9. The measured shift is in quantitative agreement with a theoretical model based on Mie theory, which makes use of size dependent dielectric functions of silver nano clusters determined with DFT calculations [76, 134]. Interestingly a single plasmonic resonance is measured down to a cluster size of Ag_9, in contrast to studies on silver clusters embedded in rare gas matrices and in the gas phase [52, 116]. In the case of supported silver clusters the size dependent blue shift of the plasmon resonance known for bigger particles [34, 158] continues down to the small size limit and it is still possible to describe the resonance with classical Mie theory in combination with a free electron spill out [147]. Furthermore it is shown, that the plasmon resonance of

supported silver clusters shifts to lower energies by $\approx 0.3\,\mathrm{eV}$ and broadens, if samples are exposed to thiophenol, which can be attributed to the high affinity of silver to thiols [132]. The shift is in agreement with an increased dielectric constant of the surrounding medium [44] and a reduction of the free electron density inside the metal clusters [164]. However it could not conclusively clarified, if the observed impact on the plasmon resonance is due to a chemisorbed thiolate solely, or if weakly physisorbed thiophenol contribute to the shift, too. Two different approaches are conceivable with the available experimental setup in order to elucidate the chemical status of the adsorbed species. Firstly, the strong divergent temperature dependence of chemisorption and physisorption, which could be observed for the adsorption of thiophenol onto gold [199], may be used in order to assign the adsorption of thiophenol onto supported silver clusters to one of these processes. Secondly, the presence or absence of the S-H stretching band of thiophenol, which is located at around 2500 cm^{-1} and could be measured by near infrared CRD spectroscopy, may be used in order to identify the chemical status of the absorbed species [18, 132]. Not only the chemical status of thiophenol could be elucidated by near infrared CRD spectroscopy but also the chemical status of other adsorbates. It has been shown, that the experimental setup has sub-monolayer sensitivity [119, 193], therefore the identification of adsorbed molecules should be possible. Sum-frequency generation spectroscopy (SFG) may be another possibility to identify adsorbed molecules and would require only slight modifications of the existing experimental setup after an extension of the existing laser-system to the IR. Sum-frequency generation is highly surface-specific and accordingly has

been developed into a powerful surface spectroscopic tool [183, 184]. In a typical setup with a picosecond-laser system the laser pumps an optical parametric amplifier to generate a tunable IR beam, which overlaps with the second harmonic output from the laser on the sample surface [182]. The generated sum-frequency signal could be detected with a photodetector.
A hot topic within cluster science are chiral metal nanoparticles, since optical activity located in metal based transitions was shown the first time for monolayer protected gold clusters by means of CD spectroscopy (circular dichroism) [55, 68, 191]. It has been shown, that chiral ligands can asymmetrize the metal core in a chiral fashion and that the chirooptical properties depend on many factors like the particle material and size, the used ligand and the number of ligands. However, optical activity was not measured in the case of supported metal nanoparticles up to now, due to the low surface coverages required to avoid agglomeration and the small excitation cross section of particles containing only a few tens of atoms in combination with small CD effects present in such systems. Fortunately linear CD spectroscopy has got a nonlinear analog and it has been shown that SHG-CD spectroscopy (second harmonic generation circular dichroism) has got the power to measure surface chirality with sub monolayer sensitivity [26, 27, 196]. The presented experimental setup was already used to investigate chiral surfaces made of enantiomerically pure 1,1'-bi-2-naphthol [78] and therefore offers all that is necessary in order to investigate chirality in supported metal clusters under controlled conditions. However, within this work it has been shown, that supported silver clusters covered by organic molecules do not contribute to the generation of second harmonic light,

which can be attributed to a reduced polarizability of the free electrons inside the metal cluster [74, 104]. Since SH intensity is mandatory for SHG-CD spectroscopy, different concepts have to be used in order to asmmetrize supported metal clusters. A possible approach may be the deposition of metal clusters on top of a chiral substrate, so that the particle surface is only partially covered by molecules. For example it has been shown that gold clusters can be soft landed onto a thiol self assembled monolayer without sinking into the molecular film [41, 201]. However it should be noted, that thiol based self assembled monolayers are usually formed onto gold films and that the used spectroscopic setup is build in order to measure samples in transmissions. In order to keep the transmittance of the samples as high as possible, the gold films has to be kept as thin as possible, or transparent SiO_2 may be functionalized directly by silanization, alternatively [88].

Appendix

Appendix A.

Experimental Results

In this part of the appendix additional informations regarding chapter 4 are given. In the first part additional information corresponding to section 4.3.1 are presented. The second part regards to section 4.3.2.
In figure A.1 it is shown that the SHG signal of supported silver clusters is almost not altered, if the sample is held in the preparation chamber for the duration of a typical evaporation process without dosing molecules. Figures A.2, A.3 and A.4 demonstrate, that the SHG signal is lost, if the samples are exposed to glutathione (SGH), 2-aza[6]helicene (helicene) and thiophenol, respectively, which can be attributed to a reduced hyperpolarizability of free conduction electrons inside the cluster caused by cluster molecule interactions.
Figure A.5 demonstrates, that the extinction spectrum of supported silver clusters is not altered, if the sample is exposed to the base pressure of

the preparation chamber for the duration of a typical evaporation process. Figure A.6 shows the evolution of the extinction spectrum of size selected Ag_{20} and Ag_{55} clusters under exposure to thiophenol. Figure A.7 shows, that the extinction spectrum of supported silver clusters saturated with thiophenol almost does not change, if the sample is stored in UHV for 24 hours. The right hand side of A.7 further demonstrates, that the extinction spectrum of a cluster sample saturated with thiophenol does not change significantly if the sample is further exposed to thiophenol, indicating that no multilayr adsorption of thiophenol takes place. Figure A.8 demonstrates the reproducibility of CRD measurements on the basis of three individual samples of Ag_{55} clusters exposed to thiophenol. Figure A.9 demonstrates the reproducibility of the adsorption kinetic of thiophenol on supported silver clusters on the basis of two individual Ag_{55} samples. Figure A.10 shows mass spectra of the background in the preparation chamber during exposure of cluster samples to thiophenol and benzene. In the thiophenol spectrum the characteristic peaks around 110, 84, 66, 51, 45 and 39 amu can be seen. In the benzene spectrum the characteristic peaks around 78, 63, 51, 39 and 26 amu can be seen.

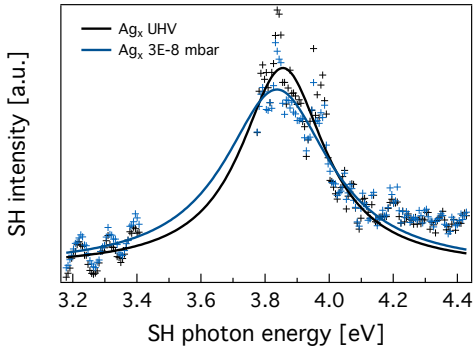

Figure A.1.: SHG Extinction spectra of Supported Silver Clusters before (black) and after (blue) Exposure to the Base Pressure of the Preparation Chamber.

A.1. SHG Studies

A.2. CRD Studies

.

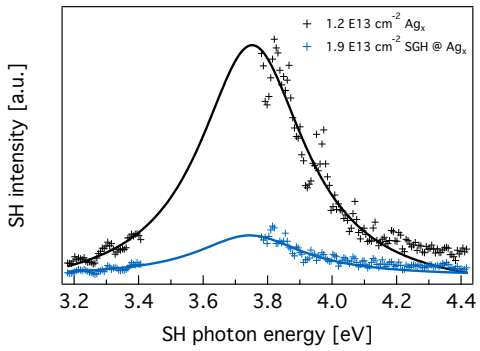

Figure A.2.: Loss of SHG Signal of Supported Silver Clusters due to Exposure to Glutathione.

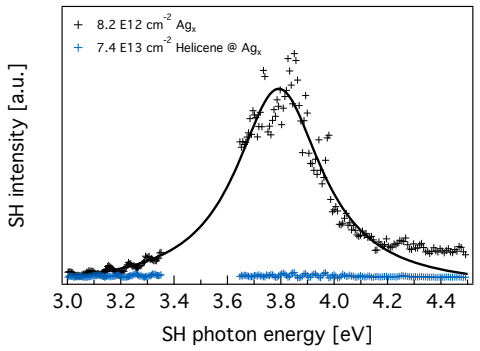

Figure A.3.: Loss of SHG Signal of Supported Silver Clusters due to Exposure to 2-aza[6]helicene.

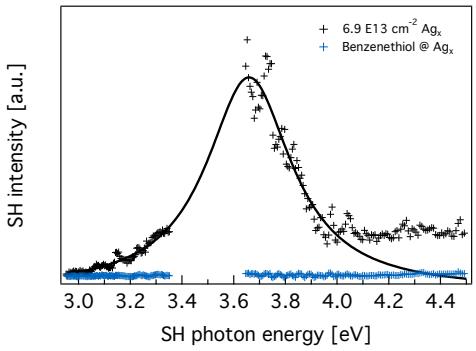

Figure A.4.: Loss of SHG Signal of Supported Silver Clusters due to Exposure to thiophenol.

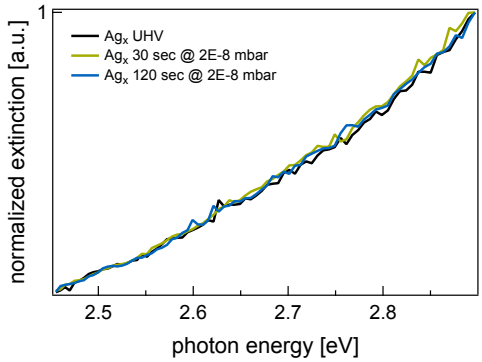

Figure A.5.: CRD Extinction Spectra of Supported Silver Clusters before (black) and after (green, blue) Exposure to the Base Pressure of the Preparation Chamber.

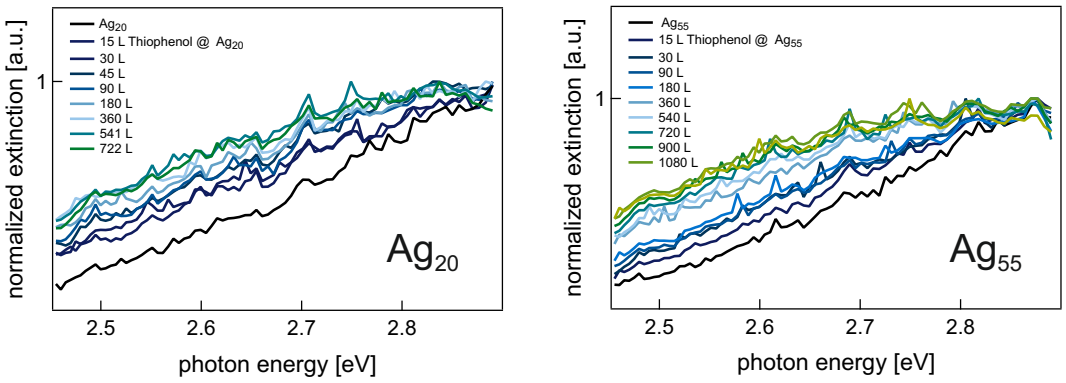

Figure A.6.: Evolution of the Extinction Spectrum of Ag_{20} and Ag_{55} Clusters under Exposure to Thiophenol.

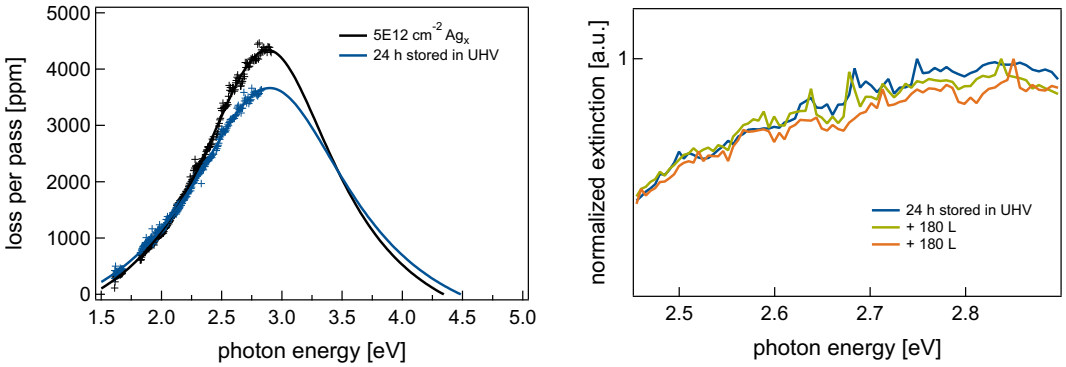

Figure A.7.: Time Behavior of the Extinction Spectrum of Supported Silver Clusters saturated with Thiophenol.

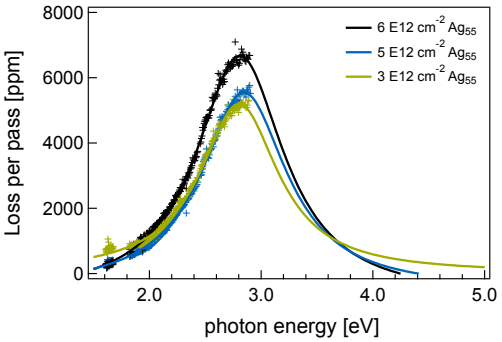

Figure A.8.: Reproducibility of CRD Measurements.

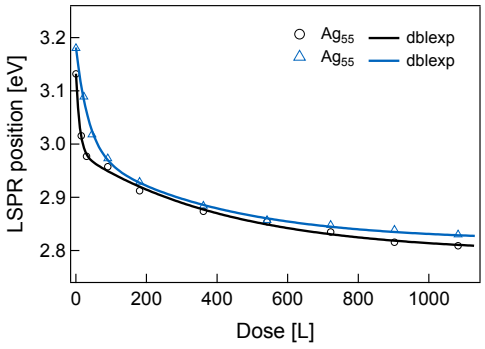

Figure A.9.: Reproducibility of the Adsorption Kinetic of Thiophenol on Supported Silver Clusters.

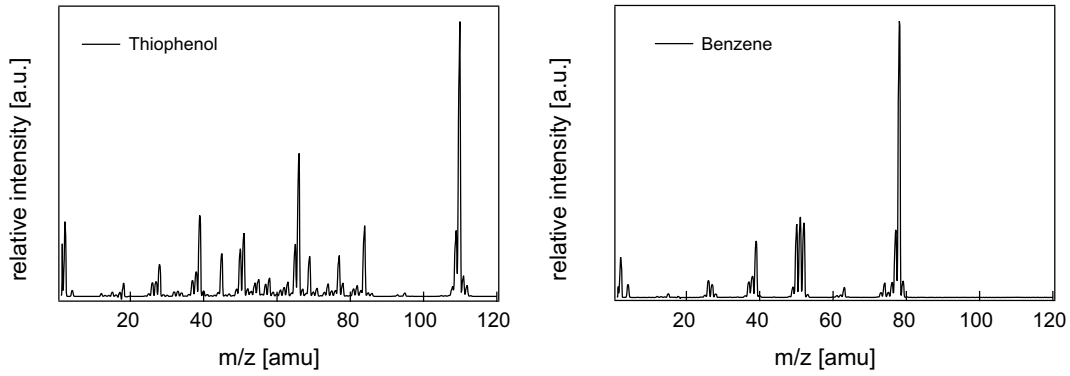

Figure A.10.: Mass Spectra of the Background in the Preparation Chamber during Exposure of Cluster Samples to Thiophenol and Benzene.

Bibliography

[1] L. G. AbdulHalim, N. Kothalawala, L. Sinatra, A. Dass, and O. M. Bakr. Neat and complete: Thiolate-ligand exchange on a silver molecular nanoparticle. *Journal of the American Chemical Society*, 136(45):15865–15868, 2014. PMID: 25345688.

[2] R. L. Aggarwal, L. W. Farrar, and S. K. Saikin. Increase of sers signal upon heating or exposure to a high-intensity laser field: Benzenethiol on an agfon substrate. *The Journal of Physical Chemistry C*, 116(31):16656–16659, 2012.

[3] C. M. Aikens, S. Li, and G. C. Schatz. From discrete electronic states to plasmons: Tddft optical absorption properties of ag n (n = 10, 20, 35, 56, 84, 120) tetrahedral clusters. *The Journal of Physical Chemistry C*, 112(30):11272–11279, 2008.

[4] P. Albella, B. Garcia-Cueto, F. González, F. Moreno, P. C. Wu, T.-H. Kim, A. Brown, Y. Yang, H. O. Everitt, and G. Videen. Shape matters:

Plasmonic nanoparticle shape enhances interaction with dielectric substrate. *Nano Letters*, 11(9):3531–3537, 2011. PMID: 21848270.

[5] Allen C. Templeton, Jeremy J. Pietron, Royce W. Murray, *, , and Paul Mulvaney*. Solvent refractive index and core charge influences on the surface plasmon absorbance of alkanethiolate monolayer-protected gold clusters. *The Journal of Physical Chemistry B*, 104(3):564–570, 2000.

[6] Alyson V. Whitney, Jeffrey W. Elam, Shengli Zou, §. Alex V. Zinovev, Peter C. Stair, George C. Schatz, , and Richard P. Van Duyne*. Localized surface plasmon resonance nanosensor: a high-resolution distance-dependence study using atomic layer deposition. *The Journal of Physical Chemistry B*, 109(43):20522–20528, 2005. PMID: 16853656.

[7] I. Ament, J. Prasad, A. Henkel, S. Schmachtel, and C. Sönnichsen. Single unlabeled protein detection on individual plasmonic nanoparticles. *Nano Letters*, 12(2):1092–1095, 2012. PMID: 22268768.

[8] D. Z. Anderson, J. C. Frisch, and C. S. Masser. Mirror reflectometer based on optical cavity decay time. *Appl. Opt.*, 23(8):1238–1245, Apr 1984.

[9] Antoine.

[10] Arnim Henglein*, , and D. Meisel†. Spectrophotometric observations of the adsorption of organosulfur compounds on colloidal silver

nanoparticles. *The Journal of Physical Chemistry B*, 102(43):8364–8366, 1998.

[11] H. A. Atwater and A. Polman. Plasmonics for improved photovoltaic devices. *Nat Mater*, 9(3):205–13, Mar 2010.

[12] H. Baida, P. Billaud, S. Marhaba, D. Christofilos, E. Cottancin, A. Crut, J. Lermé, P. Maioli, M. Pellarin, M. Broyer, N. D. Fatti, F. Vallée, A. Sánchez-Iglesias, I. Pastoriza-Santos, and L. M. Liz-Marzán. Quantitative determination of the size dependence of surface plasmon resonance damping in single ag@sio2 nanoparticles. *Nano Letters*, 9(10):3463–3469, 2009. PMID: 19719148.

[13] O. Bakr, V. Amendola, C. Aikens, W. Wenseleers, R. Li, L. DalNegro, G. Schatz, and F. Stellacci. Silver nanoparticles with broad multiband linear optical absorption. *Angewandte Chemie International Edition*, 48(32):5921–5926, 2009.

[14] N. G. Bastús, J. Piella, and V. Puntes. Quantifying the sensitivity of multipolar (dipolar, quadrupolar, and octapolar) surface plasmon resonances in silver nanoparticles: The effect of size, composition, and surface coating. *Langmuir*, 32(1):290–300, 2016. PMID: 26649600.

[15] D. Bedeaux and J. Vlieger. *Optical Properties of Surfaces*. Imperial College Press: London, 2001.

[16] C. Beitia, Y. Borensztein, R. Lazzari, J. Nieto, and R. G. Barrera. Substrate-induced multipolar resonances in supported free-electron metal spheres. *Phys. Rev. B*, 60:6018–6022, Aug 1999.

[17] G. Berden, R. Peeters, and G. Meijer. Cavity ring-down spectroscopy: Experimental schemes and applications. *International Reviews in Physical Chemistry*, 19(4):565–607, 2000.

[18] K. B. Biggs, J. P. Camden, J. N. Anker, and R. P. Van Duyne. Surface-enhanced raman spectroscopy of benzenethiol adsorbed from the gas phase onto silver film over nanosphere surfaces: † determination of the sticking probability and detection limit time. *The Journal of Physical Chemistry A*, 113:4581–4586, 2009.

[19] P. B.N.J. Polarizability of small spherical metal particles: influence of the matrix environment. *Surface Science*, 281:153–162, 1993.

[20] C. F. Bohren and D. R. Huffman. *Absorption and Scattering of Light by Small Particles*. WILEY-VCH Verlag, 1998.

[21] M. S. Bootharaju, V. M. Burlakov, T. M. D. Besong, C. P. Joshi, L. G. AbdulHalim, D. M. Black, R. L. Whetten, A. Goriely, and O. M. Bakr. Reversible size control of silver nanoclusters via ligand-exchange. *Chemistry of Materials*, 27(12):4289–4297, 2015.

[22] R. W. Boyd. *Nonlinear Optics*. Elsevier Science, 2008.

[23] P.-F. Brevet. *Surface Second Harmonic Generation*. Presses polytechniques et universitaires romandes, 1997.

[24] K. Bromann, C. Félix, H. Brune, W. Harbich, R. Monot, J. Buttet, and K. Kern. Controlled deposition of size-selected silver nanoclusters. *Science*, 274(5289):956–958, 1996.

[25] M. Brust, M. Walker, D. Bethell, D. J. Schiffrin, and R. Whyman. Synthesis of thiol-derivatised gold nanoparticles in a two-phase liquid-liquid system. *J. Chem. Soc., Chem. Commun.*, pages 801–802, 1994.

[26] J. D. Byers, H. I. Yee, and J. M. Hicks. A second harmonic generation analog of optical rotatory dispersion for the study of chiral monolayers. *The Journal of Chemical Physics*, 101(7):6233–6241, 1994.

[27] J. D. Byers, H. I. Yee, T. Petralli-Mallow, and J. M. Hicks. Second-harmonic generation circular-dichroism spectroscopy from chiral monolayers. *Phys. Rev. B*, 49:14643–14647, May 1994.

[28] A. Capretti, E. F. Pecora, C. Forestiere, L. Dal Negro, and G. Miano. Size-dependent second-harmonic generation from gold nanoparticles. *Phys. Rev. B*, 89:125414, Mar 2014.

[29] J. Carrasco, W. Liu, A. Michaelides, and A. Tkatchenko. Insight into the description of van der waals forces for benzene adsorption on transition metal (111) surfaces. *The Journal of Chemical Physics*, 140(8), 2014.

[30] N. Cathcart and V. Kitaev. Silver nanoclusters: Single-stage scaleable synthesis of monodisperse species and their chirooptical properties. *The Journal of Physical Chemistry C*, 114(38):16010–16017, 2010.

[31] . Catherine J. Murphy, T. K. Sau, A. M. Gole, C. J. Orendorff, J. Gao, L. Gou, S. E. Hunyadi, , and T. Li. Anisotropic metal nanoparticles: synthesis, assembly, and optical applications. *The Journal of Physical Chemistry B*, 109(29):13857–13870, 2005. PMID: 16852739.

[32] I. Chakraborty, J. Erusappan, A. Govindarajan, K. S. Sugi, T. Udayabhaskararao, A. Ghosh, and T. Pradeep. Emergence of metallicity in silver clusters in the 150 atom regime: a study of differently sized silver clusters. *Nanoscale*, 6(14):8024–31, Jul 2014.

[33] R. Chapman and P. Mulvaney. Electro-optical shifts in silver nanoparticle films. *Chemical Physics Letters*, 349(5–6):358 – 362, 2001.

[34] K.-P. Charle, W. Schulze, and B. Winter. The size dependent shift of the surface plasmon absorption band of small spherical metal particles. *Zeitschrift für Physik D Atoms, Molecules and Clusters*, 12(1-4):471–475, 1989.

[35] X. Chen, J. E. Moore, M. Zekarias, and L. Jensen. Atomistic electrodynamics simulations of bare and ligand-coated nanoparticles in the quantum size regime. *Nat Commun*, 6, 11 2015.

[36] H. Cheng[dagger], L. Yang[dagger], Y. Jiang, Y. Huang, Z. Sun, J. Zhang, T. Hu, Z. Pan, G. Pan, T. Yao, Q. Bian, and S. Wei. Adsorption kinetic process of thiol ligands on gold nanocrystals. *Nanoscale*, 5:11795–11800, 2013.

[37] P. Christopher, H. Xin, and S. Linic. Visible-light-enhanced catalytic oxidation reactions on plasmonic silver nanostructures. *Nat Chem*, 3(6):467–472, 06 2011.

[38] C. Clavero. Plasmon-induced hot-electron generation at nanoparticle/metal-oxide interfaces for photovoltaic and photocatalytic devices. *Nat Photon*, 8(2):95–103, 02 2014.

[39] C. L. Cleveland and U. Landman. Dynamics of cluster-surface collisions. *Science*, 257(5068):pp. 355–361, 1992.

[40] R. Corn and D. Higgins. Optical second harmonic generation as a probe of surface chemistry. *Chemical Reviews*, 94:107–125, 1994.

[41] L. Costelle, T. T. Järvi, M. T. Räisänen, V. Tuboltsev, and J. Räisänen. Binding of deposited gold clusters to thiol self-assembled monolayers on au(111) surfaces. *Applied Physics Letters*, 98(4):–, 2011.

[42] A. Curry, G. Nusz, A. Chilkoti, and A. Wax. Substrate effect on refractive index dependence of plasmon resonance for individual silver nanoparticles observed using darkfield micro-spectroscopy. *Opt. Express*, 13(7):2668–2677, Apr 2005.

[43] A. Dass. Nano-scaling law: geometric foundation of thiolated gold nanomolecules. *Nanoscale*, 4:2260–2263, 2012.

[44] J. David D. Evanoff, R. L. White, , and G. Chumanov*. Measuring the distance dependence of the local electromagnetic field from silver nanoparticles. *The Journal of Physical Chemistry B*, 108(5):1522–1524, 2004.

[45] W. A. de Heer. The physics of simple metal clusters: experimental aspects and simple models. *Rev. Mod. Phys.*, 65:611–676, Jul 1993.

[46] W. Demtröder. *Experimentalphysik 3*. Springer, 1996.

[47] A. Desireddy, B. E. Conn, J. Guo, B. Yoon, R. N. Barnett, B. M. Monahan, K. Kirschbaum, W. P. Griffith, R. L. Whetten, U. Landman, and T. P. Bigioni. Ultrastable silver nanoparticles. *Nature*, 501(7467):399–402, 09 2013.

[48] B. M. DeVetter, P. Mukherjee, C. J. Murphy, and R. Bhargava. Measuring binding kinetics of aromatic thiolated molecules with nanoparticles via surface-enhanced raman spectroscopy. *Nanoscale*, 7:8766–8775, 2015.

[49] A. Facchetti. -conjugated polymers for organic electronics and photovoltaic cell applications. *Chemistry of Materials*, 23(3):733–758, 2011.

[50] M. Farrag, M. Thaemer, M. Tschurl, T. Buergi, and U. Heiz. Preparation and spectroscopic properties of monolayer-protected silver nanoclusters. *J. Phys. Chem. C*, 116(14):8034–8043, 2012.

[51] S. Fedrigo, W. Harbich, J. Belyaev, and J. Buttet. Evidence for electronic shell structure of small silver clusters in the optical absorption spectra. *Chemical Physics Letters*, 211(2–3):166 – 170, 1993.

[52] S. Fedrigo, W. Harbich, and J. Buttet. Collective dipole oscillations in small silver clusters embedded in rare-gas matrices. *Phys. Rev. B*, 47:10706–10715, Apr 1993.

[53] Felicia Tam, Cristin Moran, , and §. Naomi Halas*, ‡. Geometrical parameters controlling sensitivity of nanoshell plasmon resonances to changes in dielectric environment. *The Journal of Physical Chemistry B*, 108(45):17290–17294, 2004.

[54] M. Finazzi, P. Biagioni, M. Celebrano, and L. Duò. Selection rules for second-harmonic generation in nanoparticles. *Phys. Rev. B*, 76:125414, Sep 2007.

[55] C. Gautier and T. Bürgi. Chiral gold nanoparticles. *Chemphyschem*, 10(3):483–92, Feb 2009.

[56] C. Gautier, R. Taras, S. Gladiali, and T. Bürgi. Chiral 1,1-binaphthyl-2,2-dithiol-stabilized gold clusters: Size separation and optical activity in the uv–vis. *Chirality*, 20(3-4):486–493, 2008.

[57] S. K. Ghosh, S. Nath, S. Kundu, Kunio Esumi, , and T. Pal*. Solvent and ligand effects on the localized surface plasmon resonance (lspr) of gold colloids. *The Journal of Physical Chemistry B*, 108(37):13963–13971, 2004.

[58] S. Gilb, K. Hartl, A. Kartouzian, J. Peter, U. Heiz, H. G. Boyen, and P. Ziemann. Cavity ring-down spectroscopy of metallic gold nanoparticles. *Eur. Phys. J. D*, 45(3):501–506, 2007. CAN 148:248949 73-4 Optical, Electron, and Mass Spectroscopy and Other Related Properties Lehrstuhl fuer Physikalische Chemie I, Technische Universitaet Muenchen, Garching, Germany. Journal 1434-6060 7440-57-5 (Gold) Role: PEP (Physical, engineering or chemical process), PRP (Properties), PROC (Process) (cavity ring-down spectroscopy of metallic Au nanoparticles).

[59] C. Goldmann, R. Lazzari, X. Paquez, C. Boissière, F. Ribot, C. Sanchez, C. Chanéac, and D. Portehault. Charge transfer at hybrid interfaces: Plasmonics of aromatic thiol-capped gold nanoparticles. *ACS Nano*, 9(7):7572–7582, 2015. PMID: 26161962.

[60] E. Gross, J. H. Liu, S. Alayoglu, M. A. Marcus, S. C. Fakra, F. D. Toste, and G. A. Somorjai. Asymmetric catalysis at the mesoscale: Gold nanoclusters embedded in chiral self-assembled monolayer as heterogeneous catalyst for asymmetric reactions. *Journal of the American Chemical Society*, 135(10):3881–3886, 2013.

[61] E. B. Guidez and C. M. Aikens. Quantum mechanical origin of the plasmon: from molecular systems to nanoparticles. *Nanoscale*, 6:11512–11527, 2014.

[62] H. Haberland. Looking from both sides. *Nature*, 494(7435):E1–E2, 02 2013.

[63] A. J. Haes, , and R. P. V. Duyne*. A nanoscale optical biosensor: sensitivity and selectivity of an approach based on the localized surface plasmon resonance spectroscopy of triangular silver nanoparticles. *Journal of the American Chemical Society*, 124(35):10596–10604, 2002. PMID: 12197762.

[64] A. J. Haes and R. P. Van Duyne. A unified view of propagating and localized surface plasmon resonance biosensors. *Anal Bioanal Chem*, 379(7-8):920–30, Aug 2004.

[65] A. J. Haes, S. Zou, . George C. Schatz, , and R. P. V. Duyne*. Nanoscale optical biosensor: short range distance dependence of the localized surface plasmon resonance of noble metal nanoparticles. *The Journal of Physical Chemistry B*, 108(22):6961–6968, 2004.

[66] A. J. Haes, S. Zou, G. C. Schatz, , and R. P. V. Duyne*. A nanoscale optical biosensor: the long range distance dependence of the localized surface plasmon resonance of noble metal nanoparticles. *The Journal of Physical Chemistry B*, 108(1):109–116, 2004.

[67] H. Häkkinen. Atomic and electronic structure of gold clusters: understanding flakes, cages and superatoms from simple concepts. *Chem Soc Rev*, 37(9):1847–59, Sep 2008.

[68] T. T. . H. Häkkinen. *Protected Metal Clusters: From Fundamentals to Applications*. Elsevier, 2015.

[69] E. Hao and G. C. Schatz. Electromagnetic fields around silver nanoparticles and dimers. *The Journal of Chemical Physics*, 120(1):357–366, 2004.

[70] M. Harb, F. Rabilloud, and D. Simon. Optical response of silver nanoclusters complexed with aromatic thiol molecules: a time-dependent density functional study. *Journal of Physics B: Atomic, Molecular and Optical Physics*, 44(3):035101, 2011.

[71] M. Harb, F. Rabilloud, D. Simon, A. Rydlo, S. Lecoultre, F. Conus, V. Rodrigues, and C. Félix. Optical absorption of small silver clusters: Agn, (n=4–22). *The Journal of Chemical Physics*, 129(19):–, 2008.

[72] W. Harbich, S. Fedrigo, and J. Buttet. The optical absorption spectra of small silver clusters (n=5–11) embedded in argon matrices. *Chemical Physics Letters*, 195(5–6):613 – 617, 1992.

[73] W. Harbich, S. Fedrigo, and J. Buttet. The optical absorption spectra of small silver clusters (n=8,äì39) embedded in rare gas matrices. *Zeitschrift für Physik D Atoms, Molecules and Clusters*, 26(1):138–140, 1993.

[74] Y. E. Harfouch, E. Benichou, F. Bertorelle, I. Russier-Antoine, C. Jonin, N. Lascoux, and P. F. Brevet. Effect of a thioalkane capping layer on the first hyperpolarizabilities of gold and silver nanoparticles. *Journal of Physics: Condensed Matter*, 24(12):124104, 2012.

[75] K. M. Harkness, Y. Tang, A. Dass, J. Pan, N. Kothalawala, V. J. Reddy, D. E. Cliffel, B. Demeler, F. Stellacci, O. M. Bakr, and J. A. McLean. Ag44(sr)304-: a silver-thiolate superatom complex. *Nanoscale*, 4:4269–4274, 2012.

[76] Y. He and T. Zeng. First-principles study and model of dielectric functions of silver nanoparticles. *The Journal of Physical Chemistry C*, 114(42):18023–18030, 2010.

[77] P. Heister. *Nonlinear Spectroscopy of Supported Size-Selected Silver Clusters (n=9-55) and Supported Chiral 2,2'-Dihydroxy-1,1'-Binaphthy (Binol) Molecules*. PhD thesis, Technische Universität München, 2014.

[78] P. Heister, T. Lunskens, M. Thamer, A. Kartouzian, S. Gerlach, T. Verbiest, and U. Heiz. Orientational changes of supported chiral 2,2[prime or minute]-dihydroxy-1,1[prime or minute]binaphthyl molecules. *Phys. Chem. Chem. Phys.*, 16:7299–7306, 2014.

[79] U. Heiz, F. Vanolli, L. Trento, and W.-D. Schneider. Chemical reactivity of size-selected supported clusters: An experimental setup. *Review of Scientific Instruments*, 65:1986–1994, 1997.

[80] C. Hendrich, J. Bosbach, F. Stietz, F. Hubenthal, T. Vartanyan, and F. Träger. Chemical interface damping of surface plasmon excitation in metal nanoparticles: Chemical interface damping of surface plasmon excitation in metal nanoparticlesa study by persistent spectral hole burning: a study by persistent spectral hole burning. *Appl. Phys. B*, 76:869–875, 2003.

[81] A. Henglein. Physicochemical properties of small metal particles in solution: "microelectrode" reactions, chemisorption, composite metal particles, and the atom-to-metal transition. *The Journal of Physical Chemistry*, 97(21):5457–5471, 1993.

[82] J. M. Herbelin, J. A. McKay, M. A. Kwok, R. H. Ueunten, D. S. Urevig, D. J. Spencer, and D. J. Benard. Sensitive measurement of photon lifetime and true reflectances in an optical cavity by a phase-shift method. *Appl. Opt.*, 19(1):144–147, Jan 1980.

[83] F. Hidalgo and C. Noguez. Optical activity of achiral ligand sch3 adsorbed on achiral ag55 clusters: Relationship between adsorption site and circular dichroism. *ACS Nano*, 7(1):513–521, 2013. PMID: 23256525.

[84] A. Hilger, N. Cüppers, M. Tenfelde, and U. Kreibig. Surface and interface effects in the optical properties of silver nanoparticles. *The European Physical Journal D - Atomic, Molecular, Optical and Plasma Physics*, 10(1):115–118.

[85] A. Hilger, M. Tenfelde, and U. Kreibig. Silver nanoparticles deposited on dielectric surfaces. *Applied Physics B*, 73(4):361–372.

[86] H. Hövel, S. Fritz, A. Hilger, U. Kreibig, and M. Vollmer. Width of cluster plasmon resonances: Bulk dielectric functions and chemical interface damping. *Phys. Rev. B*, 48:18178–18188, Dec 1993.

[87] H. Hövel, A. Hilger, I. Nusch, and U. Kreibig. Experimental determination of deposition induced cluster deformation. *Zeitschrift für Physik D Atoms, Molecules and Clusters*, page 203, 208 1997.

[88] J. A. Howarter and J. P. Youngblood. Optimization of silica silanization by 3-aminopropyltriethoxysilane. *Langmuir*, 22(26):11142–11147, 2006. PMID: 17154595.

[89] C. Hubert, L. Billot, P.-M. Adam, R. Bachelot, P. Royer, J. Grand, D. Gindre, K. D. Dorkenoo, and A. Fort. Role of surface plasmon in second harmonic generation from gold nanorods. *Applied Physics Letters*, 90(18):–, 2007.

[90] A. Iline, M. Simon, F. Stietz, and F. Träger. Adsorption of molecules on the surface of small metal particles studied by optical spectroscopy. *Surface Science*, 436(1–3):51 – 62, 1999.

[91] P. D. Jadzinsky, G. Calero, C. J. Ackerson, D. A. Bushnell, and R. D. Kornberg. Structure of a thiol monolayer-protected gold nanoparticle at 1.1 å resolution. *Science*, 318(5849):pp. 430–433, 2007.

[92] P. K. Jain, W. Huang, and M. A. El-Sayed. On the universal scaling behavior of the distance decay of plasmon coupling in metal nanoparticle pairs: A plasmon ruler equation. *Nano Letters*, 7(7):2080–2088, 2007.

[93] T. R. Jensen, M. L. Duval, K. L. Kelly, A. A. Lazarides, George C. Schatz, *, , and Richard P. Van Duyne*. Nanosphere lithography: effect of the external dielectric medium on the surface plasmon resonance spectrum of a periodic array of silver nanoparticles. *The Journal of Physical Chemistry B*, 103(45):9846–9853, 1999.

[94] P. Johnson and R. Christy. Optical constants of the noble metals. *Phys. Rev. B*, 6:4370–4379, Dec 1972.

[95] B. K. Juluri, J. Huang, and L. Jensen. Extinction, scattering and absorption efficiencies of single and multilayer nanoparticles, Jan 2016.

[96] A. Kartouzian. *Optical properties of size-selected supported metal clusters measured by cavity ring-down spectroscopy*. PhD thesis, Technische Universität München, 2010.

[97] A. Kartouzian, P. Heister, M. Thämer, S. Gerlach, and U. Heiz. Inline reference measurement for surface second harmonic generation spectroscopy. *Journal of the Optical Society of America B*, 30:541, 2013.

[98] A. Kartouzian, M. Thaemer, T. Soini, J. Peter, P. Pitschi, S. Gilb, and U. Heiz. Cavity ring-down spectrometer for measuring the optical

response of supported size-selected clusters and surface defects in ultrahigh vacuum. *J. Appl. Phys.*, 104(12):124313/1–124313/8, 2008. CAN 150:225978 73-11 Optical, Electron, and Mass Spectroscopy and Other Related Properties Lehrstuhl fuer Physikalische Chemie, Technische Universitaet Muenchen, Garching, Germany. Journal 0021-8979 81-88-9 (Rhodamine B); 7440-02-0 (Nickel); 47367-75-9 (Oxazine 1); 55804-67-6 (Coumarin 334) Role: ANT (Analyte), ANST (Analytical study) (cavity ring-down spectrometer for measuring the optical response of supported size-selected clusters and surface defects in ultrahigh vacuum).

[99] K. L. Kelly, E. Coronado, L. L. Zhao, and G. C. Schatz. The optical properties of metal nanoparticles: the influence of size, shape, and dielectric environment. *The Journal of Physical Chemistry B*, 107(3):668–677, 2003.

[100] S. A. Khan, D. Senapati, T. Senapati, P. Bonifassi, Z. Fan, A. K. Singh, A. Neeley, G. Hill, and P. C. Ray. Size dependent nonlinear optical properties of silver quantum clusters. *Chemical Physics Letters*, 512(1–3):92 – 95, 2011.

[101] Y. Kitaguchi, S. Habuka, T. Mitsui, H. Okuyama, S. Hatta, and T. Aruga. Comparative study of phenol and thiophenol adsorption on cu(110). *The Journal of Chemical Physics*, 139(4), 2013.

[102] K. Kneipp, Y. Wang, H. Kneipp, L. T. Perelman, I. Itzkan, R. R. Dasari,

and M. S. Feld. Single molecule detection using surface-enhanced raman scattering (sers). *Phys. Rev. Lett.*, 78:1667–1670, Mar 1997.

[103] M. W. Knight, Y. Wu, J. B. Lassiter, P. Nordlander, and N. J. Halas. Substrates matter: Influence of an adjacent dielectric on an individual plasmonic nanoparticle. *Nano Letters*, 9(5):2188–2192, 2009. PMID: 19361166.

[104] S. Knoppe, H. Häkkinen, and T. Verbiest. Nonlinear optical properties of thiolate-protected gold clusters: A theoretical survey of the first hyperpolarizabilities. *The Journal of Physical Chemistry C*, 119:27676–27682, 2015.

[105] U. Kreibig and M. Vollmer. *Optical Properties of Metal Clusters*. Springer, 1995.

[106] V. V. Kresin. Collective resonances and response properties of electrons in metal clusters. *Physics Reports*, 220(1):1 – 52, 1992.

[107] R. B. Kress, E. N. Duesler, M. C. Etter, I. C. Paul, and D. Y. Curtin. Solid-state resolution of binaphthyl: crystal and molecular structures of the chiral (a)1 form and racemic (b)1 form and the study of the rearrangement of single crystals. requirements for development of hemihedral faces for enantiomer identification. *Journal of the American Chemical Society*, 102(26):7709–7714, 1980.

[108] S. Kumar, M. D. Bolan, and T. P. Bigioni. Glutathione-stabilized magic-number silver cluster compounds. *Journal of the American Chemical Society*, 132(38):13141–13143, 2010.

[109] K. Laaksonen, S. Suomela, S. Puisto, N. Rostedt, T. Ala-Nissila, and R. Nieminen. Influence of high-refractive-index oxide coating on optical properties of metal nanoparticles. *J. Opt. Soc. Am. B*, 30(2):338, 2013.

[110] J. B. Lassiter, J. Aizpurua, L. I. Hernandez, D. W. Brandl, I. Romero, S. Lal, J. H. Hafner, P. Nordlander, and N. J. Halas. Close encounters between two nanoshells. *Nano Letters*, 8(4):1212–1218, 2008. PMID: 18345644.

[111] R. Lazzari and J. Jupille. Growth kinetics and size-dependent wetting of ag/-al 2 o 3 (0001) nanoparticles studied via the plasmonic response. *Nanotechnology*, 23(13):135707, 2012.

[112] R. Lazzari, J. Jupille, R. Cavallotti, and I. Simonsen. Model-free unraveling of supported nanoparticles plasmon resonance modes. *The Journal of Physical Chemistry C*, 118(13):7032–7048, 2014.

[113] R. Lazzari, J. Jupille, and J.-M. Layet. Electron-energy-loss channels and plasmon confinement in supported silver particles. *Phys. Rev. B*, 68:045428, Jul 2003.

[114] R. Lazzari, S. Roux, I. Simonsen, J. Jupille, D. Bedeaux, and J. Vlieger. Multipolar plasmon resonances in supported silver particles: The case of $Ag/\alpha - al_2o_3(0001)$. *Phys. Rev. B*, 65:235424, Jun 2002.

[115] R. Lazzari, I. Simonsen, and J. Jupille. Onset of charge localisation on coupling multipolar absorption modes in supported metal particles. *EPL (Europhysics Letters)*, 61(4):541, 2003.

[116] S. Lecoultre, A. Rydlo, J. Buttet, C. Félix, S. Gilb, and W. Harbich. Ultraviolet-visible absorption of small silver clusters in neon: Agn (n = 1–9). *The Journal of Chemical Physics*, 134(18):–, 2011.

[117] S. Lecoultre, A. Rydlo, C. Félix, J. Buttet, S. Gilb, and W. Harbich. Optical absorption of small copper clusters in neon: Cun, (n = 1–9). *The Journal of Chemical Physics*, 134(7):–, 2011.

[118] K.-S. Lee†, , and M. A. El-Sayed*. Gold and silver nanoparticles in sensing and imaging: sensitivity of plasmon response to size, shape, and metal composition. *The Journal of Physical Chemistry B*, 110(39):19220–19225, 2006. PMID: 17004772.

[119] T. Lelaidier, T. Lunskens, A. von Weber, T. Leoni, A. Ranguis, A. D'Aleo, F. Fages, A. Kartouzian, C. Becker, and U. Heiz. Optical and morphological properties of thin films of bis-pyrenyl [small pi]-conjugated molecules. *Phys. Chem. Chem. Phys.*, 18:5299–5305, 2016.

[120] J. Lermé, H. Baida, C. Bonnet, M. Broyer, E. Cottancin, A. Crut, P. Maioli, N. D. Fatti, F. Vallée, and M. Pellarin. Size dependence

of the surface plasmon resonance damping in metal nanospheres. *The Journal of Physical Chemistry Letters*, 1(19):2922–2928, 2010.

[121] J. Lermé, C. Bonnet, M. Broyer, E. Cottancin, D. Manchon, and M. Pellarin. Optical properties of a particle above a dielectric interface: Cross sections, benchmark calculations, and analysis of the intrinsic substrate effects. *The Journal of Physical Chemistry C*, 117(12):6383–6398, 2013.

[122] S. Leroy-Lhez, M. Allain, J. Oberle, and F. Fages. Synthesis and zinc(ii) complexation modulated fluorescence emission properties of two pyrene-oligo(phenylene vinylene)-2,2[prime or minute]-bipyridine conjugated molecular rods. *New J. Chem.*, 31:1013–1021, 2007.

[123] P. A. Letnes, I. Simonsen, and D. L. Mills. Substrate influence on the plasmonic response of clusters of spherical nanoparticles. *Phys. Rev. B*, 83:075426, Feb 2011.

[124] H. Li, D. R. Powell, R. K. Hayashi, , and R. West*. Poly((2,5-dialkoxy-p-phenylene)ethynylene-p-phenyleneethynylene)s and their model compounds. *Macromolecules*, 31(1):52–58, 1998.

[125] Z. Li, J. J. Foley, 4th, S. Peng, C.-J. Sun, Y. Ren, G. P. Wiederrecht, S. K. Gray, and Y. Sun. Reversible modulation of surface plasmons in gold nanoparticles enabled by surface redox chemistry. *Angew Chem Int Ed Engl*, 54(31):8948–51, Jul 2015.

[126] I. Lieberman, G. Shemer, T. Fried, E. Kosower, and G. Markovich. Plasmon-resonance-enhanced absorption and circular dichroism. *Angewandte Chemie International Edition*, 47(26):4855–4857, 2008.

[127] A. Liebsch. Surface-plasmon dispersion and size dependence of mie resonance: Silver versus simple metals. *Phys. Rev. B*, 48:11317–11328, Oct 1993.

[128] Linda S. Jung, Charles T. Campbell, *, Timothy M. Chinowsky, Mimi N. Mar, , and S. S. Yee‡. Quantitative interpretation of the response of surface plasmon resonance sensors to adsorbed films. *Langmuir*, 14(19):5636–5648, 1998.

[129] S. Linic, P. Christopher, and D. B. Ingram. Plasmonic-metal nanostructures for efficient conversion of solar to chemical energy. *Nat Mater*, 10(12):911–921, 12 2011.

[130] T. Linnert, P. Mulvaney, and A. Henglein. Surface chemistry of colloidal silver: surface plasmon damping by chemisorbed iodide, hydrosulfide (sh-), and phenylthiolate. *The Journal of Physical Chemistry*, 97(3):679–682, 1993.

[131] W. Liu, F. Maaß, M. Willenbockel, C. Bronner, M. Schulze, S. Soubatch, F. S. Tautz, P. Tegeder, and A. Tkatchenko. Quantitative prediction of molecular adsorption: Structure and binding of benzene on coinage metals. *Phys. Rev. Lett.*, 115:036104, Jul 2015.

[132] C. Love, L. A. Estroff, Jennah K. Kriebel, Ralph G. Nuzzo, *, , and George M. Whitesides*. Self-assembled monolayers of thiolates on metals as a form of nanotechnology. *Chemical Reviews*, 105(4):1103–1170, 2005. PMID: 15826011.

[133] T. L. Second-harmonic-genertion-spectroscopy of surface complexes. Master's thesis, Technische Universität München, 2012.

[134] T. Lünskens, P. Heister, M. Thamer, C. A. Walenta, A. Kartouzian, and U. Heiz. Plasmons in supported size-selected silver nanoclusters. *Phys. Chem. Chem. Phys.*, 17:17541–17544, 2015.

[135] M. A. Mahmoud, M. Chamanzar, A. Adibi, and M. A. El-Sayed. Effect of the dielectric constant of the surrounding medium and the substrate on the surface plasmon resonance spectrum and sensitivity factors of highly symmetric systems: Silver nanocubes. *Journal of the American Chemical Society*, 134(14):6434–6442, 2012. PMID: 22420824.

[136] S. A. Maier, M. L. Brongersma, P. G. Kik, and H. A. Atwater. Observation of near-field coupling in metal nanoparticle chains using far-field polarization spectroscopy. *Phys. Rev. B*, 65:193408, May 2002.

[137] M. D. Malinsky, K. L. Kelly, George C. Schatz, *, , and Richard P. Van Duyne*. Nanosphere lithography: effect of substrate on the localized surface plasmon resonance spectrum of silver nanoparticles. *The Journal of Physical Chemistry B*, 105(12):2343–2350, 2001.

[138] A. Marimuthu, J. Zhang, and S. Linic. Tuning selectivity in propylene epoxidation by plasmon mediated photo-switching of cu oxidation state. *Science*, 339(6127):1590–3, Mar 2013.

[139] K. M. Mayer and J. H. Hafner. Localized surface plasmon resonance sensors. *Chemical Reviews*, 111(6):3828–3857, 2011. PMID: 21648956.

[140] A. D. McFarland, , and R. P. V. Duyne*. Single silver nanoparticles as real-time optical sensors with zeptomole sensitivity. *Nano Letters*, 3(8):1057–1062, 2003.

[141] T. Menegotto and F. Horowitz. Anisotropic effective medium properties from interacting ag nanoparticles in silicon dioxide. *Appl. Opt.*, 53(13):2853–2859, May 2014.

[142] G. C. S. . ichelle Duval Malinsky, K. Lance Kelly and Richard P. Van Duyne*. Chain length dependence and sensing capabilities of the localized surface plasmon resonance of silver nanoparticles chemically modified with alkanethiol self-assembled monolayers. *J. Am. Chem. Soc.*, 123:1471, 2001.

[143] G. Mie. Beiträge zur optik trüber medien, speziell kolloidaler metallösungen. *Annalen der Physik*, 330(3):377–445, 1908.

[144] A. Mishra, C.-Q. Ma, and P. Bäuerle. Functional oligothiophenes: Molecular design for multidimensional nanoarchitectures and their applications. *Chemical Reviews*, 109(3):1141–1276, 2009. PMID: 19209939.

[145] J. J. Mock, D. R. Smith, and S. Schultz. Local refractive index dependence of plasmon resonance spectra from individual nanoparticles. *Nano Letters*, 3(4):485–491, 2003.

[146] K. B. Mogensen and K. Kneipp. Size-dependent shifts of plasmon resonance in silver nanoparticle films using controlled dissolution: Monitoring the onset of surface screening effects. *The Journal of Physical Chemistry C*, 118(48):28075–28083, 2014.

[147] R. C. Monreal, T. J. Antosiewicz, and S. P. Apell. Competition between surface screening and size quantization for surface plasmons in nanoparticles. *New Journal of Physics*, 15(8):083044, 2013.

[148] F. Moreno, F. Gonzalez, and J. Saiz. Plasmon spectroscopy of metallic nanoparticles above flat dielectric substrates. *Optics Letters*, 31(12), 2006.

[149] S. Mukherjee, L. Zhou, A. M. Goodman, N. Large, C. Ayala-Orozco, Y. Zhang, P. Nordlander, and N. J. Halas. Hot-electron-induced dissociation of h2 on gold nanoparticles supported on sio2. *Journal of the American Chemical Society*, 136(1):64–67, 2014.

[150] P. Mulvaney. Surface plasmon spectroscopy of nanosized metal particles. *Langmuir*, 12(3):788–800, 1996.

[151] P. Mulvaney, T. Linnert, and A. Henglein. Surface chemistry of colloidal silver in aqueous solution: observations on chemisorption and reactivity. *The Journal of Physical Chemistry*, 95(20):7843–7846, 1991.

[152] P. Mulvaney, J. Pérez-Juste, M. Giersig, L. M. Liz-Marzán, and C. Pecharromán. Drastic surface plasmon mode shifts in gold nanorods due to electron charging. *Plasmonics*, 1(1):61–66, 2006.

[153] V. Myroshnychenko, J. Rodriguez-Fernandez, I. Pastoriza-Santos, A. M. Funston, C. Novo, P. Mulvaney, L. M. Liz-Marzan, and F. J. Garcia de Abajo. Modelling the optical response of gold nanoparticles. *Chem. Soc. Rev.*, 37:1792–1805, 2008.

[154] J. Nappa, G. Revillod, I. Russier-Antoine, E. Benichou, C. Jonin, and P. F. Brevet. Electric dipole origin of the second harmonic generation of small metallic particles. *Phys. Rev. B*, 71:165407, Apr 2005.

[155] J. Nappa, I. Russier-Antoine, E. Benichou, C. Jonin, and P. F. Brevet. Second harmonic generation from small gold metallic particles: From the dipolar to the quadrupolar response. *The Journal of Chemical Physics*, 125(18):–, 2006.

[156] S. Nath, S. Kumar Ghosh, S. Praharaj, S. Panigrahi, S. Basu, and T. Pal. Silver organosol: synthesis, characterisation and localised surface plasmon resonance study. *New J. Chem.*, 29:1527–1534, 2005.

[157] S. Nie and S. R. Emory. Probing single molecules and single nanoparticles by surface-enhanced raman scattering. *Science*, 275(5303):1102–1106, 1997.

[158] N. Nilius, N. Ernst, and H.-J. Freund. Photon emission spectroscopy of individual oxide-supported silver clusters in a scanning tunneling microscope. *Phys. Rev. Lett.*, 84:3994–3997, Apr 2000.

[159] C. Noguez*. Surface plasmons on metal nanoparticles: the influence of shape and physical environment. *The Journal of Physical Chemistry C*, 111(10):3806–3819, 2007.

[160] C. Novo, A. M. Funston, A. K. Gooding, and P. Mulvaney. Electrochemical charging of single gold nanorods. *Journal of the American Chemical Society*, 131(41):14664–14666, 2009. PMID: 19824726.

[161] C. Novo, A. M. Funston, and P. Mulvaney. Direct observation of chemical reactions on single gold nanocrystals using surface plasmon spectroscopy. *Nat Nano*, 3(10):598–602, 10 2008.

[162] J. J. ock, M. Barbic, D. R. Smith, D. A. Schultz, and S. Schultz. hape effects in plasmon resonance of individual colloidal silver nanoparticles. *The Journal of Chemical Physics*, 116(15):6755–6759, 2002.

[163] A. Okeefe and D. A. G. Deacon. Cavity ring-down optical spectrometer for absorption measurements using pulsed laser sources. *Review of Scientific Instruments*, 59:2544, 1988.

[164] S. Peng, J. M. McMahon, G. C. Schatz, S. K. Gray, and Y. Sun. Reversing the size-dependence of surface plasmon resonances. *Proceedings of the National Academy of Sciences*, 107(33):14530–14534, 2010.

[165] M. Quinten. Local fields close to the surface of nanoparticles and aggregates of nanoparticles. *Applied Physics B*, 73(3):245–255, 2001.

[166] S. Raza, S. Kadkhodazadeh, T. Christensen, M. Di Vece, M. Wubs, N. A. Mortensen, and N. Stenger. Multipole plasmons and their disappearance in few-nanometre silver nanoparticles. *Nat Commun*, 6, 11 2015.

[167] S. Raza, W. Yan, N. Stenger, M. Wubs, and N. A. Mortensen. Blueshift of the surface plasmon resonance in silver nanoparticles: substrate effects. *Opt. Express*, 21(22):27344–27355, Nov 2013.

[168] W. Rechberger, A. Hohenau, A. Leitner, J. Krenn, B. Lamprecht, and F. Aussenegg. Optical properties of two interacting gold nanoparticles. *Optics Communications*, 220(1–3):137 – 141, 2003.

[169] L. M. Rodríguez, J. Esteban Gayone, E. A. Sánchez, , O. Grizzi, B. Blum*, , and R. C. Salvarezza. Room-temperature kinetics of short-chain alkanethiol film growth on ag(111) from the vapor phase. *The Journal of Physical Chemistry B*, 110(14):7095–7097, 2006. PMID: 16599469.

[170] C. E. Román-Velázquez, C. Noguez, and R. G. Barrera. Substrate effects on the optical properties of spheroidal nanoparticles. *Phys. Rev. B*, 61:10427–10436, Apr 2000.

[171] J. Romann, J. Wei, and M.-P. Pileni. Computational matching of surface plasmon resonance: Interactions between silver nanoparticles

and ligands. *The Journal of Physical Chemistry C*, 119(20):11094–11099, 2015.

[172] R. Ruppin. Optical properties of a metal sphere with a diffuse surface. *J. Opt. Soc. Am.*, 66(5):449–453, May 1976.

[173] R. Ruppin. Surface modes and optical absorption of a small sphere above a substrate. *Surface Science*, 127(1):108 – 118, 1983.

[174] M. Sanekata and I. Suzuka. Physical and chemical interface effects on mie plasmon absorption of sodium nanoclusters passivated with ch4ncln (n=1–4) molecules. *Chemical Physics Letters*, 323(1–2):98 – 104, 2000.

[175] M.-H. Schaffner, F. Patthey, and W.-D. Schneider. Size-selected agn and cun clusters supported on mgo(100) films. *The European Physical Journal D - Atomic, Molecular, Optical and Plasma Physics*, 9(1):609–612, 1999.

[176] M. Schanne-Klein, T. Boulesteix, F. Hache, M. Alexandre, G. Lemercier, and C. Andraud. Strong chiroptical effects in surface second harmonic generation obtained for molecules exhibiting excitonic coupling chirality. *Chemical Physics Letters*, 362(1–2):103 – 108, 2002.

[177] J. A. Scholl, A. L. Koh, and J. A. Dionne. Quantum plasmon resonances of individual metallic nanoparticles. *Nature*, 483(7390):421–7, Mar 2012.

[178] D. Schooss, M. N. Blom, J. H. Parks, B. v. Issendorff, H. Haberland, and M. M. Kappes. The structures of ag55+ and ag55-: trapped ion electron diffraction and density functional theory. *Nano Letters*, 5(10):1972–1977, 2005. PMID: 16218720.

[179] F. Schreiber. Structure and growth of self-assembling monolayers. *Progress in Surface Science*, 65(5–8):151–257, 2000/12// 2000.

[180] D. K. Schwartz. Mechanisms and kinetics of self-assembled monolayer formation. *Annual Review of Physical Chemistry*, 52(1):107–137, 2001. PMID: 11326061.

[181] Y. R. Shen. Optical second harmonic generation at interfaces. *Annual Review of Physical Chemistry*, 40:327–350, 1989.

[182] Y. R. Shen. A few selected applications of surface nonlinear optical spectroscopy. *Proceedings of the National Academy of Sciences of the United States of America*, 93(22):12104–12111, 10 1996.

[183] Y. R. Shen. Surface nonlinear optics. *J. Opt. Soc. Am. B*, 28(12):A56–A66, Dec 2011.

[184] Y. R. Shen. Basic theory of surface sum-frequency generation. *The Journal of Physical Chemistry C*, 116(29):15505–15509, 2012.

[185] L. J. Sherry, S.-H. Chang, . George C. Schatz, , R. P. V. Duyne*, B. J. Wiley, , and Y. Xia. Localized surface plasmon resonance spectroscopy

of single silver nanocubes. *Nano Letters*, 5(10):2034–2038, 2005. PMID: 16218733.

[186] S. Sioncke, T. Verbiest, and A. Persoons. Second-order nonlinear optical properties of chiral materials. *Materials Science Engineering R*, 42(5-6):115–155, 2003.

[187] H.-P. Steinrück, W. Huber, T. Pache, and D. Menzel. The adsorption of benzene mono- and multilayers on ni(111) studied by tpd and leed. *Surface Science*, 218(2):293 – 316, 1989.

[188] F. Strelow and A. Henglein. Time resolved chemisorption of i- and sh- on colloidal silver particles (a stopped-flow study). *The Journal of Physical Chemistry*, 99(31):11834–11838, 1995.

[189] K.-H. Su, Q.-H. Wei, X. Zhang, J. J. Mock, D. R. Smith, and S. Schultz. Interparticle coupling effects on plasmon resonances of nanogold particles. *Nano Letters*, 3(8):1087–1090, 2003.

[190] Y. Sun, S. K. Gray, and S. Peng. Surface chemistry: a non-negligible parameter in determining optical properties of small colloidal metal nanoparticles. *Phys. Chem. Chem. Phys.*, 13:11814–11826, 2011.

[191] §. T. Gregory Schaaff, *, Grady Knight, Marat N. Shafigullin, Raymond F. Borkman, , and Robert L. Whetten*, †. Isolation and selected properties of a 10.4 kda gold:glutathione cluster compound. *The Journal of Physical Chemistry B*, 102(52):10643–10646, 1998.

[192] H. Tamaru, H. Kuwata, H. Miyazaki, and K. Miyano. Resonant light scattering from individual ag nanoparticles and particle pairs. *Applied Physics Letters*, 80:1826, 2002.

[193] M. Thaemer, A. Kartouzian, P. Heister, S. Gerlach, M. Tschurl, U. Boesl, and U. Heiz. Linear and nonlinear laser spectroscopy of surface adsorbates with sub-monolayer sensitivity. *J. Phys. Chem. C*, 116(15):8642–8648, 2012.

[194] M. Thämer. *Linear and Nonlinear Surface Spectroscopy of Supported Size Selected Metal Clusters and Organic Molecules*. PhD thesis, Technische Universität München, 2012.

[195] M. Thämer, A. Kartouzian, P. Heister, T. Lünskens, S. Gerlach, and U. Heiz. Small supported plasmonic silver clusters. *Small*, 10(12):2340–2344, 2014.

[196] V. R. Thierry Verbiest, Koen Clays. *Second-Order Momlinear Optical Characterization Techniques; An Introduction*. CRC Press, 2009.

[197] J. Tiggesbäumker, L. Köller, K.-H. Meiwes-Broer, and A. Liebsch. Blue shift of the mie plasma frequency in ag clusters and particles. *Phys. Rev. A*, 48:R1749–R1752, Sep 1993.

[198] G. Toscano, J. Straubel, A. Kwiatkowski, C. Rockstuhl, F. Evers, H. Xu, N. A. Mortensen, and M. Wubs. Resonance shifts and spill-out effects in self-consistent hydrodynamic nanoplasmonics. *Nat Commun*, 6:7132, 2015.

[199] A. Tripathi, E. Emmons, S. Christesen, A. Fountain, and A. Guichetau. Kinetics and reaction mechanisms of thiophenol adsorption on gold studied by surface-enhanced raman spectroscopy. *The Journal of Physical Chemistry C*, 117:22834–22842, 2013.

[200] T. Ung, Michael Giersig, David Dunstan, , and P. Mulvaney*. Spectroelectrochemistry of colloidal silver. *Langmuir*, 13(6):1773–1782, 1997.

[201] N. Vandamme, J. Snauwaert, E. Janssens, E. Vandeweert, P. Lievens, and C. V. Haesendonck. Visualization of gold clusters deposited on a dithiol self-assembled monolayer by tapping mode atomic force microscopy. *Surface Science*, 558(1–3):57 – 64, 2004.

[202] B. Wang, B. Yoon, M. König, Y. Fukamori, F. Esch, U. Heiz, and U. Landman. Size-selected monodisperse nanoclusters on supported graphene: Bonding, isomerism, and mobility. *Nano Letters*, 12(11):5907–5912, 2012. PMID: 23057656.

[203] J. Wei, N. Schaeffer, and M.-P. Pileni. Ag nanocrystals: 1. effect of ligands on plasmonic properties. *The Journal of Physical Chemistry B*, 118(49):14070–14075, 2014. PMID: 25198062.

[204] T. Wenzel, J. Bosbach, F. Stietz, and F. Träger. In situ determination of the shape of supported silver clusters during growth. *Surface Science*, 432(3):257 – 264, 1999.

[205] M. D. Wheeler, S. M. Newman, A. J. Orr-Ewing, and M. N. R. Ashfold. Cavity ring-down spectroscopy. *J. Chem. Soc., Faraday Trans.*, 94:337–351, 1998.

[206] K. A. Willets and R. P. Van Duyne. Localized surface plasmon resonance spectroscopy and sensing. *Annu Rev Phys Chem*, 58:267–97, 2007.

[207] B. Xu, G. Gonella, B. G. DeLacy, and H.-L. Dai. Adsorption of anionic thiols on silver nanoparticles. *The Journal of Physical Chemistry C*, 119(10):5454–5461, 2015.

[208] G. Xu, M. Tazawa, P. Jin, S. Nakao, and K. Yoshimura. Wavelength tuning of surface plasmon resonance using dielectric layers on silver island films. *Applied Physics Letters*, 82:3811, 2003.

[209] T. Yamaguchi, S. Yoshida, and A. Kinbara. Optical effect of the substrate on the anomalous absorption of aggregated silver films. *Thin Solid Films*, 21(1):173 – 187, 1974.

[210] H. Yang, Y. Wang, H. Huang, L. Gell, L. Lehtovaara, S. Malola, H. Häkkinen, and N. Zheng. All-thiol-stabilized ag44 and au12ag32 nanoparticles with single-crystal structures. *Nat Commun*, 4:2422, 2013.

[211] P. Yang, H. Portalès, and M.-P. Pileni. Dependence of the localized surface plasmon resonance of noble metal quasispherical nanoparticles on their crystallinity-related morphologies. *The Journal of Chemical Physics*, 134(2), 2011.

[212] P. Zanlicki and R. N. Zare. Cavity ring-down spectroscopy for quantitative absorption measurements. *Journal of Chemical Physics*, 102:2708–2717, 1995.

[213] S. Zhang, K. Bao, N. J. Halas, H. Xu, and P. Nordlander. Substrate-induced fano resonances of a plasmonic nanocube: A route to increased-sensitivity localized surface plasmon resonance sensors revealed. *Nano Letters*, 11(4):1657–1663, 2011. PMID: 21410217.

[214] P. Zijlstra, P. M. R. Paulo, and M. Orrit. Optical detection of single non-absorbing molecules using the surface plasmon resonance of a gold nanorod. *Nat Nano*, 7(6):379–382, 06 2012.

[215] P. Zijlstra, P. M. R. Paulo, K. Yu, Q.-H. Xu, and M. Orrit. Chemical interface damping in single gold nanorods and its near elimination by tip-specific functionalization. *Angew. Chem. Int. Ed.*, 51:8352–8355, 2012.